

FLAME RETARDANCY OF POLYAMIDE COMPOUNDS AND
MICRO/NANO COMPOSITES

A THESIS SUBMITTED TO
THE GRADUATE SCHOOL OF NATURAL AND APPLIED SCIENCES
OF
MIDDLE EAST TECHNICAL UNIVERSITY

BY

HÜSEYİN ÖZGÜR GÜNDÜZ

IN PARTIAL FULFILLMENT OF THE REQUIREMENTS
FOR
THE DEGREE OF MASTER OF SCIENCE
IN
POLYMER SCIENCE AND TECHNOLOGY

JULY 2009

Approval of the thesis:

**FLAME RETARDANCY OF POLYAMIDE COMPOUNDS AND
MICRO/NANO COMPOSITES**

submitted by **HÜSEYİN ÖZGÜR GÜNDÜZ** in partial fulfillment of the requirements for the degree of **Master of Science in Polymer Science and Technology Department, Middle East Technical University** by,

Prof. Dr. Canan Özgen
Dean, Graduate School of **Natural and Applied Sciences** _____

Prof. Dr. Cevdet Kaynak
Head of Department, **Polymer Science and Technology** _____

Prof. Dr. Cevdet Kaynak
Supervisor, **Polymer Science and Technology, METU** _____

Examining Committee Members:

Prof. Dr. Teoman Tinçer
Chemistry Dept., METU _____

Prof. Dr. Cevdet Kaynak
Metalurgical and Materials Eng. Dept., METU _____

Prof. Dr. Ülkü Yilmazer
Chemical Eng. Dept., METU _____

Assoc. Prof. Dr. Necati Özkan
Central Laboratory, METU _____

Dr. H. Emrah Ünalın
Metalurgical and Materials Eng. Dept., METU _____

Date : _____

I hereby declare that all information in this document has been obtained and presented in accordance with academic rules and ethical conduct. I also declare that, as required by these rules and conduct, I have fully cited and referenced all material and results that are not original to this work.

Name, Last name: Hüseyin Özgür Gündüz

Signature:

ABSTRACT

FLAME RETARDANCY OF POLYAMIDE COMPOUNDS AND MICRO/NANO COMPOSITES

Gündüz, Hüseyin Özgür

M.S., Department of Polymer Science and Technology

Supervisor: Prof. Dr. Cevdet Kaynak

July 2009, 144 pages

In the first part of this dissertation, glass fiber reinforced/unreinforced polyamide 6 (PA6) and polyamide 66 (PA66) were compounded with three different flame retardants, which were melamine cyanurate, red phosphorus and brominated epoxy with antimony trioxide, by using an industrial scale twin screw extruder. Then, to investigate flame retardancy of these specimens, UL-94, Limiting Oxygen Index (LOI) and Mass Loss Cone Calorimeter (MLC) tests were carried out. In addition to flammability tests, thermogravimetric analysis (TGA) and tensile testing were performed. Results of the tensile tests were evaluated by relating them with fiber length distributions and fracture surface morphologies under scanning electron microscope (SEM).

Incorporation of melamine cyanurate (MCA) to PA6 led to some increase in LOI value and minor reductions in Peak Heat Release Rate (PHRR) value. However, it failed to improve UL-94 rating. Moreover, poor compatibility of MCA with PA6 matrix caused significant reductions in tensile strength.

Brominated epoxy in combination with antimony trioxide (Br/Sb) was compounded with both glass fiber reinforced PA6 and PA66. Br/Sb synergism was found to impart excellent flammability reductions in LOI value and UL-94 as V-0 rating.

Effectiveness of Br/Sb flame retardant was also proven by the MLC measurements, which showed excessive reductions in PHRR and Total Heat Evolved (THE) values. On the other hand, Br/Sb shifted the degradation temperature 100°C lower and decreased the tensile strength value, due to poor fiber-matrix adhesion and decreased fiber lengths.

Red phosphorus (RP), when introduced to glass fiber reinforced PA66 induced V-0 rating in UL-94 together with significant increase in LOI value, and major decrease in PHRR. Degradation temperature was 20°C lower while mechanical properties were kept at acceptable values compared to neat glass fiber reinforced PA66.

In the second part of this dissertation, to investigate synergistic flame retardancy of nanoclays; glass fiber reinforced PA6 was compounded by certain nanoclay and an organo-phosphorus flame retardant (OP), which contains aluminum phosphinate, melamine polyphosphate and zinc borate, in a laboratory scale twin screw extruder. Exfoliated clay structure of the nanocomposites was assessed by X-Ray Diffraction (XRD) and Transmission Electron Microscopy (TEM), while thermal stability and combustion behaviors were evaluated by TGA, LOI, UL-94 and MLC.

Replacement of a certain fraction of the flame retardant with nanoclay was found to significantly reduce PHRR and THE values, and delay the ignition. Moreover, remarkable improvements were obtained in LOI values along with maintained UL-94 ratings.

Residue characterization by ATR-FTIR and SEM ascribed the enhanced flame retardancy of nanocomposite specimens to the formation of a glassy boron-aluminum phosphate barrier reinforced by clay layers at the nanoscale.

Keywords: Polyamide, Glass Fiber, Flame Retardancy, Nanoclay, Mass Loss Cone Calorimeter

ÖZ

POLİAMİD KOMPAUNDLARININ VE MİKRO/NANO KOMPOZİTLERİNİN ALEVLENME DAYANIMI

Gündüz, Hüseyin Özgür

Yüksek Lisans, Polimer Bilimi ve Teknolojisi Bölümü

Tez Yöneticisi: Prof. Dr. Cevdet Kaynak

Temmuz 2009, 144 sayfa

Bu tezin ilk bölümünde, cam elyaf takviyeli/takviyesiz poliamid 6 (PA6) ve poliamid 66 (PA66) endüstriyel boyutlu ekstruder kullanılarak, üç farklı alev geciktirici ile karıştırılmıştır. Bu alev geciktiriciler; melamin siyanürat (MCA), kırmızı fosfor (RP) ve bromlu epoksi-antimon trioksittir (Br/Sb). Daha sonra bu numunelere, alev geciktiricilerin etkilerini incelemek için UL-94, Limit Oksijen İndeksi (LOI) ve Kütle Kaybı Konik Kalorimetre (MLC) testleri uygulanmıştır. Alevlenme testlerine ek olarak, termogravimetrik analiz ve çekme testi uygulanmıştır. Çekme testinin sonuçları, elyaf boyu dağılımı ve taramalı elektron mikroskobu (SEM) altında kırılma yüzeyi morfolojisi ile ilişkilendirilerek yorumlanmıştır.

PA6'ya MCA, LOI değerinde bir miktar artışa ve Maksimum Isı Yayma Oranında (PHRR) az miktarda düşüşe neden olmuştur. Ancak, UL-94 değerinde bir ilerleme kaydedilememiştir. Ayrıca, MCA ile PA6'nın uyumsuzluğu çekme dayanımında önemli düşüşlere neden olmuştur.

Bromlu epoksi ve antimon trioksit (Br/Sb), cam elyaf takviyeli PA6 ve PA66'ya karıştırılmıştır. Br/Sb sinerjisinin, LOI değeri ve V-0 olan UL-94 sınıflandırmasına bakıldığında alevlenmede mükemmel düşüşlere yol açtığı bulunmuştur. Br/Sb alev

geciktiricisinin etkinliđi ayrıca MLC ölçümleri ile kanıtlanmıştır. Bu ölçümlerde PHRR ve Toplam Yayılan Isı (THE) değerlerinde büyük düşüşler gözlemlenmiştir. Buna karşılık, Br/Sb ısı bozulma sıcaklığını 100°C düşürmektedir. Ayrıca, zayıflayan elyaf-matris ara yüzey bađı ve azalan elyaf boyları sonucunda çekme dayanımı düşmektedir.

Cam elyaf takviyeli PA66'ya kırmızı fosfor (RP) eklenmesi, malzemenin UL-94 testinden V-0 almasına, LOI değerinin önemli şekilde artmasına ve PHRR'nin büyük ölçüde düşmesine neden olmuştur. Isıl bozunma sıcaklığı 20°C düşerken, çekme dayanımı sadece cam elyaf takviyeli PA66'ya oranla kabul edilebilir değerlerde kalmıştır.

Bu tezin ikinci kısımda, nanokilin alev geciktiricilerle sinerjik etkilerini incelemek için; laboratuvar boyutlu çift vidalı ekstruder kullanarak, cam elyaf takviyeli PA6, özel bir nanokil ve OP diye adlandırılan (alüminyum fosfinat, melamin polifosfat ve çinko borat içeren) bir alev geciktirici ile çeşitli oranlarda karıştırılarak nanokompozit numuneler üretilmiştir. Eksfoliyeye olmuş kil yapılı nanokompozitlerin karakterizasyonu X-ışınları (XRD) ve geçirimli elektron mikroskobu (TEM) ile yapılmıştır. Isıl dayanım ve yanma davranışları ise TGA, LOI, UL-94 ve MLC kullanılarak belirlenmiştir.

Alev geciktiricinin bir miktarının yerine nano kil koyulması ile MLC ölçümlerinde PHRR ve THE değerlerinde önemli düşüşler ve tutuşma süresinde artış gözlemlenmiştir. İlave olarak, LOI değerinde dikkat çekici artışlar elde edilmiş ve zaten iyi olan UL-94 değerleri korunmuştur.

ATR-FTIR ve SEM ile yapılan kalıntı karakterizasyonları sonucunda, nanokompozitlerin artan alevlenme dayanımı; kil katmanları tarafından nano boyutta güçlendirilmiş camsı bor-alüminyum bariyerine bağlanmıştır.

Anahtar Sözcükler: Poliamid, Cam Elyafı, Alev Geciktiricilik, Nanokil, Kütle Kaybı Konik Kalorimetresi

ACKNOWLEDGEMENTS

I would like to express my deepest gratitude to my supervisor Prof. Dr. Cevdet Kaynak. Starting from the first day, he responded me very politely and always encouraged me with his positive attitude. I sincerely appreciate the time and efforts he has taken to train me and improve my thesis.

Partial financial support of this research as part of the Project 107M347 by TUBITAK, The Scientific and Technological Research Council of Turkey, is gratefully acknowledged

I am also very grateful to Murat Cansever from Eurotec Engineering Thermoplastic Inc., who gave the first advice to study flame retardancy of polymers. He also gave me the opportunity to gain some hands-on experience about polymer industry during my stay in the factory. Eurotec's twin screw extruder and UL-94 Test Machine were used in the first part of this thesis study. I am also thankful to Işık Ağıl and Murat Topsakal from the same company, for sharing their experiences.

I am thankful to Prof. Dr. Ülkü Yılmaz and Assoc. Prof. Dr. Gökür Bayram for giving permission to use laboratory scale extruder and injection molding machine in the second part of this study, and to Sertan Yeşil for instructing how to use them.

I am also thankful to Prof Dr. Teoman Tinçer and Prof. Dr. Erdal Bayramlı for giving permission to use melt flow index and injection molding machines. I also want to mention about Mehmet Doğan and Osman Yaslıtaş for their help in these studies.

I appreciate Dr. Selda Keskin for ATR-FTIR analysis, Mihrican Açıkgöz for TGA analysis, Cengiz Tan for SEM analysis and Necmi Avcı for XRD analysis.

I wish to acknowledge my laboratory mate Nihat Ali Işıtman, first for his friendship. Then, I am also respectful to him since; he gave me advices before the experiments, spared his time to help me during the experiments and also encouraged me if I felt lazy.

I am also thankful to my laboratory friends Bengü Melike Kuşcuoğlu and Ayşe Çağıl Özkaraca for their patience and politeness during my study. Also, friends from the same floor; Nagehan Duman and Muratahan Aykol are appreciated.

I sincerely acknowledge my friends; Adem Çakmaklı, Salim Çalışkan, Özer Candarlı, Fırat Hacıoğlu and Uğur Can Özel with whom I had spent most of time after working hours when preparing my thesis. They made me happy and ready for the next working day.

Finally, I want to thank to my family, Pervin and Hamit Gündüz for their endless love and support in every step of my life. I could not achieve any of these without their support and belief in me.

TABLE OF CONTENTS

ABSTRACT	iv
ÖZ	vi
ACKNOWLEDGEMENTS	viii
TABLE OF CONTENTS	x
LIST OF TABLES	xv
LIST OF FIGURES	xvi
CHAPTERS	
1. INTRODUCTION	1
1.1 Polyamides.....	1
1.1.1 Industrial Scale Production of Polyamides.....	2
(i) Polyamide 66.....	2
(ii) Polyamide 6.....	3
1.1.2 Properties of Polyamides.....	4
1.1.3 Thermal Degradation of Polyamides	5
1.2 Polyamide Composites.....	6
1.2.1 Polyamide/Short Glass Fiber Composites.....	6
1.2.2 Polyamide/Clay Nanocomposites.....	7
1.3 Flammability of Polymers.....	9
1.3.1 Flaming of Polymers.....	9
(i) General Burning Behavior of Polymers.....	9
(ii) Burning Behavior of Polyamides.....	11
1.3.2 Flame Retardants and Flame Retardancy Mechanisms.....	12

(i) Physical Action of Flame Retardancy.....	12
(ii) Chemical Action of Flame Retardancy.....	13
(iii) Flame retardancy of nanoclays.....	14
1.3.3 Using Flame Retardants Together.....	14
(i) Halogen-Antimony Synergism.....	15
(ii) Phosphorus-Phosphorus (P-P) and Nitrogen-Phosphorous (N-P) Synergism.....	16
(iii) Zinc Borate as a Synergist.....	16
(iv) A Commercial Example of Synergism.....	17
1.3.4 Fire and Flammability Tests.....	17
(i) UL-94 Tests.....	18
(ii) Limiting Oxygen Index Test (LOI)	20
(iii) Mass Loss Cone Calorimeter.....	22
1.4 Previous Studies.....	25
1.4.1 Previous Studies on the Flammability of Polyamides Using Conventional Flame Retardants.....	25
(i) Brominated Flame Retardants.....	25
(ii) Melamine Cyanurate.....	25
(iii) Red Phosphorous.....	26
(iv) Organic Phosphorus Additives.....	28
1.4.2 Previous Studies on the Flammability of Polyamides Using Conventional Flame Retardants in Combination with Nanofillers.....	29
1.5 Aim of This Study.....	30
2. EXPERIMENTAL.....	33
2.1 Materials Used.....	33
2.1.1 Polyamides.....	33
2.1.2 Glass Fiber.....	34

2.1.3 Flame Retardants.....	34
(i) Melamine Cyanurate.....	34
(ii) Brominated Epoxy and Antimony Trioxide	34
(iii) Red Phosphorous	36
(iv) Organophosphorous Flame Retardant.....	36
2.1.4 Nanoclay.....	36
2.2 Production of the Specimens.....	37
2.2.1 Specimen Groups.....	37
2.2.2 Compounding by Twin Screw Extruder.....	39
2.2.3 Shaping by Injection and Compression Molding.....	40
(i) Drying.....	40
(ii) Shaping by Injection Molding.....	40
(iii) Shaping by Compression Molding.....	41
2.3 Characterization of the Specimens.....	43
2.3.1 Water Absorption Value.....	43
2.3.2 Melt Flow Index (MFI).....	44
2.3.3 Tensile Testing.....	44
2.3.4 Fiber Length Distribution.....	45
2.3.5 X-Ray Diffraction (XRD) Analysis.....	45
2.3.6 Scanning Electron Microscopy (SEM)	46
2.3.7 Transmission Electron Microscopy (TEM)	46
2.3.8 Attenuated Total Reflection Fourier Transform Infrared (ATR- FTIR) Spectroscopy.....	47
2.3.9 Thermogravimetric Analysis (TGA)	48
2.4. Flammability Tests of the Specimens.....	48
2.4.1 UL-94 Vertical Burning Test.....	48

2.4.2 Limiting Oxygen Index (LOI) Test.....	49
2.4.3 Mass Loss Calorimeter (MLC)	51
3. RESULTS AND DISCUSSION.....	53
3.1 Short Glass Fiber Reinforced/ Unreinforced PA6 and PA66 with Flame Retardants.....	53
3.1.1 Water Absorption Values.....	53
3.1.2 Mechanical Properties.....	56
3.1.3 Fiber Length Distributions.....	59
3.1.4 Fracture Surface Morphology.....	62
3.1.5 Thermogravimetry.....	67
3.1.6 Flammability and Fire Performance.....	71
(i) Flammability Tests: Limiting Oxygen Index (LOI) and UL-94 Vertical Burning Test.....	71
(ii) Fire Performance Assessment by Mass Loss Cone Calorimeter (MLC).....	75
3.1.7 Residue Characterization.....	81
3.2 Short Glass Fiber Reinforced PA6 with a Flame Retardant and Nanoclay.....	83
3.2.1 Melt Flow Index (MFI)	84
3.2.2 Mechanical Properties.....	85
3.2.3 Fiber Length Distribution.....	89
3.2.4 Fracture Surface Morphology.....	91
3.2.5 Nanoclay Dispersion.....	93
3.2.6 Thermogravimetry.....	97
3.2.7 Flammability and Fire Testing.....	101
(i) Flammability Tests: Limiting Oxygen Index (LOI) and UL-94 Vertical Burning.....	101

(ii) Fire Performance Assessment by Mass Loss Cone Calorimeter (MLC).....	103
3.2.8 Residue Characterization.....	113
(i) Morphology of the Char.....	113
(ii) Infrared Spectroscopy.....	115
4. CONCLUSIONS.....	119
REFERENCES.....	124
APPENDICES	
A. AN EXAMPLE OF THE CALCULATION OF LIMITING OXYGEN INDEX BY DIXON’S UP AND DOWN METHOD.....	131
B. AN EXAMPLE OF THE CALIBRATION OF THE MASS LOSS CONE CALORIMETER	134
C. REPRESENTATIVE STRESS-STRAIN CURVES FOR EACH SPECIMEN GROUPS.....	138

LIST OF TABLES

TABLES

Table 1.1 Requirements for the UL-94 Vertical Burning Test Ratings.....	19
Table 2.1 Flame Retardants Used in This Study.....	35
Table 2.2 Physical Properties of Cloisite 30B.....	37
Table 2.3 Compositions of the Specimens Studied in the First Group.....	38
Table 2.4 Compositions (wt%) of the Specimens Studied in the Second Group..	38
Table 2.5 Extrusions Parameters Used in the First Group.....	39
Table 2.6 Drying Conditions of the Materials.....	40
Table 2.7 Injection Molding Parameters Used in the First Group.....	41
Table 2.8 Injection Molding Parameters Used in the Second Group.....	41
Table 2.9 Compression Molding Parameters Used.....	42
Table 2.10 Tensile Test Specimen Dimensions.....	45
Table 3.1 Results of Thermogravimetric Analyses for PA6 and PA66 Based Specimens.....	70
Table 3.2 LOI and UL-94 Results of PA6 and PA66 Based Specimens.....	71
Table 3.3 Mass Loss Cone Calorimeter Results for PA6 and PA66 compounds..	77
Table 3.4 Results of the Thermogravimetric Analysis.....	97
Table 3.5 Results of the Flammability Tests.....	102
Table 3.6 Cone Calorimeter Results for Nanoclay and Glass Fiber Reinforced PA6.....	109
Table A.1 Values of k for calculating Limiting Oxygen Index.....	133
Table B.1 Calibration Data for Converting Cone Temperature to External Heat Flux.....	134
Table B.2 Calibration Data for Converting Thermopile Reading to Heat Release Rate.....	136

LIST OF FIGURES

FIGURES

Figure 1.1 Levels of Dispersion in Polymer/Clay Nanocomposites	8
Figure 1.2 Start of a Flame in Polymeric Materials.....	10
Figure 1.3 Physical and Chemical Processes During Burning of a Polymer.....	11
Figure 1.4 Schematic Representation of UL-94 Vertical Burning Test.....	20
Figure 1.5 Schematic Representation of Limiting Oxygen Index (LOI) Test Apparatus.....	21
Figure 1.6 Schematic Representation of Mass Loss Cone Calorimeter.....	23
Figure 1.7 Representative Heat Release Rate and Total Heat Evolved Curves...	24
Figure 2.1 Chemical Structure of the Organic Modifier of Cloisite 30B.....	37
Figure 2.2 Compression Molding Machine.....	43
Figure 2.3 Dog Bone Shaped Specimen for Tensile Testing.....	44
Figure 2.4 Ceast Flammability Meter UL-94 Test Device.....	49
Figure 2.5 Fire Testing Technology LOI Device.....	50
Figure 2.6 Fire Testing Technology Mass Loss Cone Calorimeter.....	51
Figure 3.1 Water Absorption Values of (a) PA6 Compounds and Composites (b) PA66 Compounds and Composites.....	55
Figure 3.2 Mechanical Properties of PA6 Based Specimens (a) Tensile Strength, (b) Elastic Modulus, (c) % Elongation at Yield for Unreinforced Specimens and % Elongation at Break for Fiber Reinforced Specimens.....	57
Figure 3.3 Mechanical Properties of PA66 Based Specimens (a) Tensile Strength, (b) Elastic Modulus, (c) % Elongation at Yield for Unreinforced Specimens and % Elongation at Break for Fiber Reinforced Specimens.....	58
Figure 3.4 Optical Micrographs of (a) PA6-GF and (b) PA66-GF-RP.....	59

Figure 3.5 Fiber Length Probability Density Functions and Corresponding Mean Fiber Lengths of PA6 Composites.....	60
Figure 3.6 Fiber Length Probability Density Functions and Corresponding Mean Fiber Lengths of PA66 Composites.....	61
Figure 3.7 SEM Micrographs of PA6-GF (a) General View; (b) Closer View...	63
Figure 3.8 SEM Micrographs of (a) PA6-MCA and (b) PA6-GF-Br/Sb.....	64
Figure 3.9 SEM micrographs of PA66-GF (a) General view, (b) Closer view...	65
Figure 3.10 SEM Micrographs of (a) PA66-GF-RP and (b) PA66-GF-Br/Sb....	66
Figure 3.11 (a) Thermogravimetric (TG) and (b) Differential Thermogravimetric (DTG) Curves of PA6 Based Specimens.....	68
Figure 3.12 (a) Thermogravimetric (TG) and (b) Differential Thermogravimetric (DTG) Curves of PA66 Based Specimens.....	69
Figure 3.13 (a) Heat Release Rate vs. Time, (b) Total Heat Evolved vs. Time, and (c) Mass Loss Rate vs. Time graphs for PA6 based specimens.....	78
Figure 3.14 (a) Heat Release Rate vs. Time, (b) Total Heat Evolved vs. Time, and (c) Mass Loss Rate vs. Time Graphs for PA66 Based Specimens.....	79
Figure 3.15 Appearances of the PA6 and PA66 Based Specimens after LOI Test.....	82
Figure 3.16 SEM Micrographs Taken from Chars of Flame Retarded Specimens (a) PA6-MCA, (b) PA6-GF-Br/Sb, (c) PA66-GF-Br/Sb, (d) PA66-GF-RP.....	83
Figure 3.17 Melt Flow Index Values for PA6 Based Specimens.....	84
Figure 3.18 Effect of Flame Retardant, Glass Fibers and Nanoclay on the Mechanical Properties of PA6: (a) Tensile Strength, (b) Young's Modulus and (c) Elongation at Break.....	87
Figure 3.19 Mechanical Properties of Flame Retarded PA6 Specimens with/without Nanoclay at Equal Total Additive Content: (a) Tensile Strength, (b) Young's Modulus and (c) Elongation at Break.....	88
Figure 3.20 Optical Micrograph of PA6/GF-OP15.....	89

Figure 3.21 Fiber Length Probability Density Functions and Corresponding Mean Fiber Lengths for Representative Composite Samples.....	90
Figure 3.22 Debonding at Flame Retardant/Polymer Interface as a Consequence of Poor Adhesion in PA6/OP.....	91
Figure 3.23 SEM Micrographs of (a) PA6/GF, (b) nPA6/GF, (c) PA6/GF-OP15, (d) nPA6/GF-OP15.....	92
Figure 3.24 TEM images of nPA6 Nanocomposite at (a) Low Magnification and (b) High Magnification.....	95
Figure 3.25 XRD Patterns after the First Extrusion of the Specimens (a) Nanoclay, (b) nPA6/GF, (c) nPA6/GF-OP15, (d) nPA6.....	96
Figure 3.26 XRD Patterns after the Second Extrusion of the Specimens (a) Nanoclay, (b) n-PA6, (c) n-PA6/GF, (d) n-PA6/GF-OP15, (e) n-PA6/GF-OP10, and (f) n-PA6/GF-OP5.....	96
Figure 3.27 (a) Thermogravimetric, and (b) Differential Thermogravimetric Curves of the Specimens Tested.....	98
Figure 3.28(a) Thermogravimetric, and (b) Differential Thermogravimetric Curves for the Evaluation of the Effects of Flame Retardant Content.....	99
Figure 3.29 Cone Calorimeter Data to Compare generally the Effects of Glass Fibers (GF), Organo-phosphorus Flame Retardant (OP) and Nanoclay (n),: (a) HRR, (b) THE and (c) MLR Curves.....	106
Figure 3.30 Cone Calorimeter Data to Compare the Effects of OP Content in the Glass Fiber Reinforced PA6.....	107
Figure 3.31 Cone Calorimeter Data to Compare the Effects of OP Content in the Glass Fiber and Nanoclay Reinforced PA6.....	108
Figure 3.32 Heat Release Rate Curves Showing the Synergistic Effect of Nanoclay with OP.....	110
Figure 3.33 Re-evaluation of Cone Calorimeter Data for Nanoclay Synergism;(a) Peak Heat Release Rate, (b) Total Heat Evolved, (c) Time to Ignition, and (d) Fire Growth Index. (Dashed lines indicate equal nominal filler contents, i.e. nanoclay + flame retardant)	111

Figure 3.34 Macroscopic Appearances of Char Residues after Cone Calorimetry (Full Upper Surfaces of 100x100 mm Specimens are Displayed): (a) n-PA6/GF, (b) PA6/GF-OP15, (c) n-PA6/GF-OP5, and (d) n-PA/GF-OP15	114
Figure 3.35 SEM Micrographs Displaying the Char Morphologies of (a) PA6/OP, (b) n-PA6/GF, (c) PA6/GF-OP15, and (d) n-PA6/GF-OP	115
Figure 3.36 ATR-FTIR Spectra of Combustion Residues from Specimens without Nanoclay: (a) PA6/GF, (b) PA6/OP, (c) PA6/GF-OP15	117
Figure 3.37 ATR-FTIR Spectra of Combustion Residues from Specimens with Nanoclay: (a) PA6/GF, (b) n-PA6/GF, and (c) n-PA6/GF-OP15	118
Figure B.1 Correlation of Thermopile Reading to Heat Release Rate for a neat PA6 specimen	137
Figure B.2 Correlation of Thermopile Reading to Heat Release Rate for a PA66-GF-Br/Sb specimen	137
Figure C.1 Representative Stress vs. Strain Curve for a PA6 specimen	138
Figure C.2 Representative Stress vs. Strain Curve for a PA6-MCA specimen	138
Figure C.3 Representative Stress vs. Strain Curve for a PA6-GF specimen	139
Figure C.4 Representative Stress vs. Strain Curve for a PA6-GF-Br/Sb specimen	139
Figure C.5 Representative Stress vs. Strain Curve for a PA66 specimen	139
Figure C.6 Representative Stress vs. Strain Curve for a PA66-GF specimen	140
Figure C.7 Representative Stress vs. Strain Curve for a PA66-GF-RP specimen	140
Figure C.8 Representative Stress vs. Strain Curve for a PA66-GF-Br/Sb specimen	140
Figure C.9 Representative Stress vs. Strain Curve for a PA6 specimen	141
Figure C.10 Representative Stress vs. Strain Curve for a PA6/OP specimen	141
Figure C.11 Representative Stress vs. Strain Curve for a PA6/GF specimen	142
Figure C.12 Representative Stress vs. Strain Curve for a PA6/GF-OP20 specimen	142

Figure C.13 Representative Stress vs. Strain Curve for a PA6/GF-OP15 specimen	142
Figure C.14 Representative Stress vs. Strain Curve for a PA6/GF-OP10 specimen	143
Figure C.15 Representative Stress vs. Strain Curve for an <i>n</i> PA6 specimen	143
Figure C.16 Representative Stress vs. Strain Curve for an <i>n</i> PA6/GF specimen .	143
Figure C.17 Representative Stress vs. Strain Curve for an <i>n</i> PA6/GF-OP15 specimen	144
Figure C.18 Representative Stress vs. Strain Curve for an <i>n</i> PA6/GF-OP10 specimen	144
Figure C.19 Representative Stress vs. Strain Curve for an <i>n</i> PA6/GF-OP5 specimen	144
Figure C.19 Representative Stress vs. Strain Curve for an <i>n</i> PA6/GF-OP5 specimen	144

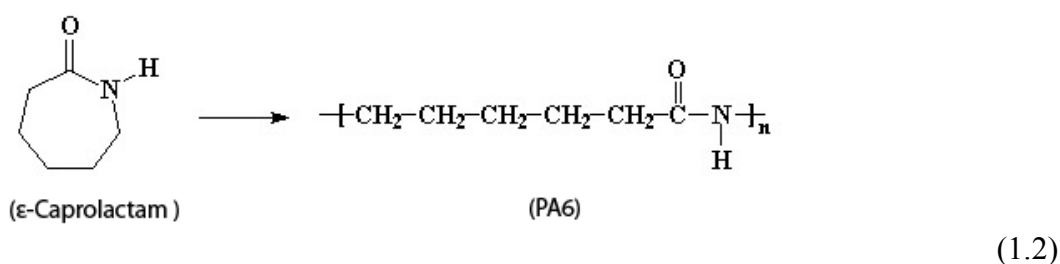
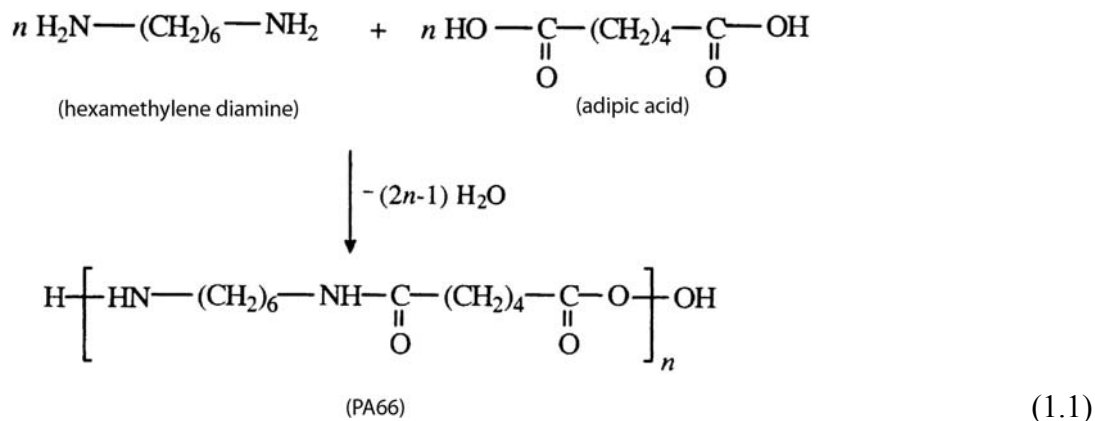
CHAPTER 1

INTRODUCTION

1.1 Polyamides

Polyamides are a class of polymeric materials which contain regularly spaced amide linkages (-CONH-) in their backbones. They are also known as nylons from the trade name of DuPont. Nylon history began in 1938 when Wallace Carothers and his research team at DuPont succeeded to synthesize a fiber which can replace some abundantly used natural fibers; such as silk. That synthetic fiber named as Nylon 66 (PA66), was the product of the condensation polymerization of hexamethylene diamine and adipic acid. In order to take a position in this new field of manufacture, Paul Schlack at I. G. Farbenindustrie in 1938, developed another new polymer having similar properties with Nylon 66, named Nylon 6 (PA6), which was synthesized from the ring opening polymerization reaction of ϵ -Caprolactam [1].

Polyamides have been conventionally accompanied by some digits indicating the number of carbon atoms in the structural unit. The first digit shows the carbon atoms of the diamine, the second those of the dicarboxylic acid. The nylon invented by Carothers is known as nylon 66 or polyamide 66, or poly(hexamethylneadipamide), which means that it is composed of two structural units, each with six carbon atoms, namely the residues of hexamethylene diamine ($\text{H}_2\text{N}(\text{CH}_2)_6\text{NH}_2$) and adipic acid ($\text{HOOC}(\text{CH}_2)_4\text{COOH}$). Nylon 6 or poly (6-caprolactam), is composed of a single structural unit, namely the apparent residue of 6-aminocaproic acid ($\text{H}_2\text{N}(\text{CH}_2)_4\text{COOH}$). Synthesis reactions of PA66 and PA6 are given in below respectively.



First product from polyamides was the nylon bristled toothbrushes, then it became popular with women stockings, and in following years replaced silk in many applications. Today about 70% of the polyamides produced is used in fibers industry, whereas the remaining parts find many applications in automotive, electronics, construction and consumer goods industries. Approximately, 90% of all polyamides are PA6 and PA66, whereas other polyamides are preferred only for some special applications.

1.1.1 Industrial Scale Production of Polyamides

(i) Polyamide 66

PA66 is synthesized from the reaction of adipic acid and hexamethylenediamine. The diamine is usually stored at approximately 85% concentration in water. It is diluted to 50% final salt concentration before production. Then a slight excess of diacid is added to diamine solution and thoroughly dissolved and neutralized. This salt

solution is held under inert gas until it is sent to the polymerization process. The salt solution is concentrated to about 75% by boiling in an evaporator. After the salt is concentrated, it is fed into an autoclave, which is a large and stirred pressure vessel, where the polymerization takes place. The temperature of the autoclave is increased up to a value, corresponding to a pressure of 1.75 MPa. During this step most of the diamine and diacid reacts to form oligomers. Then, boiling mass is held at this temperature to reach the equilibrium for the molecular weight to increase. In the final step, the temperature is raised to 275°C while the pressure is held at 1 atm. The polymerization then approaches equilibrium.

Upon the polymerization is finished, the polymer is removed from the autoclave through a die which forms a series of continuous polymer strands. These are fed into a casting machine which cools and solidifies the polymer in water, cuts it into small pellets. The pellets are then dried and stored for further processing or sale [1].

(ii) Polyamide 6

PA6 is synthesized from the ring opening reaction of ϵ -Caprolactam via hydrolytic or anionic mechanisms. Mostly, hydrolytic process is preferred, in which controlling the process is easier. The polymerization process for polyamide-6 via the hydrolytic mechanism can be batch or continuous.

In batch process, the caprolactam, which is a molten liquid, is mixed with the desired processing additives, and then charged to an autoclave. During the two-stage polymerization cycle, the temperature is raised from 80 to 260°C. In the first stage, water is held in the reactor, the pressure rises, and the hydrolysis and addition steps occur. After a predetermined time the pressure is released and the final condensation reaction step occurs. The final polymer is then drained through a die to form ribbons of polymer, which are then cooled in water and cut into pellets. The difference of the continuous process is that; it takes place in a series of connected vessels or in a single long, vertical, tubular reactor [1].

1.1.2 Properties of Polyamides

Polyamides are semi-crystalline materials. The crystalline regions contribute to the stiffness, strength, chemical resistance, creep resistance, temperature stability, and electrical properties; whereas amorphous areas contribute to the impact resistance and high elongation at break. However, they are notch sensitive; thus their impact strength decreases drastically when notched.

Strong hydrogen bonds are present between carbonyl and NH groups; favoring strong intra- and inter-chain segmental association and high crystallinity due to their polar amide groups. Polyamides have rather higher melting points as a result of both strong hydrogen bonds between their chains and higher crystallinity levels.

Absorption of significant amounts of water is another characteristic property of polyamides. Water molecules can easily coordinate around polar amide groups. Water absorption interrupts the hydrogen bonding, making it more flexible and increase the impact strength.

Polyamides tend to be particularly resistant to non-polar solvents such as hydrocarbons. However some strong acids and phenols may disrupt the hydrogen bonding and dissolve the polyamides. They are known to be soluble in formic acid, chloral hydrate, pyridine, m-cresol, dimethyl sulfoxide, and hexamethyl phosphoric triamide.

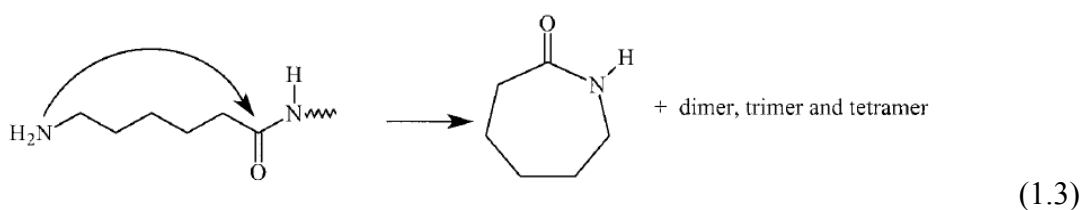
Polyamides are a class of materials that are easily ignitable: They are said to be self extinguishing; however, their flammability performance is far from passing in certain flammability tests.

Moreover, they are good electrical insulators at low temperatures and low humidity. Polyamides also show particular advantages in abrasion resistance and coefficient of friction over most of the polymers.

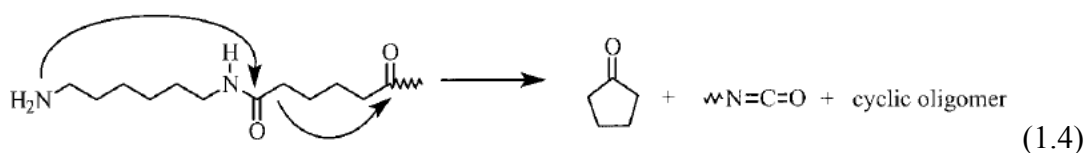
1.1.3 Thermal Degradation of Polyamides

Polyamides are preferred for many applications due to their good thermal stability. However, when kept at elevated temperatures for long time, they tend to degrade. Degradation negatively affects the physical and mechanical properties and causes some difficulties in processing. The chemical changes during the degradation of polyamides are cross-linking, formation of aromatic conjugated material and finally formation of involatile black char.

It is reported that main degradation product of Polyamide 6 is ϵ -caprolactam, where the other products at trace amounts are cyclic oligomers and acrylonitrile [2,3]. The formation of caprolactam is achieved by the cleavage of relatively weak N-H bond followed by cyclization. Predominant degradation reaction for PA6 is intermolecular end biting reaction shown below [2].



In polyamide 66, the main degradation product is cyclopentanone, which is formed by cleavage of two N-H bonds to give a diradical and two carbonyl esters, whereas isocyanate and some cyclic oligomers are also detected. Main degradation mechanism for PA66 is intermolecular end biting and shown in Reaction 1.4 [2].



During degradation of polyamides; crystallinity decreases with the formation of cross links which leads to the formation of the conjugated aromatic structure.

Discoloration to yellow-brown indicates the formation of the conjugated structure. Finally, an insoluble gel fraction remains.

It is stated by Holland et al. [2,4] that the amount of char remained decreases at high temperatures noting that the char yield of PA66 is greater than that of PA6 at any temperature because PA66 has higher extend of hydrogen bonding remained at elevated temperatures compared to PA6. The reason behind the increased amount of residue when degraded at low temperatures is the favor of cross linking to cleavage of C-H or N-H bond loss, due to the lowest activation energy of cross linking in these three processes.

1.2 Polyamide Composites

1.2.1 Polyamide/Short Glass Fiber Composites

Reinforcing the thermoplastic materials with short glass fiber increases both strength and stiffness of the composite as a function of the fraction of the fibers, their length and their orientation [5]. These composites have the potential to integrate the easy processing solutions available for short fiber reinforced composites with the high mechanical performance of continuous fiber reinforced composites. Short glass fiber reinforced composites have found extensive applications in automobiles, business machines, durable consumer items, sporting goods and electrical products owing to their low cost, easy processing and superior mechanical properties over the parent polymers.

Despite the good electrical strength and ductility of polyamides, for applications requiring higher strength and modulus, better dimensional stability and lower water absorption, they require to be reinforced. Short glass fibers are the commonly used reinforcing fillers for polyamides since they are economical, readily available and easily processed.

According to the material data sheets of DuPont [6], 20 wt% glass fiber reinforcement in PA66 matrix increases tensile strength from 60 MPa to 120 MPa and Young's modulus from 2.2 GPa to 6.4 GPa. Significant increase is also observed in heat deflection temperature (HDT at 0.45 MPa) reaching to 237°C from 117°C. Elongation at break value on the other hand is decreased to 3.9% from 160%.

1.2.2 Polyamide/Clay Nanocomposites

Recent developments in the chemistry of nanoclays, led up to their use as fillers in polymer materials to enhance physical and mechanical properties. These nanocomposites, when compared with conventional composites, exhibit lower permeability, higher optical transparency, lower density, enhanced thermal and mechanical properties in addition to reduced flammability, at just a little loading levels (1-10 wt%). The fineness of the reinforcement and the nanoscale interaction between the matrix and the reinforcement at the nanoscale contribute to the refinement of the properties.

Extend of the property enhancement mainly depends on many factors such as: degree of dispersion, aspect ratio of the fillers, orientation in the matrix and the interfacial strength between the matrix and the filler [7]. Degree of dispersion of nanoclays is referred in three groups as shown in Figure 1.1: Unmixed (also referred as microcomposite or tactoids), intercalated and exfoliated (delaminated). If the nanoclays are unmixed; a phase separated composite is obtained which shows the similar properties like conventional composites. In the intercalated case, polymer chains interpenetrate stacked silicate layers with small separation distances (few nanometers) between the layers. In the exfoliated or delaminated morphology, the silicate layers are well dispersed within the polymer matrix.

Layered silicates such as montmorillonite have received a great deal of attention as reinforcing materials for polymers due to their high aspect ratio and unique intercalation / exfoliation characteristics. Generally, inorganic materials have poor dispersion and weak interfacial strength in polymer matrices; therefore their surfaces

are organically modified to increase compatibility with the polymer matrix. To make a better interaction with the organic polymers: the cations (typically sodium) on the surface of the montmorillonite to balance the negative charge of aluminum/magnesium silicate layer are exchanged with organic molecules with a cation group such as alkyl ammonium ions. Final product of this ion exchange reaction is also referred as organoclays.

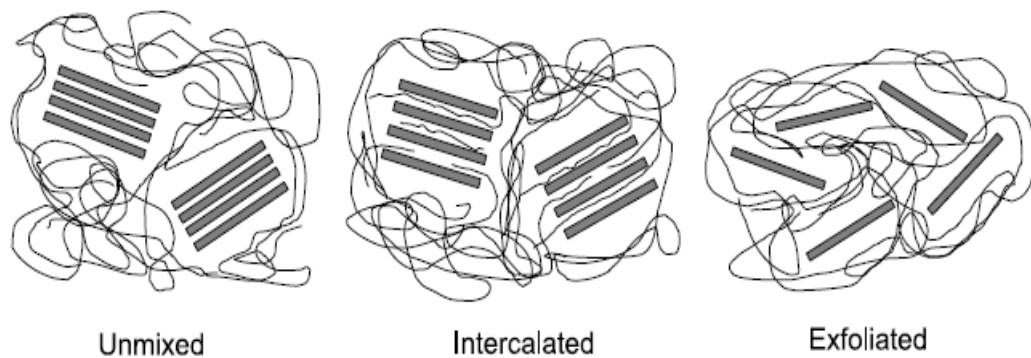


Figure 1.1 Levels of Dispersion in Polymer/Clay Nanocomposites

Studies on the incorporation of organoclays to polymers date back to 1950's [8,9]. In 1976, Fujiwara and Sakomoto [10] of the Unichika Co. described the first organoclay hybrid polyamide nanocomposite. One decade later, a research team from Toyota disclosed improved methods for producing PA6 – clay nanocomposites using in situ polymerization similar to Unichika process [11]. Toyota demonstrated a 70% increase in room temperature tensile modulus, an 87°C increase in heat distortion temperature and a significant decrease in water permeability of the nanocomposite.

More recently, Cho et al. [7] investigated the mechanical properties and morphology of PA6 nanoclay composites processed with different equipments and at different conditions. They concluded that; in nanocomposites compounded by twin screw extruder, strength and modulus were substantially increased with respect to neat

nylon while toughness or impact strength is not altered significantly. Moreover, nanocomposites showed superior increase in modulus without decreasing the elongation at break too much, compared to conventional composites.

1.3 Flammability of Polymers

Flammability is referred to the ease of ignition and rapidness of burning for a material. Polymeric materials, in general, are flammable as a consequence of their hydrocarbon backbones. 95% of commodity polymers continue to burn after exposure to a small flame, where as only 5% of engineering polymers have enhanced flammability characteristics [12].

However, current regulations limit usage of some plastic materials which are below a certain flammability rating for using in consumer electronics, electrical equipment, building and construction, home furnishings, automobiles, and public transportation. Therefore, the market for fire retarded polymers is continuously growing.

1.3.1 Flaming of Polymers

(i) General Burning Behavior of Polymers

There are three ingredients that cause the flame. The combustion takes place only, when all three of the combustible material, oxidizing agent and ignition source are present. For polymeric materials; fuel is the combustible volatiles produced from breaking of the chemical bond upon exposure to a heat source, which is also the ignition source. These volatiles react with the oxygen in the air and a fire starts. Large amount of heat is emitted during the combustion and some part of it is fed to the burning polymer. This process is illustrated in Figure 1.2.

After the ignition of polymeric materials, several chemical and physical processes take place in three separate phases: gas, mesophase and condensed phase. The mesophase is the interface between the condensed and gas phases during burning of a

polymer. Figure 1.3 shows the chemical and physical processes happening in this three phases. The physical processes during the combustion are; (1) heat transfer by radiation and convection between gas phase and mesophase, (2) energy loss from the mesophase by conduction to solid and vaporization of pyrolysis gases. The chemical processes, on the other hand are (1) thermal degradation of the polymer in the mesophase, (2) mixing of combustible volatiles with air, and (3) combustion of air-fuel mixture producing radiant heat.

Flames of the polymers are hydrocarbon flames comprising of mainly $H\cdot$, $O\cdot$ and $OH\cdot$ radicals. Besides these radicals, $H_2O\cdot$, $HCO\cdot$ and $CH_3\cdot$ can be observed in trace amounts. Chain branching reactions during combustion accelerate the burning process, since more radicals are formed as a result of these reactions

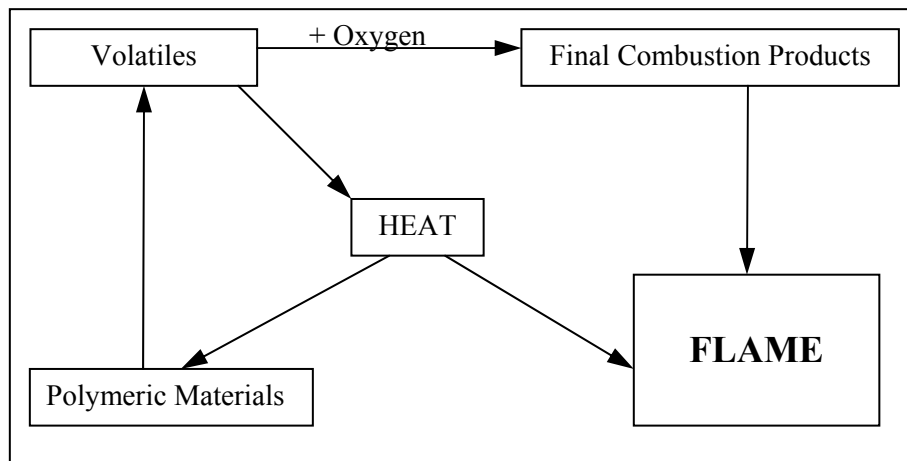


Figure 1.2 Start of a Flame in Polymeric Materials [13]

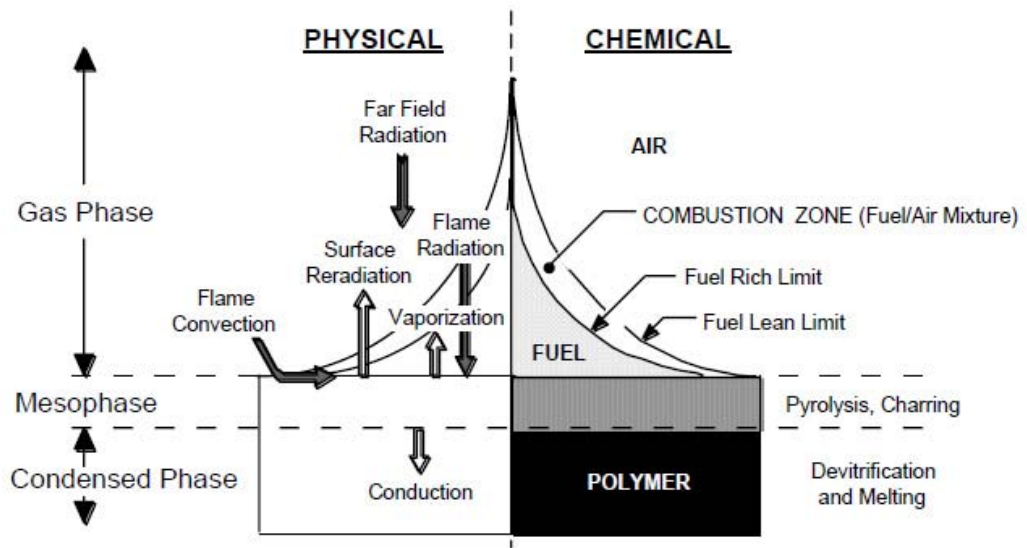


Figure 1.3 Physical and Chemical Processes During Burning of a Polymer [12]

(ii) Burning Behavior of Polyamides

Polyamides are relatively easily ignitable. Self ignition temperature of polyamides upon exposure to preheated air in thermogravimetric analyzer is determined. For PA66 it was found that the ignition temperature at a heating rate of 20°C /min is 370°C whereas at a heating rate of 100°C /min it is 405°C. For PA6, ignition temperature decreased from 530°C to 470°C with the increase of heating rate from 2°C /s to 50°C/s as a result of the severe bubbling of the polymer [14].

Polyamides, burn with a stable yellow flame; having a pool of the melt located above the burning sample. Low molecular weight samples drip away from the flaming zone due to their very low melt viscosities.

Polyamides produce very little vision obscuring smoke during combustion. The smoke is formed from the incomplete oxidation of the thermal degradation products. The smoke is very corrosive and has a basic character. It is mainly composed of CO₂, H₂O, NH₃, NO_x, CO, HCN; from which CO and HCN are the primary toxic constituents of the smoke of polyamide combustion.

1.3.2 Flame Retardants and Flame Retardancy Mechanisms

According to a commonly accepted definition: a “flame retardant” is a material which resists burning when exposed to low energy flame source, while a “fire retardant” is a material which resists burning when exposed to a very energetic flame, as in the case of real fires [15]. Since the flammability measurements carried throughout in this study could not simulate the real fire scenarios; the term “flame retardant” is preferred for the additives which improve flammability performance of the polymers.

A material which inhibits or suppresses the flaming process is said to be flame retardant. Many chemicals interfere with combustion during heating, ignition, decomposition or flame spread. These chemicals act physically or chemically in condensed or gas phase. In general, they do not have a single mechanism action and may act in more than one phase.

(i) Physical Action of Flame Retardancy

Some additives form a protective layer with low thermal conductivity in the condensed phase, which reduces the heat transfer to the material from external heat sources. As a result, degradation and fuel production at the flaming zone is decreased. Boric acid derivatives and borates are known to act in this manner. They produce a vitreous protective layer, restricting the diffusion and heat transfer [16]. A similar mechanism is observed in silicon containing flame retardants [17].

Upon thermal degradation of some flame retardants release water in the gas phase. These flame retardants degrade endothermically, cooling the specimen below a temperature suitable to sustain the flaming. Inorganic hydroxides such as; aluminum trihydrate and magnesium hydrate are the most common flame retardants acting accordingly. However, very high amounts of additive should be incorporated to the polymer to obtain acceptable flame retardancy [18,19].

The water release in the vapor phase by inorganic hydroxides may also be given as an example for another main flame retardancy mechanism; dilution of the gas phase. According to this mechanism, degradation products of some flame retardants release incombustible gases like H₂O, CO₂ and NH₃ in the vapor phase lowering the partial pressures of the combustible gases and the oxygen. Therefore, they slow down the reaction rate.

Some incombustible materials dilute the fuel by lowering its combustible portion. Therefore, total heat evolved during burning can be decreased. Talc and calcium carbonate are examples of this kind of additives [20].

(ii) Chemical Action of Flame Retardancy

Some flame retardant additives catalyze the degradation of the polymer, leading to a decrease in molecular weight and the viscosity of the polymer which leads to flowing away of the molten polymer from the flaming zone. Melamine cyanurate, is mainly known to be a flame retardant increasing the dripping away of the burning polymer [21].

Upon heating, some flame retardants may react with the polymer forming double bonds. They form carbonaceous layer via cyclizing and cross-linking reactions. This char layer limits the mass and heat transfer from the polymer to the flame. Phosphorous compounds thermally decompose into phosphoric acid causing the extraction of water in the condensed phase from the pyrolyzing substrate, causing it to char. Besides this main flame retardancy mechanism of phosphorous compounds they also act in vapor phase diluting the combustible gases and scavenging the free radicals [22].

The combustion processes may be interrupted in the gas phase by the degradation products of some flame retardants. In general, the flame retardancy is achieved by the trapping of radicals interrupting the exothermic combustion process. The most important example of radical trapping is in halogenated flame retardants. Very energetic H•, O• and OH• radicals react with the degradation products of the

halogenated flame retardants forming less energetic halogen radicals ($X\bullet$) and inactive molecules [23].

(iii) Flame Retardancy of Nanoclays

During combustion, delaminated structure of nanoclays collapses and clay layers rises above to the surface of the polymer. This forms a protective barrier composed of accumulated clay layers and a small amount of carbonaceous char, acting as a thermal insulator and slowing down the diffusion of volatile degradation products to the flame.

The accumulation of clay particles on the surface of the sample is achieved in two ways. First, recession of polymer from the surface by pyrolysis leaves clay particles behind. Clay particles tend to stick each other since their organic modifier is degraded and they are not compatible with polymer resin. Second, clay particles are moved from the interior of the polymer sample to the surface as a result of rising bubbles of the degradation products of the polymer by convection [24].

Gilman et al. [25] reported on the presence of nanodispersed montmorillonite clay in polyamide 6 produces a substantial improvement in fire performance at loadings as low as 3–5%. In fact, the improvement can be as high as 60% decrease in PHRR. The proposed mechanism is that the formation of a char layer which lacks major cracks covering the surface of the specimen and accordingly restricting the heat and mass transfer to and from the sample. Flame retardancy of polyamide nanocomposites is investigated by various researchers [24,26-28], concluding that the flame retardancy effect is independent of the nano-dispersion level [29] and for improved flame retardancy performance they should not be used alone but in combination with conventional flame retardants [30,31].

1.3.3 Using Flame Retardants Together

If the flame retardancy effect of two additives used in combination is greater than the sum of the effects of them when used individually, these additives are said to

“*synergist*” with respect to flame retardancy. In general, when a synergist flame retardant additive is introduced to an already flame retarded composition, either the degradation pathway is altered or the barrier effect is enhanced [13].

On the other hand, two flame retardants each having a positive effect if used separately, when used in combination may be less effective than the either one used alone in the same concentration. In other words, the observed effect in flame retardancy is less than the computed additive effect. These flame retardants are said to be “*antagonist*” or “*anti-synergist*” [13]. Anti-synergism may be observed in flame retarded samples where one additive enhances dripping while other restricts it by charring.

(i) Halogen-Antimony Synergism

In most cases, halogenated flame retardants are used in combination with antimony trioxide, the most common form of antimony, for improving the flammability performance. This also optimizes the cost.

During combustion, halogen additives and antimony trioxide interact to form antimony trihalides. Antimony trihalides are volatile flame poisons scavenging H•, O• and OH• radicals. They give metal oxides in the flame by the elimination of hydrogen halides. Moreover, antimony halides act in the condensed phase catalyzing the charring. The cross-linking enhanced by these molecules leads to the formation of a barrier, restricting the melt flow and delaying the evolution of the flammable gases.

It is stated by Zhang et al. [32] that; about 40 wt% of chlorine containing or 20 wt% of bromine containing flame retardant should be added to polyolefins to achieve a reasonable level of flame retardancy, but by introducing the antimony trioxide this amount can be decreased significantly.

In the study of Galip et al. [15], addition of 2 wt% antimony trioxide to flame retarded polyester containing 2 wt% decabromodiphenyloxide (DBDPO) increased

the LOI value from 18.5% to 20.6%. It is observed that incorporation of antimony trioxide to the flame retarded system gave better results than the use of either DBDPO or antimony trioxide alone in the same total concentration.

(ii) Phosphorus-Phosphorus (P-P) and Nitrogen-Phosphorous (N-P) Synergism

Previous studies revealed that phosphorous containing flame retardants have more than one mechanism of action. Therefore, two or three phosphorous containing species may be used in combination for improved flammability performance. In these cases, often one additive is char former and the second is the catalyst and blowing agent. A third phosphorus compound, possibly having a vapor phase action, may also be incorporated to system.

In most cases, the synergy between phosphorus containing additives is accompanied by nitrogen-phosphorus synergy. In these cases, nitrogen compounds extend the decomposition temperature range of the polymer, reducing the production of the combustible volatiles. Also the release of inflammable ammonia gas dilutes the fuel. In the condensed phase, nitrogen compounds aid the retention of phosphorus compounds in the char, thus making it more stable. This is very advantageous in charrable polymers; however, in less charrable polymers it may not be useful due the decreased vapor phase activity [13].

A typical example can be given by the combination of: pentaerythritol as char former, ammonium polyphosphate as the catalyst and melamine as the blowing agent [33].

(iii) Zinc Borate as a Synergist

Despite the limited usage of zinc borate (ZB) alone, as a flame retardant, it shows some synergistic effects in flame retarded composites. Most of the commercial zinc borates are hydrates. Therefore, they release water endothermically upon heating. It also forms a glassy protective layer over the burning surface restricting the diffusion of gases and the transfer of heat. Moreover, it was proved that zinc borate in a polymer promotes the formation of char.

Cartentier et al. [34] studied the EVA composites with magnesium hydroxide and zinc borate where synergist effects of zinc borate are clearly illustrated. Samyn et al. [35] investigated zinc borate system with ammonium polyphosphate (APP) concluding that formation of borophosphates and zinc phosphates which stabilize phosphorous species in the char increases the effect of the physical barrier.

(iv) A Commercial Example of Synergism

About 30 years ago, various metal salts of dialkylphosphinates were prepared and tested for their flame retardancy efficiency. It is observed that, addition of 20 wt% aluminum (Al) or calcium (Ca) salts of ethylmethylphosphinic acid are effective flame retardant additives granting a UL-94 V-0 rating for non-reinforced polyamides. On the other hand, for glass fiber filled polyamides 30 wt% addition was required for a V-0 rating [36].

Later Clariant Inc. found that it is easier to manufacture diethylphosphinate salts and commercialized the Al salt as Exolit® OP 930. The effectiveness of dialkylphosphinic acid salts did not meet the criteria for the flame retardancy of polyamides. However, they were found synergistic with some nitrogen-containing products like melamine cyanurate, melamine phosphate, or melamine polyphosphate. Upon this discovery, Clariant commercialized two new flame retardants Exolit® OP 1311 and OP 1312; containing aluminum phosphinate in combination with melamine polyphosphate and zinc borate. OP 1312 also contains a stabilizer which makes it suitable for PA66, which is processed at higher temperatures.

1.3.4 Fire and Flammability Tests

In order to quantify the fire performance of plastic materials many tests are standardized for various specific fire scenarios. These tests can be divided into two groups as specific tests for the end products and general laboratory scale tests. Most common lab scale tests include two small scale flammability tests: UL-94, LOI and a bench scale fire test MLC.

These tests are insufficient to evaluate the burning behavior and should not be used for regulations relating to safety control and consumer protection. They only provide a sensitive measure of burning materials under controlled laboratory conditions.

(i) UL-94 Tests

UL-94 Tests for Flammability of Plastic Materials for Parts in Devices and Appliances, a standard developed by Underwriters Laboratories (USA), is one of the simplest and most widely used flammability test method employed in plastic industry in order to determine the acceptability of a plastic material in means of flammability.

Most common configuration for the UL-94 test is “vertical burning”, where the specimen is suspended vertically. Standard bar specimens are to be 125 ± 5 mm long by 13.0 ± 0.5 mm wide, and specimen thickness is 1.3 mm or 3.2 mm. However, the test results are dependent extensively on sample thickness. Generally, thinner specimens burn more rapidly. Therefore, sample thickness should be stated in the UL-94 ratings.

A schematic representation of the UL-94 Vertical Burning is given in Figure 1.6. Here, the specimen is subjected to a calibrated methane flame, and there is a piece of surgical cotton below the specimen. Flame is introduced to the sample for 10 seconds and its extinguishment time (afterflame time, t_1) is recorded. This procedure is repeated once more after the ceasing of the first flame. Then, second afterflame time (t_2) and afterglow time (the time required for the fire glow to disappear, t_3) is recorded. During the application of the flame, the distance between burner and specimen must remain constant. If drops fall, the burner must be tilted through a maximum angle of 45° or slightly isolated from the specimen flame. This test should be carried on 5 individual specimens. There are four ratings in the UL-94 vertical burning test and they are summarized in Table 1.1.

Table 1.1 Requirements for the UL-94 Vertical Burning Test Ratings

Criteria	Ratings			
	V-0	V-1	V-2	Fail
Afterflame time of each individual specimen (t_1 or t_2) in seconds	≤ 10	≤ 30	≤ 30	> 30
Total afterflame time for 5 specimens ($t_1 + t_2$) in seconds	≤ 50	≤ 250	≤ 250	
Afterflame plus afterglow time for each individual specimen after the second flame application ($t_2 + t_3$)	≤ 30	≤ 60	≤ 60	
Afterflame or afterglow of any specimen up to the holding clamp	No	No	No	
Cotton indicator ignited by flaming particle or drops	No	No	Yes	

To sum up, UL-94 vertical burning test is a non ventilated test measuring the material response to a removed fire threat and its time to self-extinction. Materials taking V-0 ratings from UL-94 are said to be self-extinguishing.

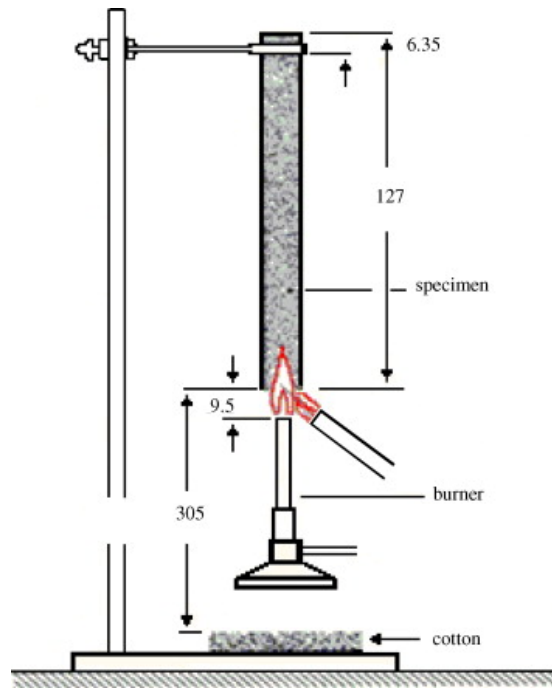


Figure 1.4 Schematic Representation of UL-94 Vertical Burning Test [37]

(ii) Limiting Oxygen Index Test (LOI)

Limiting Oxygen Index Test (LOI) is first described by Fenimore and Martin [38] in 1966 and now subjected to the international standard ISO 4589 *Determination of burning behavior by oxygen index*. It is one of the most important flammability tests used for screening and quality control, by industry and academic researchers.

Bar shaped specimen oriented vertically inside a glass chimney is ignited by a propane flame from the top. Then, minimum oxygen concentration in a mixture of oxygen/nitrogen flowing through a glass chimney at ambient temperature which will sustain the burning of the specimen for 3 minutes or consume a length of 5 cm of the sample is determined by varying the oxygen concentration, and named as the Limiting Oxygen Index value. A schematic representation of the test apparatus is given in Figure 1.5.

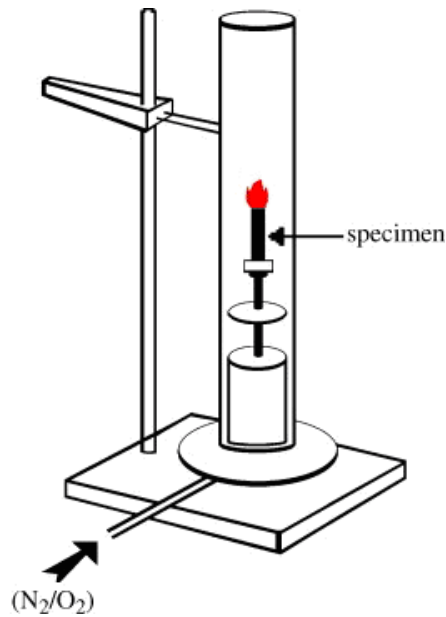


Figure 1.5 Schematic Representation of Limiting Oxygen Index (LOI) Test Apparatus [37]

As air contains 21% oxygen, materials with a LOI value below 21% may be classified as “*combustible*” whereas those with a LOI above 21% may be classified as “*self-extinguishing*”, since their combustion can not be sustained at ambient temperature without an external energy contribution. Higher LOI values indicate better flame retardancy. However, this “*self-extinguishing*” property should not be taken as a strict indication for the real fire cases, since materials with high LOI values at room temperature may burn without extinguishing under intense fire conditions. It should be noted that the test is carried out at ambient temperature and the obtained values are very sensitive to the temperature.

Depending on the burning characteristics, sample thickness may or may not affect the LOI value. For dripping samples, LOI value changes significantly with the sample thickness, thinner materials dripping more and having lower LOI values, whereas for charring and non-dripping materials it is not altered much. Moreover for dripping polymers, it should also be taken into account that, dripping can extinguish the flame and lower than actual values of LOI, can be recorded.

(iii) Mass Loss Cone Calorimeter (MLC)

Today, heat release rate calorimetry is accepted as the most scientific way for the flame retardancy measurements. The instrument used for this method is named as the “Cone Calorimeter” due to the conic shape of its heaters. Generally, cone calorimeter uses oxygen consumption principle for the measurement. This principle states that there is a direct relationship between the mass of oxygen consumed from the air and the amount of the heat released. The corresponding standard for heat release measurements by cone calorimeter is ISO 5660 *Reaction to fire tests: Heat release, smoke production and mass loss rate*.

However, the instrument used in this study, named Mass Loss Cone Calorimeter (MLC), employs a different principle than the oxygen consumption principle of cone calorimeters. In MLC, heat release is determined from the outputs of the thermopiles located in the chimney above the burning specimen which is subjected to a specified radiant heat flux from the cone heaters. The output from the thermopiles, which in the unit of millivolts (mV), is converted to the heat release rate, in the units of kW/m², by using the calibration graph which is obtained by burning propane with a known calorific value, in the same apparatus. Besides this, the mass of the specimen is continuously recorded by the load cell. A schematic drawing of the mass loss calorimeter is shown in Figure 1.6 and the corresponding standard for measuring the heat release rate by this method is ISO 13927 *Simple heat release test using a conical radiant heater and a thermopile detector*.

A rigid specimen with a smooth surface, having the dimensions of 100x100x4 mm is placed in the sample holder above the load cell in order to measure the evaluation of mass loss during the experiment. Conic Heaters, set to the corresponding temperature for the preferred external heat flux, continuously radiates the sample from above. The combustion is triggered by an electric spark.

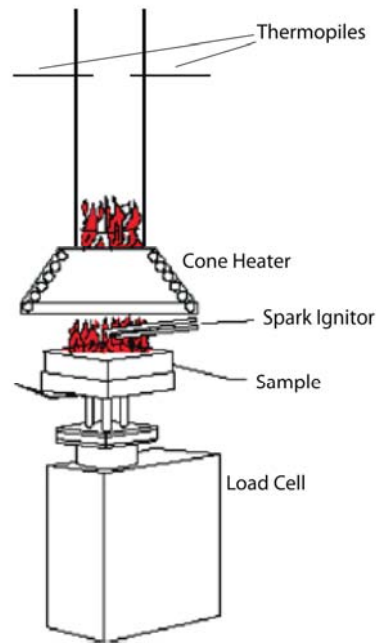


Figure 1.6 Schematic Representation of Mass Loss Cone Calorimeter [37]

Representative *Heat Release Rate versus Time* and *Total Heat Evolved (THE) versus Time* graphs for a neat and flame retarded polymer is shown in Figure 1.7. The maximum value of the heat release rate curve, the “peak heat release rate” (PHRR) is an important property to quantify the fire performance of the polymers. PHRR is the maximum energy emitted during burning and it corresponds to the flashover of the flame. Generally, effectiveness of a flame retardant is given as the percentage reduction in PHRR value compared to that of neat polymer. As seen in Figure 1.7 neat polymers have sharp heat release rate curves with higher PHRR values while the flame retarded polymers have broad curves with smaller peak values.

By integrating the heat release rate versus time curve “total heat evolved during combustion” (THE) is determined. THE value is the total fire load of the specimen during cone calorimeter scenario therefore, it is as important as the PHRR in assessing the fire hazard. Significant reductions in THE values are observed in Figure 1.7 upon addition of a flame retardant.

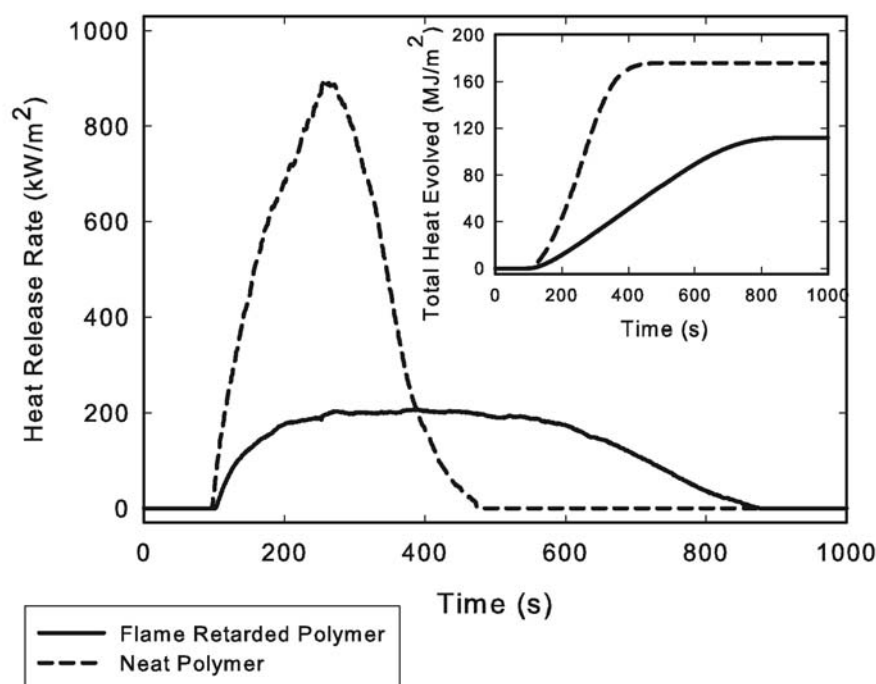


Figure 1.7 Representative Heat Release Rate and Total Heat Evolved Curves

Total mass loss (TML), time to ignition (TTI) and total time of burning (TTB) are also recorded. Total Mass Loss (TML) is the difference of the initial and final weights of the test specimen. Time to Ignition (TTI) is the time between introduction of the spark and ignition, which shows the ease of ignitability of the specimen. Total Burning Time (TBT) is the time between ignition and extinguishment of flame. Generally, flame retardants with condensed phase mechanism increase Total Time of Burning (TBT) while flame retardants with gas phase mechanism decrease it.

Fire Growth Index (FGI) is determined by dividing PHHR with TTI as proposed by Petrella [39]. FGI value addresses the flame spread. Another important data about the flame retardancy mechanism of additives can be obtained by dividing total heat release rate to total mass loss (THE/TML Ratio). If THE/TML Ratio of flame retarded composition greatly differs from that of pure one it is stated that the flame retardant has a gas phase action.

1.4 Previous Studies

1.4.1 Previous Studies on the Flammability of Polyamides Using Conventional Flame Retardants

(i) Brominated Flame Retardants

Brominated flame retardants are the class of additives which obtains the best ratings for flame retardancy in polyamides. Despite the lack of academic studies on this subject, there are several patents available on the use of brominated flame retardants for polyamides.

In the U.S. patent by Richardson [40] 22-25 wt% of brominated polystyrene in combination with 4-6 wt% antimony trioxide was sufficient to obtain a V-0 rating for PA6/PA66 copolymer. Yamakana et al. [41] granted a patent for the use of brominated tetra-acetyl aromatic diamines in PA6 at a concentration of 5 wt%, which increased the LOI value to 28-31%. In the patent of Kahan [42] immediate extinguishment is observed in PA6 / PA66 copolymer filled with 25 wt% glass fiber and containing 13.4 wt% decabromodiphenyl ether, 3.35 wt% antimony trioxide and 4 wt% low density polyethylene. Similarly in the patent of Tjahjadi [43] 8 wt% brominated epoxy with 3 wt% antimony trioxide in combination with 21 wt% talc and 4 wt% pyrophosphate gave a V-1 rating for 20 wt% glass fiber reinforced PA6. So in another patent by Williams [44] V-0 in glass filled PA66 is achieved by the use of 18-22 wt% brominated epoxy with 5-7 wt% antimony trioxide [44]. In the patent granted by Yaakov and Minke [45]; 12 wt% brominated epoxy with 4 wt% antimony trioxide increased the LOI of PA66 to 29% where the use of 15 wt% brominated epoxy with 5 wt% antimony trioxide helped PA6 to reach a LOI value of 28%.

(ii) Melamine Cyanurate

Melamine salts, such as melamine cyanurate, are effective flame retardants for polyamides. Melamine cyanurate and its degradation products are non-toxic. Moreover, small amounts are sufficient to achieve acceptable flame retardancy, which would conserve mechanical properties. Since melamine cyanurate works by

increasing the dripping of the polymer; it is not effective in composites where the dripping is constrained, such as glass fiber reinforced systems.

Condensed phase mechanism of melamine cyanurate in polyamides is stated by Casu et al. [21] observing that LOI value increases steadily by increasing the concentration of melamine cyanurate. They showed that an addition of 10 wt% melamine cyanurate to commercial PA6 / PA66 copolymer increased the LOI value to 32%, while decreasing the heat release rate and time to ignition in cone calorimeter. Levchik et al. [46] found that 10 wt% melamine cyanurate is enough to reach a V-0 rating and a LOI value of 35% for PA6. Gijsman et al. [47] concluded that effectiveness of melamine cyanurate is higher in PA66, where 5-10 wt% is sufficient for V-0 rating, compared to PA6 in which 8-15 wt% addition is required for V-0. This is due to the higher reactivity of cyclopentanone (primary degradation product of PA66) compared to caprolactam (primary degradation product of PA6) with melamine cyanurate and its degradation products at 350-450°C.

Lui et al. [48] used polyamide resin encapsulated melamine cyanurate/melamine phosphate (MCA/MP) composite flame retardant for glass fiber reinforced polyamides. They found that at a loading level of 20 wt% flame retardant, containing 25 wt% encapsulated resin with MCA to MP ratio of 4:1, V-0 rating is achieved without a significant loss in mechanical properties for glass fiber filled PA6. Lui et al. [49,50] also studied the microencapsulation of red phosphorous with melamine cyanurate for PA6 and PA66 concluding that condensed phase mechanism is enhanced with N-P synergism. Microencapsulated additives show improved flame retardancy and mechanical properties compared to conventional flame retardants.

(iii) Red Phosphorous

It is interesting that; a highly flammable material is used as one of the most effective flame retardants. Elemental phosphorus, in the dark-red color, is generally stored in the form of phenolic masterbatches to prevent the ignition.

Incorporation of these masterbatches to polyamides gives excellent flammability ratings at low filler contents. Davis et al. [51] stated that 6-8 wt% red phosphorous may lead to a V-0 rating with reduced dripping, and acceptable mechanical strength. Whereas, it is stated in the study of Levchik et al. [36] that for glass filled polyamides 8-12 wt% red phosphorous is required to obtain a V-0 rating. In the same study, 7 wt% red phosphorus, 5 wt% phenolic resin and 25 wt% glass fiber containing PA66 obtained the V-0 rating.

Jou et al. [52] studied the flame retardancy of glass fiber filled PA66 containing red phosphorous. They found that 6 wt% red phosphorous in 23 wt% glass filled PA6 is enough for V-0. Increasing the phosphorus content to 8 wt% causes the LOI to increase 30.5% from 28.6%. A further increase in the phosphorus content to 16 wt% has no significant effect on LOI. Moreover, they also observed that addition of red phosphorus decreases the time to ignition. After ignition has occurred, formation of stable char like residues retards the combustion. Schartel et al. [53] stated that the use of red phosphorus in PA6 results in an increased amount of residue and in a corresponding decrease in total heat release. They attribute this decrease to the dominant condensed phase mechanism of red phosphorus.

Levchik et al. [54] studied the flame retardancy of red phosphorus in PA6, improved by co-addition of ferric/ferrous oxides. They showed that PA6 gets a V-0 rating with an addition of 10 wt% red phosphorus and 5 wt% ferric oxide (Fe_2O_3). However at the same composition with ferrous oxide (Fe_3O_4) only a V-2 rating is possible. This is attributed to the catalytic activity of ferric oxide, having a larger active surface. Balanovic et al. [55] investigated the effects of red phosphorus, which had been intermolecularly cross-linked by radiation, on flame retardancy of PA66. They concluded that an improved flame resistance is achieved if red phosphorus is used at least 7 wt% in combination with 5 wt% triallyl cyanurate.

Disadvantages of red phosphorus as a fire retardant for polyamides are its red color and generation of toxic phosphine gas through reaction with water [14]. To decrease

phosphine evolution, a low concentration of potassium iodide (0.6 wt%) can be added to the red phosphorus masterbatches [56].

(iv) Organic Phosphorus Additives

Recent patents and technical works indicate a growing interest in halogen-free solutions with the predominance of the literature focusing on various phosphorus-based flame retardants.

In a recent study by Braun et al. [57] flame retardancy mechanism of aluminum diethylphosphinate, melamine polyphosphate and zinc borate used separately and in combination is investigated in glass fiber reinforced PA66. It has been reported that, aluminum diethylphosphinate mainly acts as a flame inhibitor; melamine polyphosphate dilutes the gaseous fuel besides the condensed phase barrier effect, where addition of zinc borate stabilizes the char barrier. Synergistic effects are clearly observed from LOI and Cone Calorimeter studies.

Liping et al. [58] used zinc-ion modified melamine polyphosphate as a new flame retardant for glass fiber filled PA66. They observed that in 25 wt% glass fiber containing PA66, 22 wt% zinc ion modified melamine polyphosphate achieves a V-0 rating and LOI value of 37.8%. At the same composition without the zinc ion modification, despite the LOI of 31.5%, only V-1 rating is obtained in UL-94 test.

The effect of melamine polyphosphate on thermal degradation of PA6 and PA66 is investigated by Jahromi et al.[59]. It is concluded that melamine polyphosphate is more effective in PA66 than PA6, due the higher cross-linking capability of PA66.

Chen et al. [60] synthesized a halogen free flame retardant from melamine and phosphoric acid and incorporated it to glass fiber reinforced PA6. It is observed that flame retardant shifts the degradation temperature to lower temperatures and increases charring. In 35 wt% glass fiber containing composition V-0 rating is granted by the addition of 25 wt% flame retardant.

It is proven by Wang et al. [61] that; with 30 wt% of melamine polyphosphate and 3 wt% of thermoplastic polyurethane encapsulated solid acid as a synergistic agent, the 30 wt% glass fiber reinforced PA6 can pass UL-94 V-0 rating.

1.4.2 Previous Studies on the Flammability of Polyamides Using Conventional Flame Retardants in Combination with Nanoclays

It is generally indicated that; addition of very small amounts of nanoclays significantly reduces the peak heat release rate (PHRR) of the polymer composites [24,62]. However, comparing the UL-94 and LOI results of nanocomposites with the virgin polymer, no progress in flame retardancy is observed [30,31,63].

Therefore for improved flame retardancy nanoclays should not be used alone, but in combination with conventional flame retardants where the nanoclay promotes the charring of the polymer, forming an insulating barrier [31,64,65].

There are some recent studies investigating the effect of nanoclays in flame retarded polyamides. Bourbigot et al. [30] showed that incorporation of 2 wt% organoclay to PA6 with OP 1311 increased the LOI value and granted the V-0 rating in UL-94. Shanmuganathan et al. [66] investigated the effect of nanoclay alone and in combination with zinc borate in PA6 nanocomposites. They observed that in the presence of the clay and intumescent effects of zinc borate, a well-blown stable char structure is formed, which reduces the PHRR about 70%, much larger than the reduction caused by nanoclay or zinc borate alone.

Song et al. [67] prepared halogen free flame retarded PA6 nanocomposites by using magnesium hydroxide and red phosphorous in combination with organoclay. PA6 containing 8 wt% magnesium hydroxide and 5 wt% red phosphorous achieves a V-0 rating. By substituting 2 wt% of magnesium hydroxide with organoclay they observed that; LOI value increases to 31% from 29%, PHRR is reduced by 33% and char residue is increased 1.5 times; becoming more stable. Dong et al. [68] observed that in a nanocomposite of PA6 containing 10 wt% silicon elastomeric rubber, by

replacing 2 wt% of additive with nanoclay the PHRR value is further decreased about 21.5%.

In the study of Song et al [28], PA66 nanocomposites with melamine polyphosphate were synthesized via in situ polymerization. It is stated that presence of clay in combination with melamine provides better thermal stability and higher char residue. Moreover, synergistic effects in flame retardancy are seen as a further 50% decrease in PHRR after addition of 4 wt% nanoclay to 7 wt% melamine polyphosphate containing PA66 composition.

Hu et al. [69] investigated the effect of nanoclay in two different flame retarded PA6 compositions. They found that nanoclay has synergistic flame retardancy effects in PA6 containing decabromodiphenyloxide and antimony trioxide, decreasing the PHRR and obtaining a V-0 rating. However, in PA6 containing 15 wt% melamine cyanurate, which already satisfies a V-0 rating, addition of 5 wt% nanoclay decreased the PHRR to a minor extent but changed the UL-94 rating to “fail”. Antagonist (anti-synergistic) action of nanoclay in flame retarded compositions of PA6 with melamine cyanurate is also revealed by the studies of Kiliaris et al. [70] and Zhang et al. [71].

1.5 Aim of This Study

Polyamides, especially PA6 and PA66, are the most widely used engineering thermoplastics. The main reasons behind the widespread utilization of polyamides are their high strength and ductility, good electrically insulating properties, high melting point, as well as excellent resistance to solvents and abrasion. Therefore, in addition to their usage to manufacture high strength fibers, they are preferred in automotive, electrical, consumer and many other industries. However, for applications requiring higher strength and modulus, better dimensional stability and lower water absorption, polyamides are reinforced with short glass fibers

PA6 and PA66 are easily ignitable and they continue to burn after ignition. For instance, unfilled and unreinforced PA6 and PA66 have an UL-94 rating of V-2 and a limiting oxygen index (LOI) of around 20-25% [14,72]. Dripping is another problem regarding the combustion of polyamides during which the reduced melt viscosity causes the material to flow downwards increasing the exposed surface area. Consequently, degradation occurs for a longer time and flame spread increases. Therefore, various flame retardant additives are compounded with polyamides to attain the required flame retardancy.

Flame retarded polyamides are suitable for electrical applications requiring polymers which do not ignite easily or at least do not spread the flame further. Recently, polyamides are replacing thermosetting polymers in electrical connectors, terminal blocks, switch components, wire ties and many other commercial parts [21,52]. It is noteworthy that compounding industrial flame retardants to polymers significantly deteriorates strength. Accordingly, in order to have enhanced mechanical properties together with substantial flame retardancy; it is common to compound flame retardant additives to short fiber reinforced polymers. As a matter of fact, researchers continually investigate the mechanical properties of short fiber composites based on flame retarded polyamides [52,58].

Incorporation of nanofillers, such as organically modified montmorillonite (organoclay), leads to enhanced thermal and mechanical properties in addition to reduced flammability at loading levels less than 10 wt%. Use of organoclays in combination with some conventional flame retardants further improves the flammability rating of the polymers. Many researchers are investigating the use of commercial flame retardants together with nanoclays in polyamide matrix [66-69]. However, studies on the use of nanoclays and glass fibers together as reinforcements in polyamides are very limited [73,74]. None of these studies are concerned about the flame retardancy. Moreover, there seems to be lack of studies on the synergistic effect of nanoclays in flame retarded and glass fiber reinforced polyamides.

Therefore, the first aim of this study was to evaluate and compare the flame retardancy effects of various commercial flame retardants used in glass fiber reinforced/ unreinforced PA6 and PA66. The second aim was to investigate the synergistic flame retardancy of nanoclays when used in combination with a commercial flame retardant in glass fiber reinforced PA6 matrix.

For the first purpose, PA6 and PA66 with or without glass fiber reinforcement containing three different commercial flame retardants were produced by an industrial scale extruder. In order to deeply understand the flame retardancy effects of different commercial flame retardants with different acting mechanisms, various characterization techniques were employed. Detailed flammability measurements were done on the samples by means of UL-94, Limiting Oxygen Index (LOI) and Mass Loss Cone Calorimetry (MLC). In addition to flammability test, samples were also characterized by mechanical tests, SEM and XRD.

For the second purpose, eleven different compositions are prepared by a lab scale twin screw extruder. The morphology of the nanocomposites is characterized by means of XRD and TEM. Flammability measurements are carried out by UL-94, LOI and MLC methods. Flame retardancy mechanism is assessed by TGA and by conducting ATR-FTIR and SEM studies on burned samples.

CHAPTER 2

EXPERIMENTAL

In this study, first PA6 and PA66 containing commercial flame retardants and reinforced with short glass fiber were compounded by an industrial scale extruder and then characterized by: tensile testing, SEM, TGA, LOI, UL-94, MLC and by means of fiber length distribution and water absorption value.

In the second part, certain nanoclay was added to short glass fiber filled PA6 containing another commercial flame retarded by using a laboratory scale extruder, in order to investigate the synergistic effects of nanoclays when used in combination with commercial flame retardants. Prepared samples were characterized by: tensile testing, XRD, SEM, TEM, ATR-FTIR, MFI, TGA, LOI, UL-94, and MLC and by fiber length distribution studies.

2.1 Materials Used

2.1.1 Polyamides

PA6 used was DSM Akulon K125, low viscosity polyamide having the specific gravity of 1.13. PA66 is a general purpose polyamide 66, obtained from DuPont as Zytel FE 210021 having a specific gravity of 1.14.

2.1.2 Glass Fiber

Silane treated short glass fibers were supplied by CAMELYAF (Turkey). They have an initial length of 3 mm and diameter of 10.5 μm . Aminosilane treatments with APS (γ -aminopropyltrimethoxysilane) makes them compatible with polyamide matrices.

2.1.3 Flame Retardants

In this study, four different commercial flame retardants which were kindly supplied from various sources were used. Concentrations of the active species of the flame retardants and their chemical structures are summarized in Table 2.1.

(i) Melamine Cyanurate (MCA)

Melamine cyanurate is a non-halogenated flame retardant, which possess good thermal stability. It is suitable for increasing flame retardancy of thermoplastics and especially polyamides. It is a white fine powder with a bulk density of 0.3-0.4 g/cm^3 and particle size of 12-17 μm .

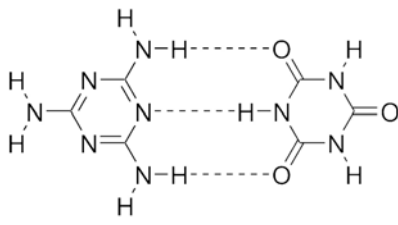
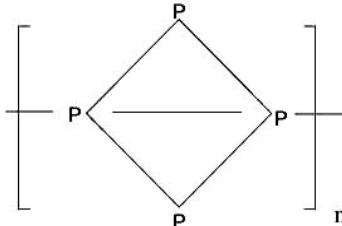
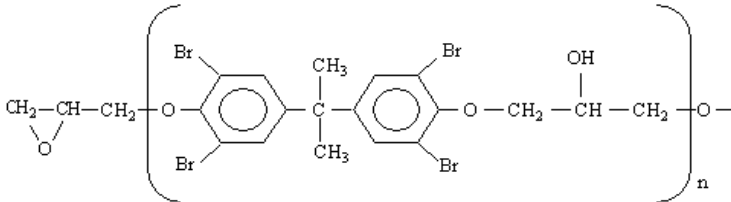
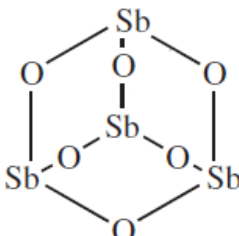
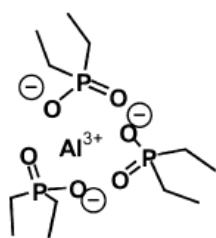
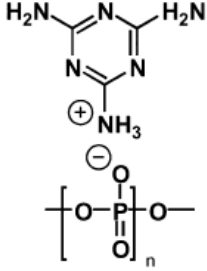
(ii) Brominated Epoxy and Antimony Trioxide (Br/Sb)

Bromine containing additives are one of the most widely used halogenated flame retardants. Also it is understood by recent studies that; aromatic bromine compounds are much better than aliphatic bromine compounds in providing flame retardancy.

Aromatic bromine compound employed in this study is tetrabromobisphenol-A epoxy polymer (2,6,2',6'-tetrabromo-4,4'-isopropylidene-di phenol) or with the commercial name of; *brominated epoxy* (BEP). It is obtained in the form of white-off white powder, having density of 1.9 g/cm^3 and containing 52% Br by weight.

Antimony trioxide (Sb_2O_3) is fine white powder having the average size of 0.3-1.1 μm and containing at least 99% antimony trioxide.

Table 2.1 Flame Retardants Used in This Study

Flame Retardant	Active Species Content	Chemical Structure
Melamine Cyanurate	99.5 wt% MCA	
Red Phosphorus	60 wt% P	
Brominated Epoxy	52 wt% Br	
Antimony Trioxide	99 wt% Sb ₂ O ₃	
Organo-phosphorous Flame Retardant (OP 1312)	18.7-19.7 wt% P	<div style="display: flex; justify-content: space-around;"> <div style="text-align: center;">  <p>aluminium diethylphosphate AlPi</p> </div> <div style="text-align: center;">  <p>melamine polyphosphate MPP</p> </div> </div>

(iii) Red Phosphorous (RP)

Elemental red phosphorous has an amorphous inorganic macromolecular structure. Despite being violently flammable, it is used as an effective flame retardant in oxygen and nitrogen containing polymers. It is one of the most effective flame retardant additives used for polyamides. Red phosphorus master batch (RPM) used in this study contains 60 wt% red phosphorous dispersed in phenolic matrices.

(iv) Organophosphorous Flame Retardant (OP)

It is the mixture of aluminum diethyl phosphinate and melamine polyphosphate with zinc borate. This flame retardant with the brand name of Exolit® OP 1312 was kindly supplied by Clariant in the form of white powder having a specific gravity of 1.5. OP 1312 flame retardant contains 18.7-19.7% phosphorous.

2.1.4 Nanoclay

The layered silicate for this study was Cloisite 30B purchased from Southern Clay Products (USA). Cloisite 30B has the lowest surface hydrophobicity compared to other clay products; therefore it is the most suitable one for the incorporation with the polyamide matrix.

Cloisite 30B is a montmorillonite produced from the cation exchange reaction between sodium montmorillonite and *methyl, tallow, bis-2-hydroxyethyl quaternary ammonium* (MT₂EtOH) with the anion of chloride. The chemical structure of this organic modifier is given in Figure 2.1. (T in Figure 2.1 stands for hydrogenated tallows; long organic molecules having ~65% C¹⁸; ~30% C¹⁶; ~5% C¹⁴.) The physical properties of Cloisite 30B is given in Table 2.2.

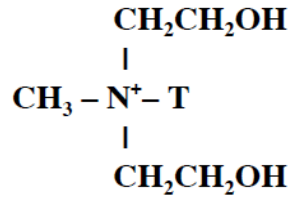


Figure 2.1 Chemical Structure of the Organic Modifier of Cloisite 30B

Table 2.2 Physical Properties of Cloisite 30B

Property	Value
Specific Gravity	1.98
Color	Off-white
Dry Particle Size	10% < 2 μm,
	50% < 6 μm
	90% < 13 μm
d Spacing	D ₀₀₁ = 18.5 Å
Organic Content	30 wt%
Modifier Concentration	90 meq/100g clay

2.2 Production of the Specimens

Specimens were first produced by twin screw extrusion compounding of polyamides, glass fiber, nanoclay and commercial flame retardants, and then shaped by injection and compression molding.

2.1 Specimen Groups

In this study, there were two main groups of specimens. The first group being PA6 and PA66 compositions with/without glass fiber and three different commercial

flame retardants, and the second group being PA6 compositions with glass fiber and a commercial flame retardant in combination with a nanoclay. Designations and compositions of the specimens studied in the first and second group are given in Tables 2.3 and 2.4, respectively.

Table 2.3 Compositions of the Specimens Studied in the First Group

Specimens	Composition
PA6	100% PA6
PA6-MCA	88% PA6, 12% MCA
PA6-GF	85% PA6, 15% SGF
PA6-GF-Br/Sb	58.5% PA6, 15% SGF, 20% BEP (10.6% Br), 6.5% Sb ₂ O ₃
PA66	100% PA66
PA66-GF	75% PA6, 25% SGF
PA66-GF-RP	63% PA6, 25% SGF, 12% RPM (7.2% RP)
PA66-GF-Br/Sb	48.5% PA6, 25% SGF, 20% BEP (10.6% Br), 6.5% Sb ₂ O ₃

Table 2.4 Compositions (wt%) of the Specimens Studied in the Second Group

Specimens	Short Glass Fiber (GF)	Nanoclay¹ (n)	Flame Retardant (OP)
PA6	-	-	-
PA6/OP	-	-	20
PA6/GF	15	-	-
PA6/GF-OP20	15	-	20
PA6/GF-OP15	15	-	15
PA6/GF-OP10	15	-	10
<i>n</i> PA6	-	5	-
<i>n</i> PA6/GF	15	5	-
<i>n</i> PA6/GF-OP15	15	5	15
<i>n</i> PA6/GF-OP10	15	5	10
<i>n</i> PA6/GF-OP5	15	5	5

¹ Nanoclay content is the nominal value instead of silicate basis

2.2.2 Compounding by Twin Screw Extruder

Specimens of the first group were compounded by an industrial scale twin screw extruder. Melt mixing of glass fiber, melamine cyanurate, red phosphorous and brominated epoxy in combination with antimony trioxide to PA6 and PA66 was achieved by ZSK 70 twin screw extruder having an L/D ratio of 40. Extrusions parameters for the samples produced in the first group are given in Table 2.5.

Table 2.5 Extrusions Parameters Used in the First Group

Specimens	Screw		Temperature Profile (°C)
	Speed (rpm)		
PA6's without retardant	Flame	1150	260-250-240-230-220-210-210-210-270
PA6's with retardant	Flame	500	260-250-230-210-190-180-170-170-260
PA66's without retardant	Flame	1100	290-280-270-260-250-240-240-240-270
PA66's with retardant	Flame	600	270-260-250-230-200-190-190-190-270

Specimens in the second group were prepared by a lab-scale extruder. Compounding of glass fibers, OP and nanoclay with PA6 was carried out by using Thermo Prism Twin Screw Extruder 16 TC with L/D ratio of 24. The temperature profile was 230-240-240-240-240°C and the screw speed was set at 200 rpm.

The compositions were prepared by dry-mixing prior to processing. Then the mixture was fed in equal portions of approximately 1 gram per equal time intervals of 10 seconds; from the main feeder. This feed rate asserts that the torque of the machine has not increased too much. Due to the difficulties encountered in continuously feeding the polyamide to the pelletizer, the product from the extruder die was pulled out and coiled up. Then, they were pelletized. In order to certify the homogeneity of

the products and the dispersion of the nanoclays: Pelletized samples were dried as stated below and extruded once more with the same process parameters.

2.2.3 Shaping by Injection and Compression Molding

(i) Drying

Polyamides are very hydrophilic materials. They absorb significant amounts water; which lead to swelling and shrinkage of the moulded parts. The granules should have a moisture content less than 0.2 wt% before any molding process. Otherwise air gaps and bubbles will occur in the test specimen, which negatively affects nearly any property of the material. Therefore, all granules were dried prior to processing. The drying conditions are given in Table 2.6.

Table 2.6 Drying Conditions of the Materials

Condition	Value
Temperature	80°C
Pressure (Vacuum)	- 400 mm Hg
Time	18 hours

Dried polyamides should be instantly molded. Else, they should be kept inside the desiccators.

(ii) Shaping by Injection Molding

In the first group, specimens for the tensile testing were prepared by laboratory scale injection molding machine (Microinjector, DACA Instruments). The operation parameters for PA6 and PA66 are given in Table 2.7.

Table 2.7 Injection Molding Parameters Used in the First Group

Injection Molding Parameters	Unit	PA6	PA66
Nozzle Temperature	°C	240	280
Mold Temperature	°C	80	80
Heating Time	min	3.5	3.5
Injection Pressure	bar	8	8

Specimens in the second group were injection molded by DSM Micro 10 cc Injection Molding Machine for tensile and LOI tests. The operation parameters are given in Table 2.8. Injection pressure was increased compared to the samples in the first group, which was done at DACA Microinjector, in order to prevent freezing of the molten polymer at the mold runner and to certify the full filling of the mold; due to the increased viscosity caused by the addition of fiber, clay and flame retardant additives.

Table 2.8 Injection Molding Parameters Used in the Second Group

Injection Molding Parameters	Unit	Value
Nozzle Temperature	°C	240
Mold Temperature	°C	80
Heating Time	min	3.5
Injection Pressure Profile	bar	10-10-15-15-10

(iii) Shaping by Compression Molding

Compression molding machine was used to prepare the specimens for LOI and MLC tests. A photograph of the compression molding machine is given in Figure 2.2.

Owing to the difficulties in mold filling and higher mold shrinkage in the molds with small cavities, especially bar shaped cavities: Molds with the cavity dimensions 100 mm x 100 mm x 4 mm were used.

Teflon sheets of 0.5 mm thickness were put on the bottom and top of the molds; to obtain smooth surfaces and prevent sticking of the molten polymer to the mold. Aluminum sheets were also employed on the both sides of the mold, to prevent sticking of the molten polymer to the hot plates. The compression parameters for PA6 and PA66 are given in Table 2.9.

For the LOI measurements, prepared samples were cut into 10x100x4 mm specimens by METACUT Cutting Machine.

Table 2.9 Compression Molding Parameters Used

Compression Molding Parameters	Unit	PA6	PA66
Mold Temperature	°C	235	265
Mold Pressure	bar	100	100
Pre heating Time	min	5	5
Pressure Applied Time	min	3	3
Cooling Method	---	Quench to room temperature	Quench to room temperature

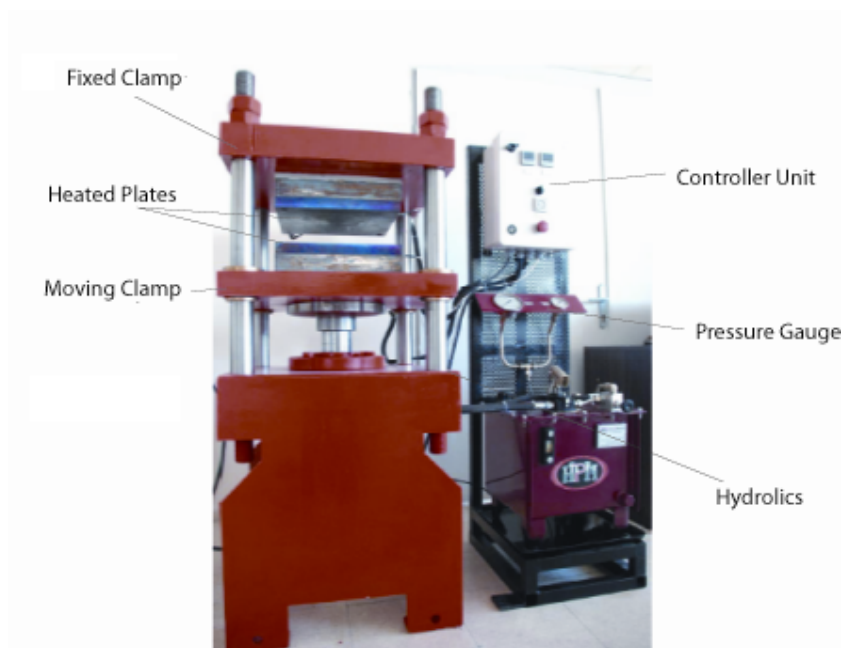


Figure 2.2 Compression Molding Machine

2.3 Characterization of the Specimens

Although the main purpose of this study is to improve fire retardancy, specimens were characterized by various methods before and after the flammability tests.

2.3.1 Water Absorption Value

Water absorption value of polyamide compounds was determined by immersing them in boiling water according to ISO 62 Method 2 *Determination of water absorption*. Boiling water is the harshest case and in this way the maximum amount of water that can be absorbed by polyamides is determined.

Samples were dried at 50°C for 24 hours and weighted prior to testing; then they were put in a pan containing boiling water. For every 30 minutes; samples were removed from the pan, dried by a towel and kept in a desiccator then weighted until the difference between two proceeding weightings is ± 0.1 mg.

2.3.2 Melt Flow Index (MFI)

The melt flow index (MFI) is defined as the amount of polymer passing through a specified capillary in ten minutes. It is generally used to measure the uniformity of the material's flow rate at process conditions.

MFI measurements, for the samples prepared in the second part, were carried out by Coesfeld MFI Tester according to ISO 1133 *Determination of the melt mass-flow rate (MFR) and the melt volume-flow rate (MVR) of thermoplastics*. Temperature was set to 240°C, which is the temperature used in the extrusion of these samples. Preferred load was 2.16 kg.

2.3.3 Tensile Testing

In tensile testing, specimen is elongated at a constant rate while the instantaneous applied load and the resulting elongations are recorded simultaneously.

Tensile tests were conducted using a 10 kN universal testing machine (Shimadzu AGS-J) at a crosshead speed of 1mm/min according to ISO 527 *Plastics - Determination of tensile properties*. The shape and dimensions of the specimens are given in Figure 2.3 and Table 2.10, respectively. Tensile strength, Young's modulus and percent elongation at break values are determined by using stress-strain curves.

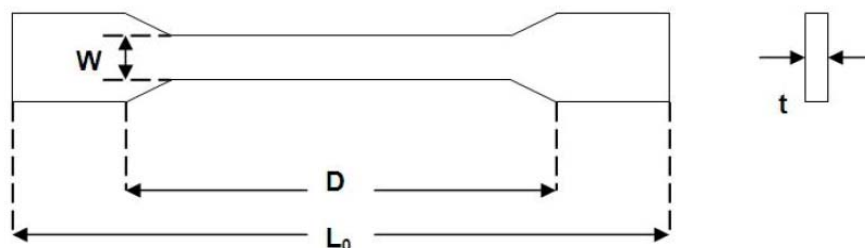


Figure 2.3 Dog Bone Shaped Specimen for Tensile Testing

Table 2.10 Tensile Test Specimen Dimensions

Term, Symbol	Specimen Dimensions (mm)	
	First Group	Second Group (ISO 527 Type 5A)
Distance between the grips, D	80	40
Overall length, L_0	110	75
Thickness, t	2	2
Width of narrow section, W	7.5	4
Gauge length	50	30

2.3.4 Fiber Length Distribution

Mechanical properties of short glass fiber reinforced polymers are related to the lengths of glass fibers. Fiber lengths are decreased drastically during processing due to fiber-polymer, fiber-fiber and fiber-machine interactions.

Fiber lengths were determined according to ISO 22314 *Glass-fibre-reinforced products - Determination of fibre length*, by burning out the volatile fraction of samples; that is polyamide, organic modifier in nanoclay, and various volatile fractions of flame retardant additives. Samples containing flame retardants were burnt at 850°C, whereas samples without flame retardants were burned at 650°C. Residues were dispersed in water by using ultrasonic bath. Then, fiber lengths were measured by using an optical microscope.

2.3.5 X-Ray Diffraction (XRD) Analysis

X-Ray Diffraction (XRD) Analysis is one of the most widely used characterization techniques for polymeric materials. A beam of X-rays incident to a material is partly absorbed and partly scattered, and the rest is transmitted unmodified. The scattering of X-rays occurs as a result of interaction with electrons in the material. The X-rays

scattered from different electrons interfere with each other and produce a diffraction pattern that varies with scattering angle. The variation of the scattered and diffracted intensity with angle provides information on the electron density distribution and hence the atomic positions within the material.

Composites were analyzed with a Rigaku D-Max 2200 X-ray diffractometer with a monochromatic Cu K α radiation. The diffraction angle 2θ is scanned from 1° to 10° at scanning speed of 1°/min. Sectioned injection molding specimens were analyzed in rigid solid form.

2.3.6 Scanning Electron Microscopy (SEM)

Scanning Electron Microscope (SEM) is used to determine the surface morphology of the specimens. Its working principle lies on; scanning the specimen surface by a beam of electrons then collecting and displaying the back scattered electron beam on a cathode ray tube.

In order to observe the interfacial relations between polyamides, glass fibers and flame retardant additives; the fracture surface of the tensile testing specimens were examined by a low voltage SEM (JEOL JSM-6400). Also, the burnt specimens from LOI test were examined to observe the char-microstructures and fiber orientations.

The sample surfaces were coated with a thin layer of gold to provide conductive surfaces thus avoiding electrostatic charging during observation. Several micrographs of fracture surfaces and burnt specimens were taken for each sample at various magnifications.

2.3.7 Transmission Electron Microscopy (TEM)

Transmission electron microscopy (TEM) is an imaging technique to obtain the enlarged image of the sample by focusing a beam of electrons onto it. Electrons are generated by a process known as thermionic discharge in the same manner as the

cathode in a cathode ray tube, or by field emission. Then, they are accelerated by an electric field and focused by electrical and magnetic fields onto the sample.

Transmission electron microscopy was conducted with FEI Tecnai G2 F30 at an acceleration voltage of 100 kV.

Thin sections of the injection molded dog-bone specimens were sharpened by using a glass knife and then 50-80 nm thin samples were cut by ultra microtome Lecia EM UC 6, having a diamond knife, operated at room temperature.

2.3.8 Attenuated Total Reflection Fourier Transform Infrared (ATR-FTIR) Spectroscopy

Attenuated total reflection Fourier Transform Infrared Spectroscopy (ATR-FTIR) uses the phenomena of total internal reflection. It operates by measuring the changes that occur in a totally reflected infrared (IR) beam when the beam comes into contact with a sample. When an IR beam is directed onto an optically dense crystal with a high refractive index at a certain angle, it will totally internally reflect. At the wavelengths of the IR spectrum where the sample absorbs energy, the reflected wave will be attenuated or altered. The attenuated energy from each reflected wave is passed back to the IR beam, which then exits the opposite end of the crystal and is passed to the detector in the IR spectrometer. The resultant attenuated radiation is measured and plotted as a function of wavelength.

ATR-FTIR Spectroscopy technique was used to determine the products formed during the combustion the specimens. ATR-FTIR spectrums were recorded by Bruker Optics Tensor having a diamond internal reflection element. Samples were scanned from 4000 cm^{-1} to 600 cm^{-1} with a resolution of 4 cm^{-1} .

2.3.9 Thermogravimetric Analysis (TGA)

Thermogravimetric Analysis (TGA) of the samples was performed at Shimadzu DTG 60-H thermogravimetric analyzer. It was carried out in nitrogen atmosphere at a nitrogen flow rate of 50 ml/min. Samples were analyzed from room temperature to 900°C at a heating rate of 10°C/min.

Mass loss and char yield are determined from TGA results and average decomposition temperature is determined by taking the derivative of the TGA curve (DTG).

2.4. Flammability Tests of the Specimens

2.4.1 UL-94 Vertical Burning Test

This test indicates the acceptability of polymeric materials in terms of flammability for a particular application. Since it is very easy to carry out and it categorizes materials as “pass” or “fail” ; UL 94 Vertical Burning Test is the most widely, and generally the only, test conducted in industry for flame retardancy.

In this test a small calibrated flame is applied twice to the vertically oriented specimen for 10 seconds. Then, the time to extinguishment of the flame and dripping behavior is observed. It gives information about the materials response for removed fire threat, in poor ventilated atmosphere.

This test was conducted at Ceast Flammability Meter, according to the UL-94 standard *Tests for Flammability of Plastic Materials for Parts in Devices and Appliances* developed by Underwriters Laboratories. A photograph of the instrument is given in Figure 2.4.

UL-94 measures the material response to a removed fire threat and its time to self-extinction. The specimen prepared in the dimensions of 125 ± 5 mm x 13.0 ± 0.5 mm x 1.6 ± 0.1 mm, is suspended vertically from the top. A small calibrated flame is applied from the bottom of the sample for 10s, twice. There is a layer of surgical cotton below the flame. Time to extinguishment after each flame application is measured; also ignition of the cotton by the drips of burning polymer is observed. The UL-94 Vertical Burning test has four ratings; V-0, V-1, V-2 and fail.



Figure 2.4 Ceast Flammability Meter UL-94 Test Device

2.4.2 Limiting Oxygen Index (LOI) Test

Limiting oxygen index (LOI) values, which is the minimum concentration (in volume percent) of oxygen in a mixture of nitrogen and oxygen that will sustain

burning, were measured, by an oxygen index apparatus (Fire Testing Technology, UK) having a paramagnetic oxygen analyzer so that precise adjustments of the oxygen concentration can be performed and repeatable results are obtained. A picture of the FTT LOI device is shown in Figure 2.5.

Bar shaped test specimens were used for determination of LOI; having dimensions of 100x10x4 mm. Oxygen concentrations were varied according to Dixon's up-and-down procedure explained in ISO 4589 *Determination of burning behavior by oxygen index*. This method entails the use of a large number of specimens of the same type to determine oxygen index with a low standard deviation. An example of the calculation of limiting oxygen index by this method is shown in Appendix A.



Figure 2.5 Fire Testing Technology LOI Device

2.4.3 Mass Loss Cone Calorimeter (MLC)

In addition to small scale flammability tests such as UL-94 and LOI, flame resistance of polymeric samples were also characterized by a medium scale fire test instrument, which is mass loss cone calorimeter (MLC), according to ISO 13927 *Simple heat release test using a conical radiant heater and a thermopile detector*. The instrument used is Fire Testing Technology Mass Loss Cone Calorimeter with Keithley- K-USB-3108 Data Accusation System, a photograph of the FTT Mass Loss Cone Calorimeter is shown in Figure 2.6.

Firstly, the cone temperature is calibrated to a value which is enough to generate an external flux of 35 kW/m^2 on the sample. Then, the thermopiles were calibrated to correspond to heat releases by burning propane. These calibrations are illustrated in more detail in Appendix B.



Figure 2.6 Fire Testing Technology Mass Loss Cone Calorimeter

Specimens having the dimensions of 100x100x4 mm were tested at an external heat flux of 35 kW/m². Specimens were ignited by a spark igniter and their ignition times were recorded.

Load cell and thermopile readings were recorded by data accusation system. Heat Release Rates (HRR) were calculated by the calibration mentioned above; and HRR versus time. Total Heat Evolved (THE) is the integral of the heat release rate with respect to time. Then, THE versus Time curves were also drawn. By taking the derivative of load cell readings with respect to time; mass loss rates were calculated and mass loss rate versus time curves were drawn.

Consequently, the values obtained from mass loss cone calorimeter measurements are as follows: Total Heat Evolved (THE), Peak Heat Release Rate (PHRR), Time to Ignition (TTI), Total Burning Time (TBT), Fire Growth Index (FGI), Total Mass Loss (TML), and THE / TML ratio.

CHAPTER 3

RESULTS AND DISCUSSION

The work in this thesis may be grouped in two parts: (1) short glass fiber reinforced/unreinforced PA6 and PA66 with flame retardants, and (2) short glass fiber reinforced PA6 with a flame retardant and nanoclay as a synergist.

3.1 Short Glass Fiber Reinforced/ Unreinforced PA6 and PA66 with Flame Retardants

In this part, three different commercial flame retardants were compounded with short glass fiber reinforced/unreinforced PA6 and PA66 with an industrial scale twin screw extruder. Flame retardants used in this study were melamine cyanurate (MCA), red phosphorus (RP) and brominated epoxy with antimony trioxide (Br/Sb). After compounding and shaping, water absorption values, mechanical properties, fiber length distributions were determined, and morphological studies were conducted. Then, thermogravimetric analysis (TGA) and flammability tests; UL-94, Limiting Oxygen Index (LOI) and Mass Loss Cone Calorimeter (MLC) measurements were carried out. Following the flammability tests, residues of the burnt samples were examined by SEM for their char microstructures.

3.1.1 Water Absorption Values

Polyamides are known to be hydrophilic due to the presence of polar amide groups in their backbones. They absorb significant amounts of water, which devastates their

processability. Therefore, they should be dried to decrease their moisture content below 0.2 wt% prior to processing.

In this study, specimens of PA6 and PA66 compounds and composites were immersed in boiling water to determine the maximum amount of water that will be absorbed. Figure 3.1 shows the moisture content of PA6 and PA66 compounds and composites with respect to time.

It is observed that neat PA6 and PA66 can absorb a maximum of more than 8 wt% and 6wt% water, respectively. Affinity to absorb water is considerably decreased with the incorporation of glass fibers and flame retardant additives. In the case of neat glass fiber reinforced composites, if the dilution of the matrix weight fractions are also taken into consideration, the water absorption behavior seems unchanged when compared to neat polyamides. However, considering the dilution of water absorbing polyamide matrices present in the flame retarded compositions, the absorbed percentage of water is still low compared to neat polyamides. This behavior can be attributed to rather lower water affinity developed in the system. However, the moisture content is still much higher than an appropriate value for processing, thus all polyamide compounds should be dried as stated on their data sheets, prior to any processing.

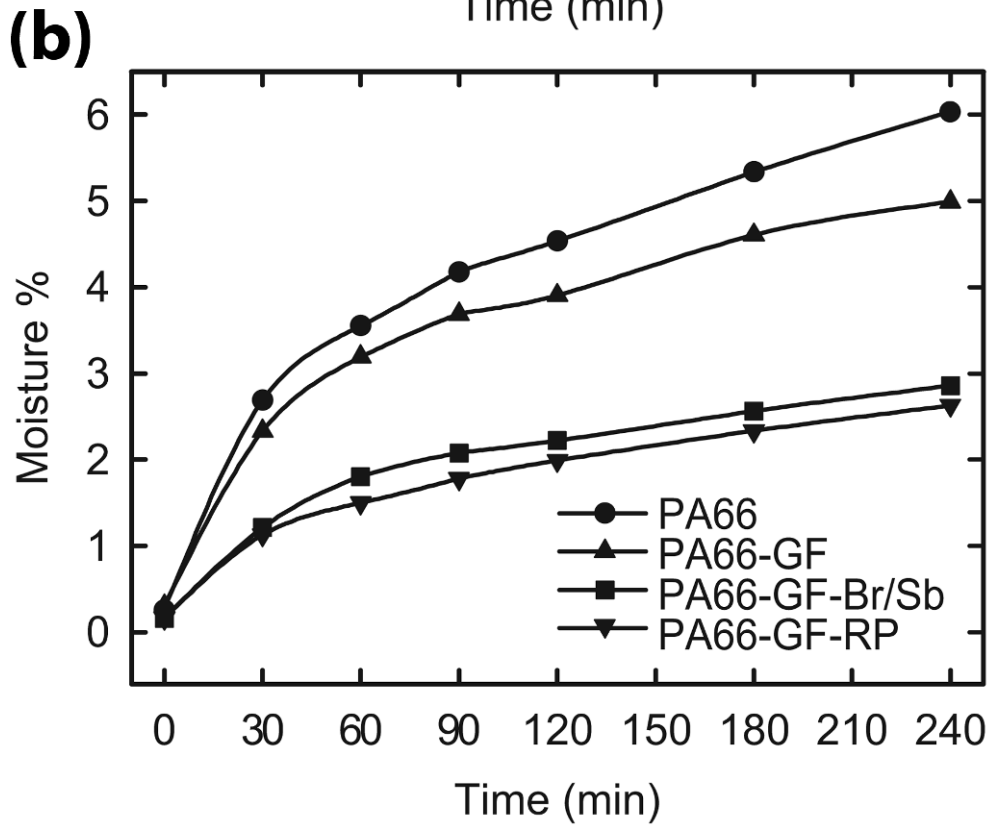
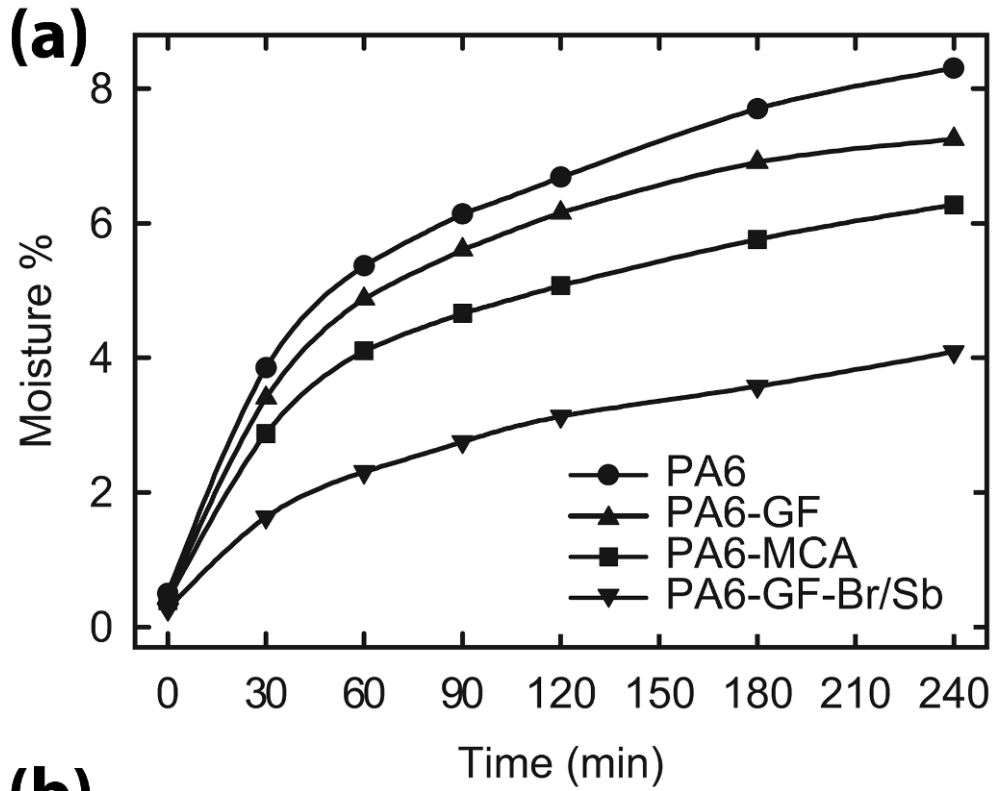


Figure 3.1 Water Absorption Values of (a) PA6 Compounds and Composites (b) PA66 Compounds and Composites

3.1.2 Mechanical Properties

Strength, stiffness and elongation values obtained from the tensile tests of PA6 based and PA66 based specimens are given in Figure 3.2 and Figure 3.3, respectively.

Figure 3.2 shows that the presence of melamine cyanurate (MCA) leads to a decrease in tensile strength, while it bringing a modest increase in elastic modulus. The decrease in the tensile strength compared to neat PA6 can be attributed to the poor interfacial interaction and incompatibility between melamine cyanurate and polyamide matrix [70]. Ductility of the specimen is not altered much, which can be seen in the SEM micrographs (Figure 3.8(a)) as fibrous matrix.

Comparing the results of PA6-GF-Br/Sb with PA6-GF, tensile strength and ductility are reduced to some extent, but substantial improvement in elastic modulus is present. The reason behind modulus improvement can be the presence of inorganic fillers with high modulus. The cause for decreased strength can be due to the much shorter fiber lengths resulting in lowered load carrying capability of the reinforcement (details are explained in the next section). Additionally, number of fiber ends per volume of fibers is drastically increased which reduced ductility as a consequence of stress concentration effects at fiber ends. Moreover, the presence of stress concentrating brominated epoxy and antimony trioxide (Br/Sb) at a relatively large fraction further lowers ductility and tensile strength due to poor interfacial strength (Figure 3.8(b)). Regarding PA66-GF and PA66-GF-Br/Sb, although a fair increase in elastic modulus is obtained, tensile strength decreased to about 60% of the glass fiber reinforced polymer. The reasons for lowered strength should be similar to those explained above for PA6-GF-Br/Sb.

Considering PA66-GF-RP; tensile strength is lower compared to PA66-GF due to substantial reduction in the fiber lengths. However, ductility reduction is not as much as in the case of PA66-GF-Br/Sb owing to the lower amount of additive present in PA66-GF-RP flame retarded system (apart from glass fibers, PA66-GF-Br/Sb contains 26.5 wt% additive while PA66-GF-RP contains 12 wt% additive).

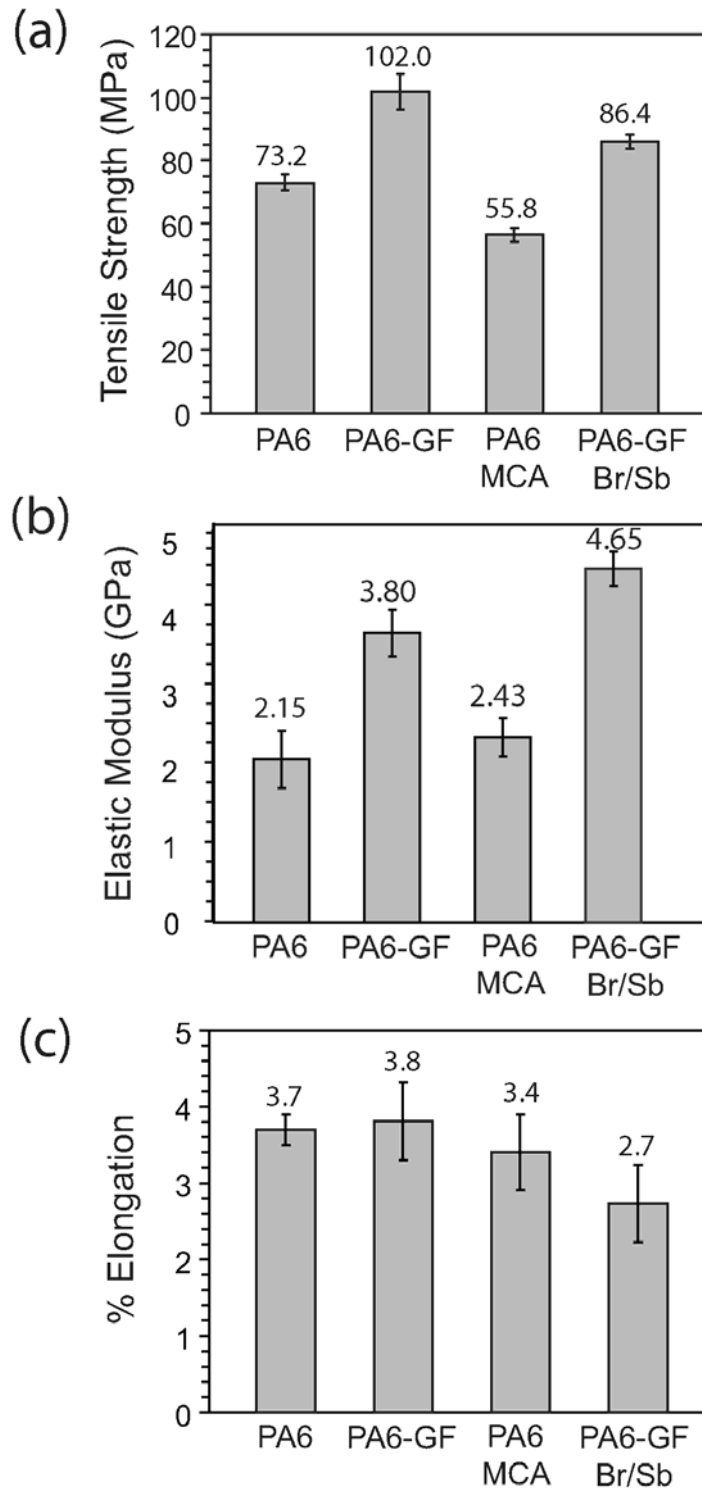


Figure 3.2 Mechanical Properties of PA6 Based Specimens (a) Tensile Strength, (b) Elastic Modulus, (c) % Elongation at Yield for Unreinforced Specimens and % Elongation at Break for Fiber Reinforced Specimens

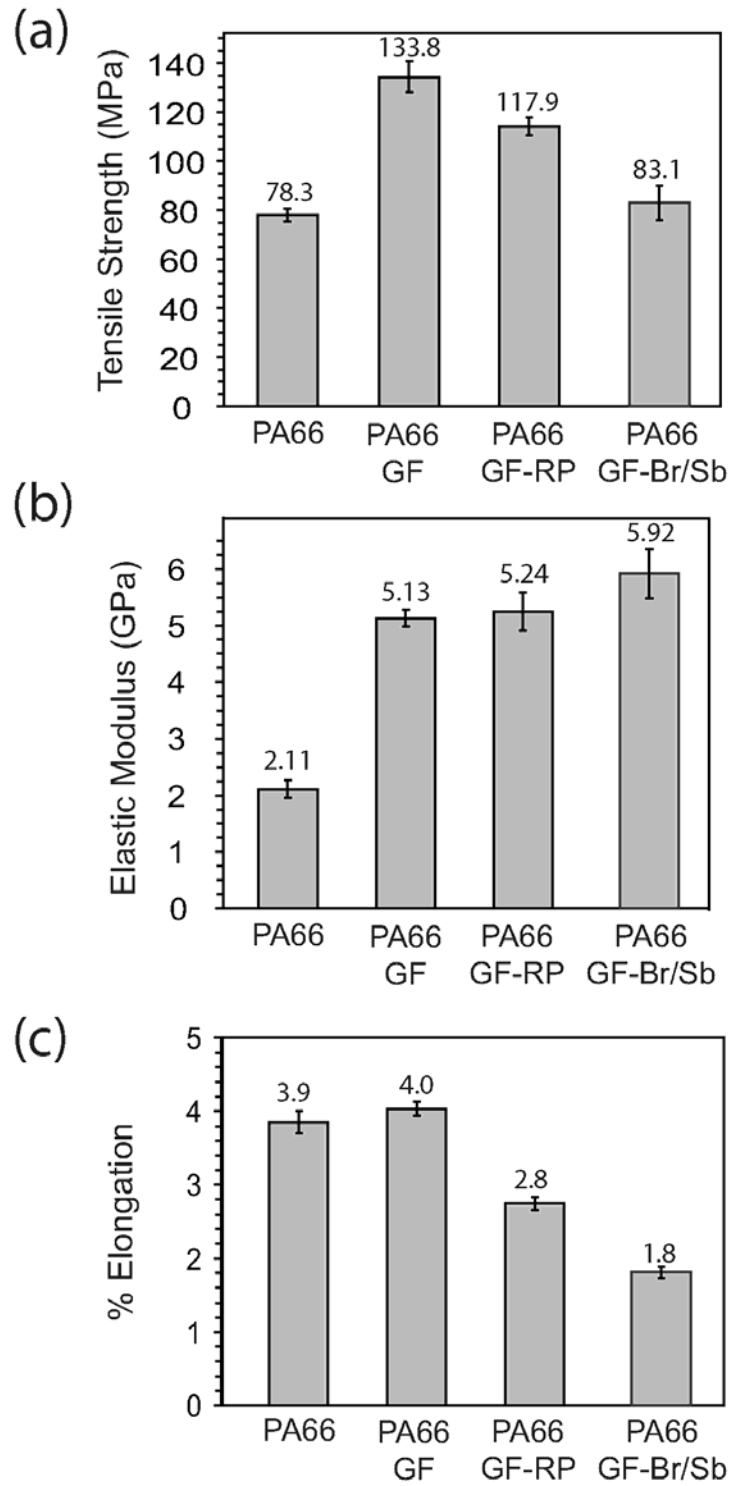


Figure 3.3 Mechanical Properties of PA66 Based Specimens (a) Tensile Strength, (b) Elastic Modulus, (c) % Elongation at Yield for Unreinforced Specimens and % Elongation at Break for Fiber Reinforced Specimens

3.1.3 Fiber Length Distributions

Aspect ratio of the fibers is one of the most important parameters affecting the mechanical strength of reinforced polymers. The glass fibers are fragmented into shorter lengths during extrusion as a result of fiber-fiber, fiber-machine and fiber-flame retardant interactions. Figure 3.4 shows micrographs of PA6-GF and PA66-GF-RP taken by an optical microscope at 40X magnification. It is clearly seen that, in the second specimen (Figure 3.4(b)) containing higher fiber reinforcement level and red phosphorus flame retardant, fiber lengths are much shorter.

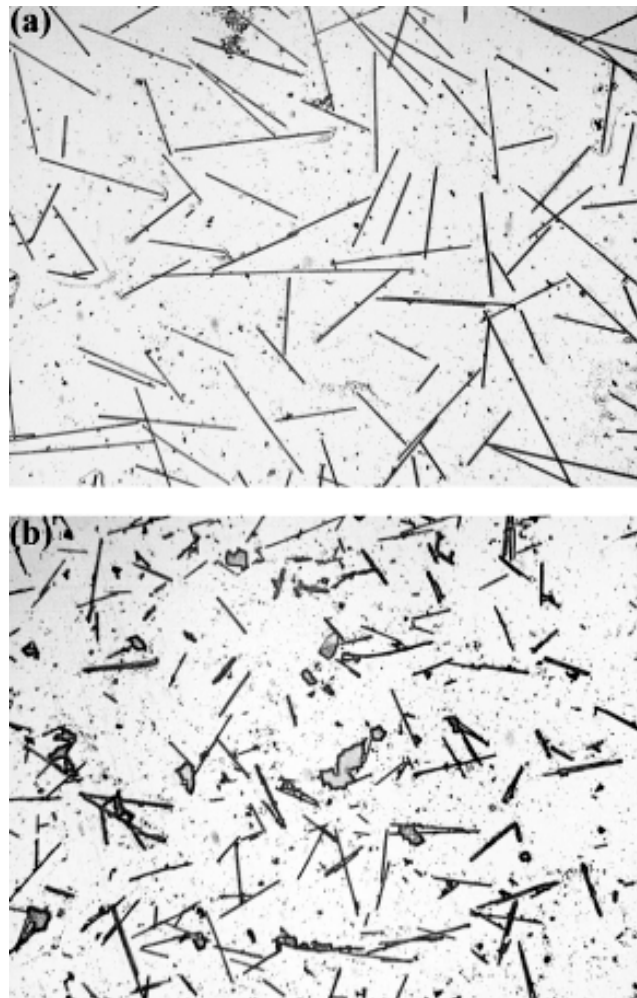


Figure 3.4 Optical Micrographs of (a) PA6-GF and (b) PA66-GF-RP (40X magnification)

By counting approximately 600 fibers using semi-automated image analysis software, fiber length distributions were determined as probability density functions. The residual fiber length distributions in terms of fiber length probabilities and mean fiber lengths are given in Figure 3.5 and Figure 3.6 for PA6 composites and PA66 composites respectively, $\bar{\ell}_n$ being the number of the average fiber lengths.

It is seen that fiber lengths are shorter for composites incorporating the flame retardant additives. This is attributed to the increased fiber attrition occurring in extrusion through further abrasion of fiber surfaces by the additive particles. This is one of the main reasons explaining the decreased tensile strengths in the flame retarded composites.

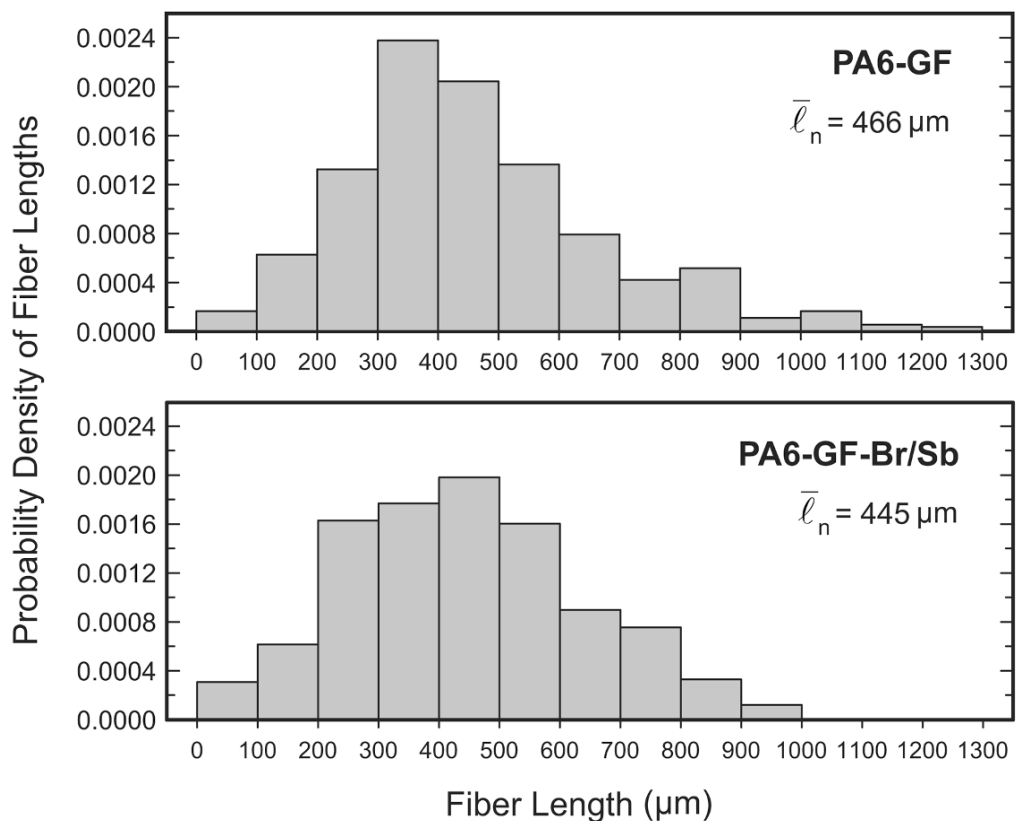


Figure 3.5 Fiber Length Probability Density Functions and Corresponding Mean Fiber Lengths of PA6 Composites

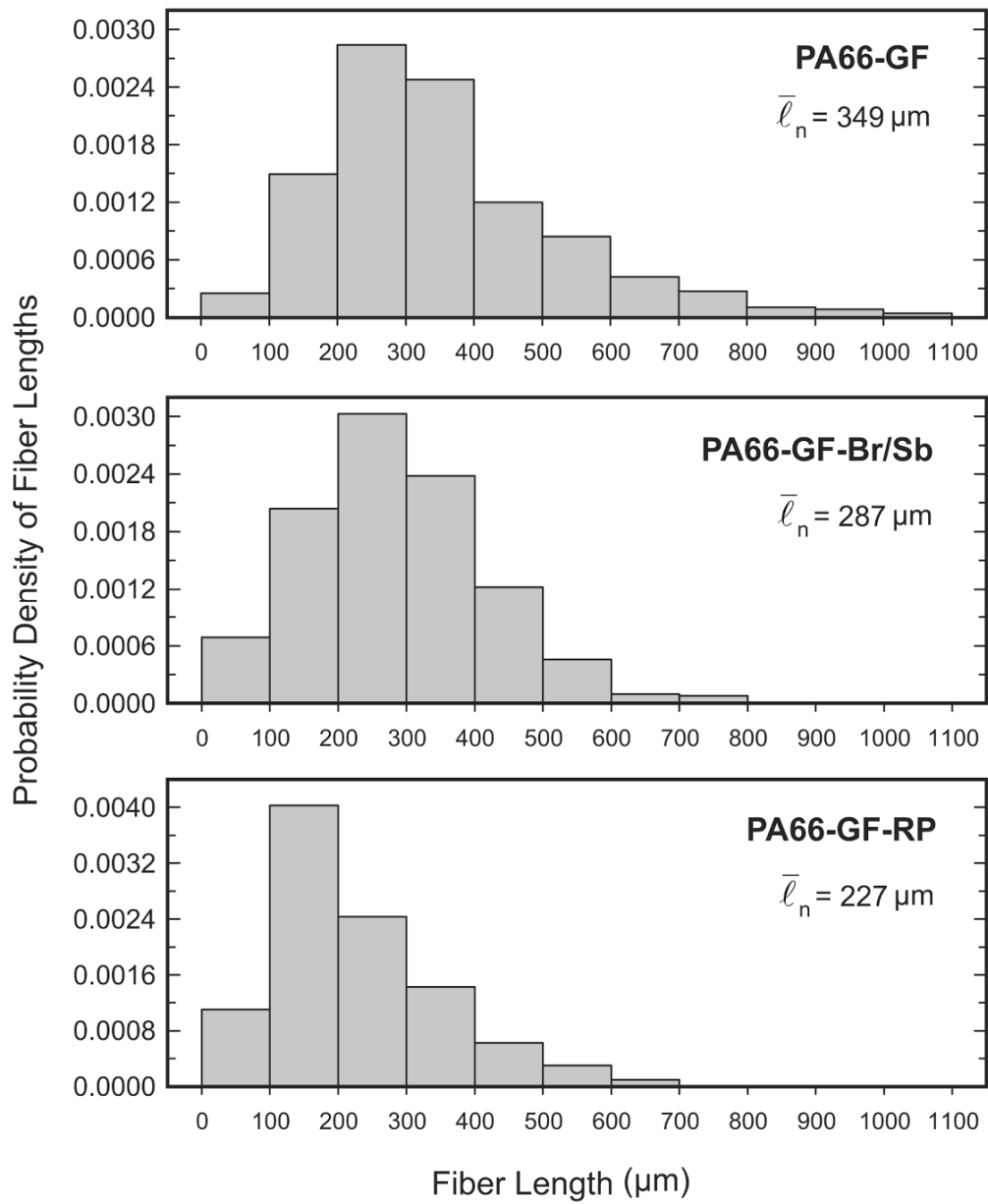


Figure 3.6 Fiber Length Probability Density Functions and Corresponding Mean Fiber Lengths of PA66 Composites

3.1.4 Fracture Surface Morphology

Scanning Electron Microscope (SEM) micrographs were taken from the fracture surfaces of the tensile test specimen at various magnifications. Figure 3.7 and Figure 3.8 show the SEM micrographs of PA6 based specimens.

Figure 3.7 show that there is a certain level of adhesion between the PA6 matrix and the glass fibers, leading to improved mechanical strength values. Figure 3.7(a) also shows that fibers are well oriented along the injection direction.

On the contrary, poor compatibility of MCA with PA6, which is the cause of the reduction in the tensile strength, is clearly seen in Figure 3.8(a) showing high levels of debonding. However fibrils are observed, indicating that the matrix preserved its ductile character.

A similar incompatibility between Br/Sb flame retardant and PA6 matrix is expected. However, brominated epoxy is miscible with PA6 matrix and only antimony trioxide molecules (in the range of 1 μm diameter) are seen. In this case, the interface between the matrix and the fibers are also not very good. Figure 3.8(b), shows debonding of the fibers, indicating a poor interface between glass fibers and PA6.

SEM micrographs of PA66 based specimens are given in Figure 3.9 and Figure 3.10. Figure 3.9 also shows that there is a good adhesion between the PA66 matrix and glass fibers. In Figure 3.10(a), no significant debonding between the matrix and glass fibers is seen. In PA66-GF-RP, red phosphorus containing phenolic flame retardant resin is well dissolved in PA66 matrix. On the other hand, certain level of debonding is observed in PA66-GF-Br/Sb as shown in Figure 3.10(b).

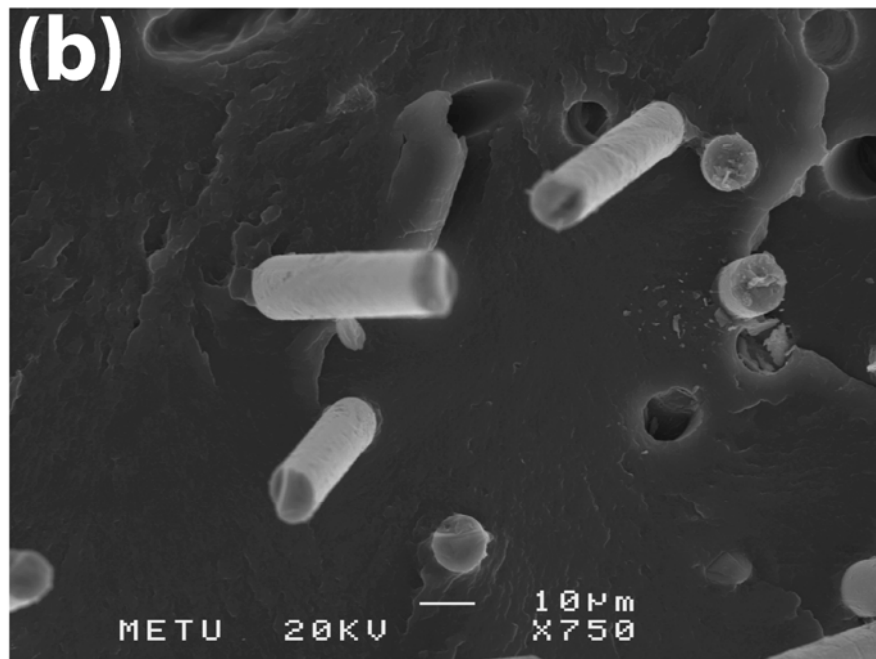
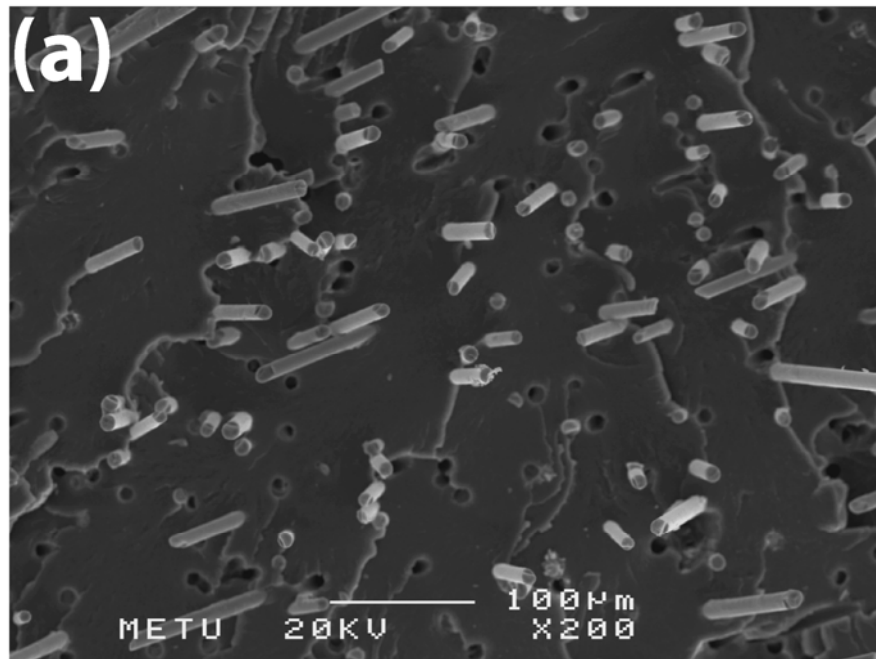


Figure 3.7 SEM Micrographs of PA6-GF (a) General View, (b) Closer View

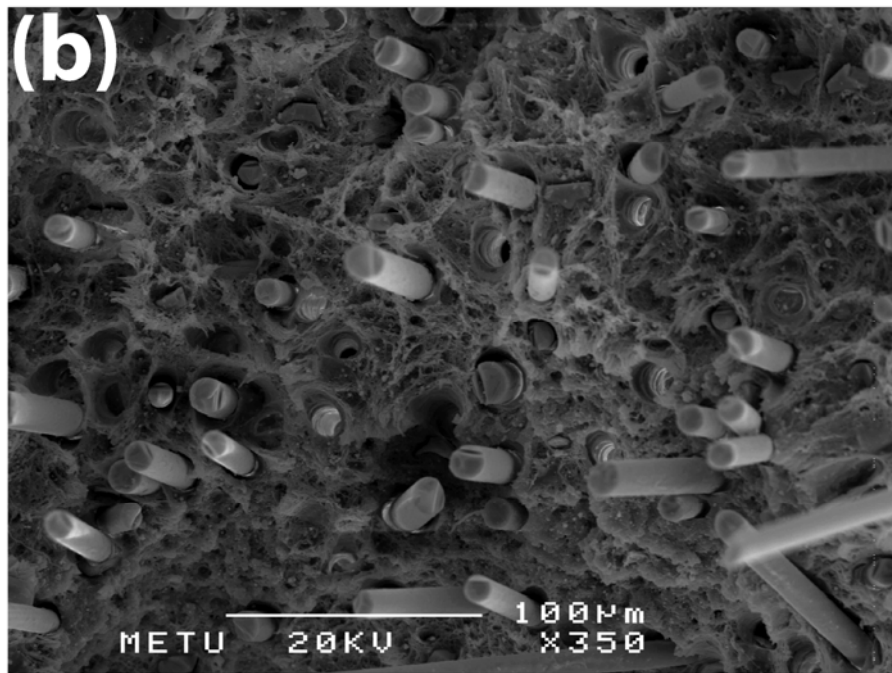
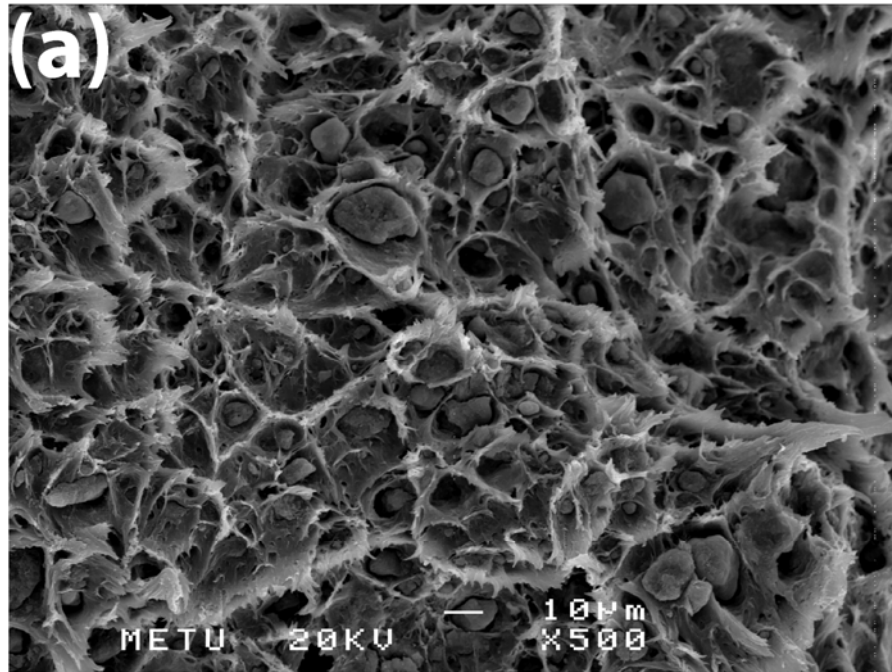


Figure 3.8 SEM Micrographs of (a) PA6-MCA and (b) PA6-GF-Br/Sb

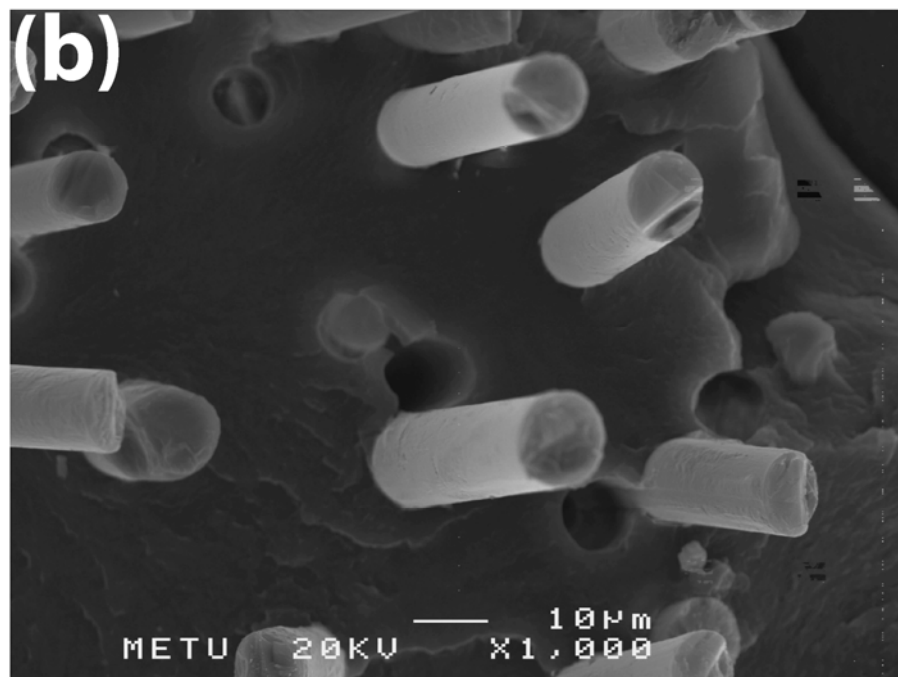
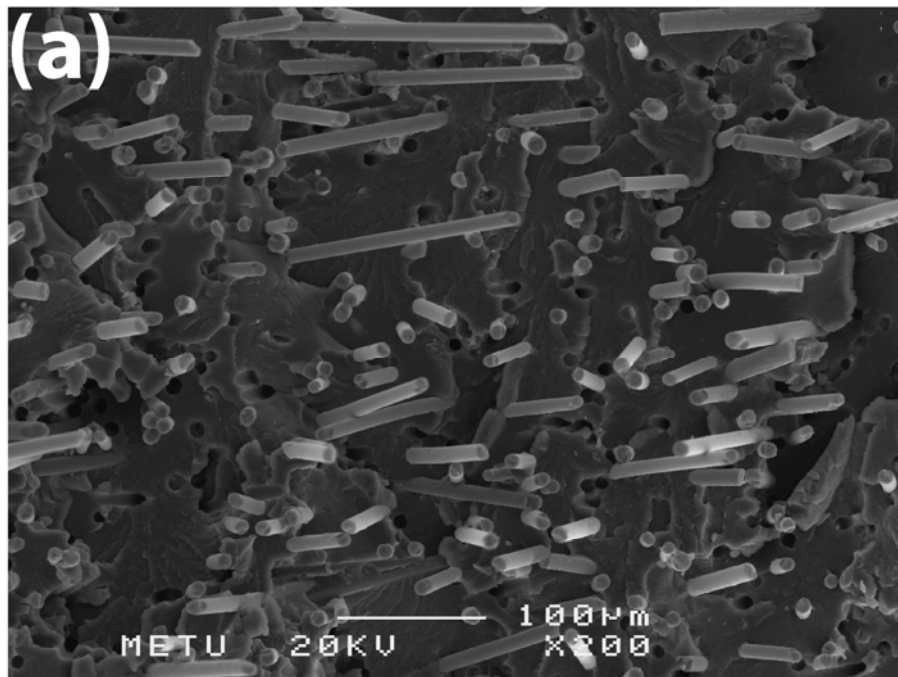


Figure 3.9 SEM Micrographs of PA66-GF (a) General View, (b) Closer View

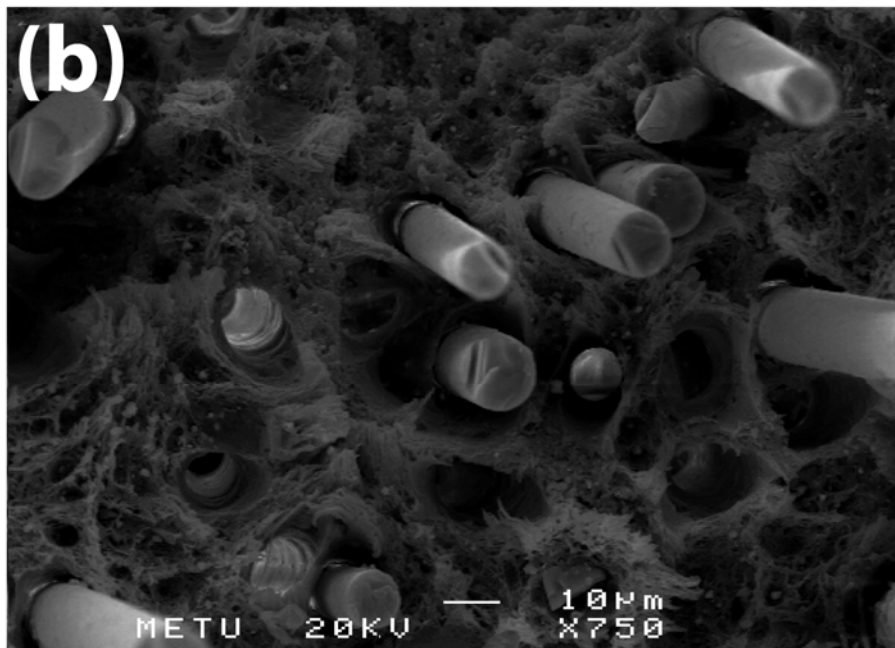
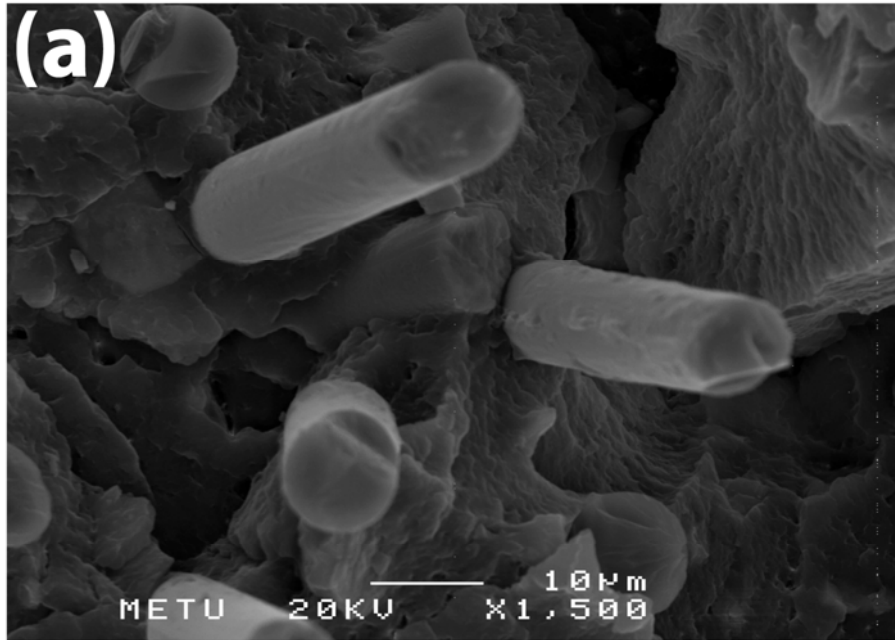


Figure 3.10 SEM Micrographs of (a) PA66-GF-RP and (b) PA66-GF-Br/Sb

3.1.5 Thermogravimetry

Thermogravimetric analysis (TGA) was carried on representative samples to investigate the effect of the employed flame retardants on the thermal degradation of PA6 and PA66 based specimens. Figure 3.11 and Figure 3.12 show the thermogravimetric (TGA) and differential thermogravimetric (DTG) curves of PA6 and PA66 samples, respectively. Peak temperatures of differential thermogravimetry ($T_{\text{DTG-Peak}}$), 10% mass loss temperature ($T_{10\%}$) and % residue values are given in Table 3.1.

Neat PA6 and PA66 decomposes totally in a single step, giving nearly no char residue. When glass fiber is introduced into PA6-GF (15 wt%) and PA66-GF (25 wt%) neither $T_{\text{DTG-Peak}}$ nor $T_{10\%}$ temperatures are altered compared to neat PA6 and PA66. However; peak mass loss rate values decrease in both cases. It can be concluded that residues of PA6-GF and PA66-GF solely consists of glass fibers.

As seen in Figure 3.11, PA6-MCA decomposes in two steps having peak values of 335.1°C and 447.5°C. First peak corresponds to endothermic volatilization of melamine cyanurate and the second peak corresponds to evaporation of the unaltered salt and its thermal dissociation to melamine and cyanuric acid [21]. It is also observed in Table 3.1 that first peak in DTG coincides with the 10% weight loss. PA6-MCA sample gives exactly no residue at 900°C.

Figure 3.12 shows that decomposition pathway of PA66-GF-RP also consists of two steps. However, at a heating rate of 10°C/min, decomposition steps overlap and second step forms only a shoulder in DTG curve as observed in Figure 3.12(b). Similarly, overlap of two decomposition steps is also observed by Schartel et al.[53] and Balabanovich et al. [55]. By adding red phosphorus to glass fiber reinforced PA66, thermal stability of the sample is reduced. That is, $T_{\text{DTG-Peak}}$ and $T_{10\%}$ values decreased by 18.2°C and 10.9°C, respectively, compared to PA66-GF. Moreover, red phosphorus induces charring, increasing the char residue from 25.9% (PA66-GF) to 32.3% (PA66-GF-RP).

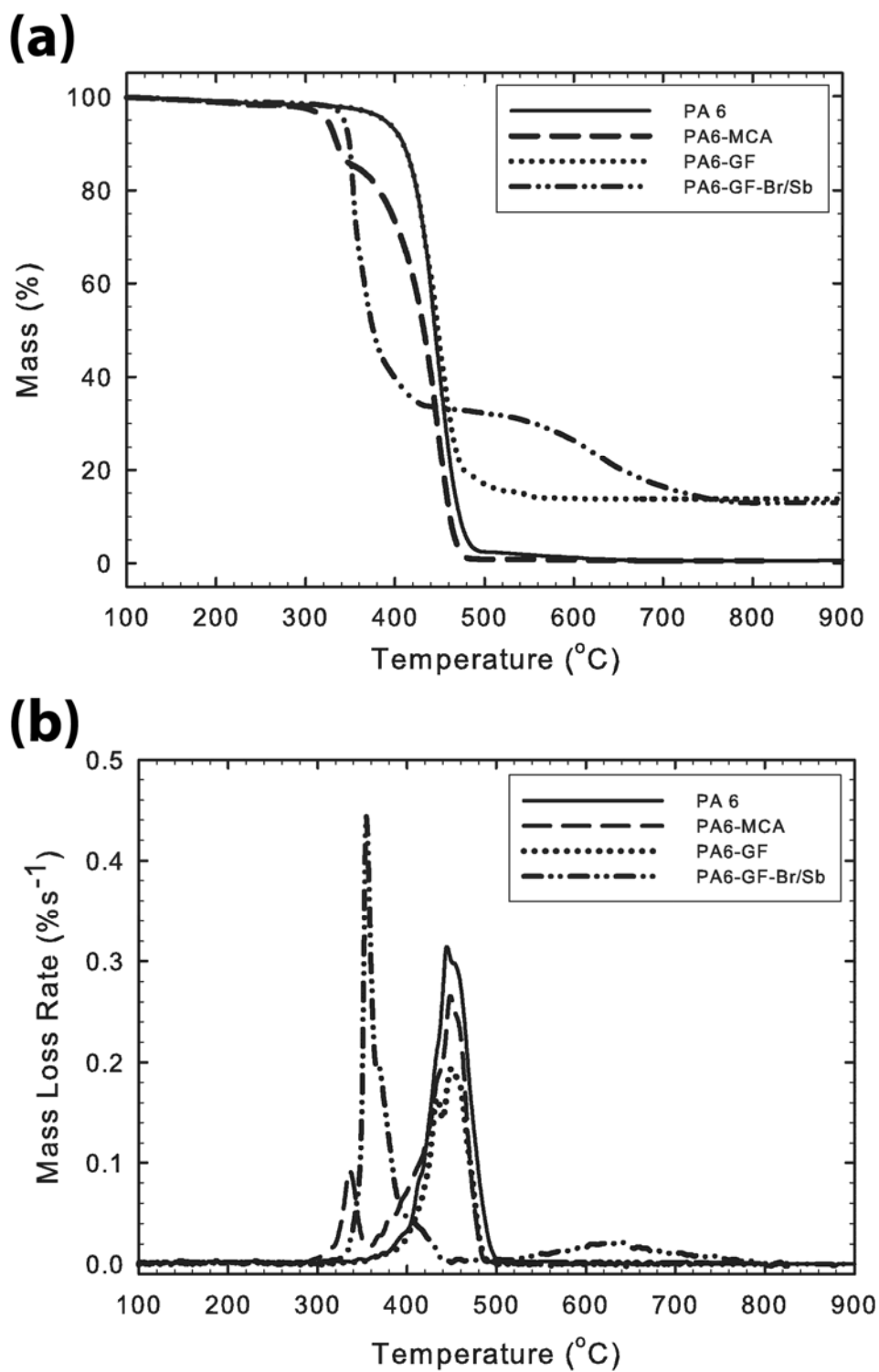


Figure 3.11 (a) Thermogravimetric (TG) and (b) Differential Thermogravimetric (DTG) Curves of PA6 Based Specimens

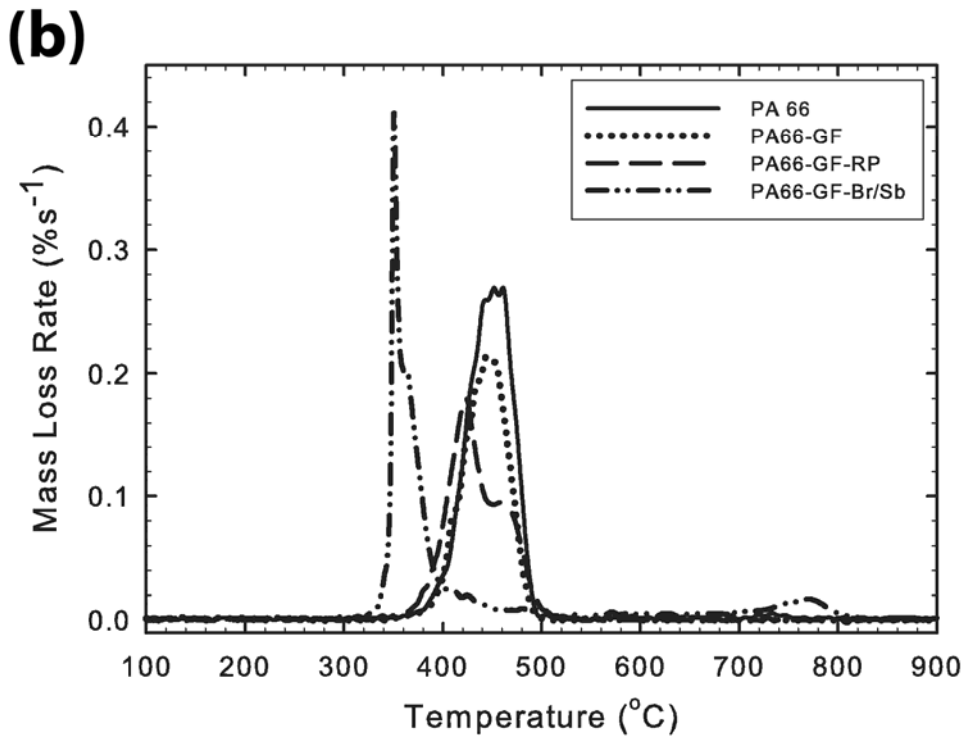
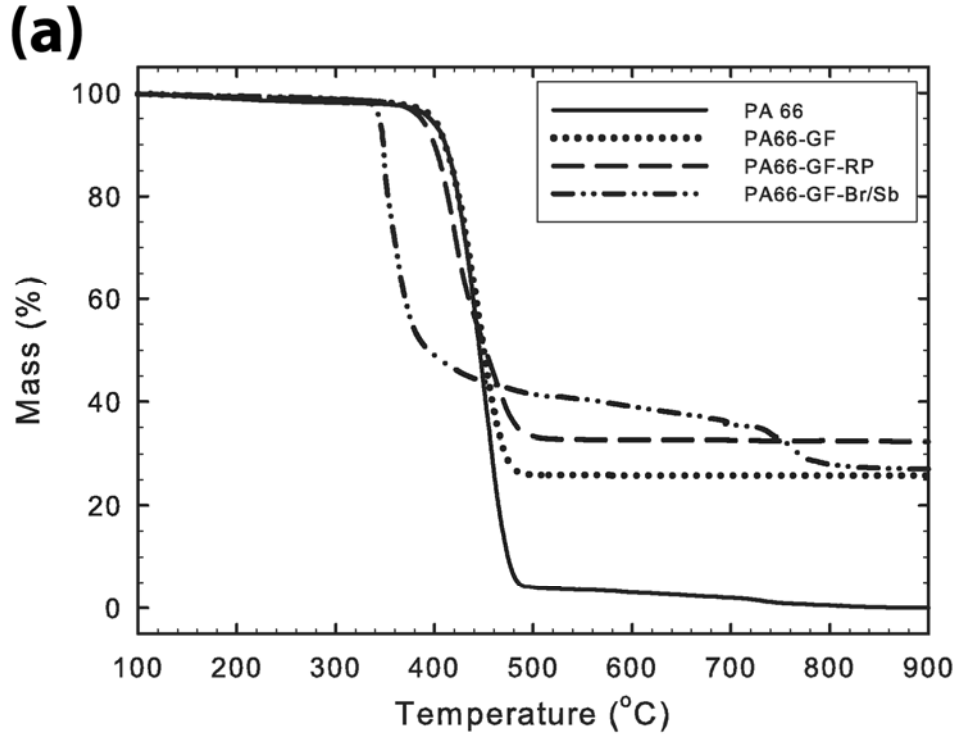


Figure 3.12 (a) Thermogravimetric (TG) and (b) Differential Thermogravimetric (DTG) Curves of PA66 Based Specimens

Figure 3.11 and Figure 3.12 indicate that PA6-GF-Br/Sb and PA66-GF-Br/Sb specimens also have two step decomposition pathways. First decomposition step which occurs at substantially lower temperatures compared to neat polyamides corresponds to dehydrobromination catalyzed polymer decomposition. The second step corresponds to reaction of HBr and Sb₂O₃; forming SbBr₃ which is an effective radical scavenger. Due to the dominant gas phase action of the flame retardant, DTG curves have much narrow shapes with increased mass loss rates as seen in Figure 3.11(b) and Figure 3.12(b).

For PA6-GF-Br/Sb, $T_{DTG-Peak}$ and $T_{10\%}$ values are lowered by 92°C and 58.9°C, respectively, compared to PA6-GF. Similarly, $T_{DTG-Peak}$ and $T_{10\%}$ values of PA66-GF-Br/Sb are 92.9°C and 62.2°C lower than that for PA66-GF. The main reason behind these shifts of thermal decomposition temperatures of polyamides to lower values are the acid catalysis induced by the formation of HBr. There are slight changes in the char residues. That is; from 13.8% to 13.0% comparing PA6-GF and PA6-GF-Br/Sb, and from 25.9% to 27.1% comparing PA66-GF and PA66-GF-Br/Sb. Thus, it can be concluded that Br/Sb flame retardant mainly acts in the gas phase and do not induce significant charring.

Table 3.1 Results of Thermogravimetric Analyses for PA6 and PA66 Based Specimens

Specimens	$T_{DTG-Peak}$ (°C)	$T_{10\%}$ (°C)	% Residue
PA6	443.1	409.8	0.7
PA6-MCA	335.1 and 447.5	335.0	0.5
PA6-GF	449.8	408.6	13.8
PA6-GF-Br/Sb	357.8	349.7	13.0
PA66	451.7	411.8	0.5
PA66-GF	443.2	411.0	25.9
PA66-GF-RP	425.0	400.1	32.3
PA66-GF-Br/Sb	350.3	348.8	27.1

3.1.6 Flammability and Fire Performance

Limiting Oxygen Index (LOI) Test, UL-94 Vertical Burning Test and Mass Loss Cone Calorimetry (MLC) measurements were conducted for the PA6 and PA66 based specimens.

(i) Flammability Tests: Limiting Oxygen Index (LOI) and UL-94 Vertical Burning Test

Results of LOI and UL-94 tests are given in Table 3.2. LOI tests were conducted according to Dixon's up and down method as explained in Appendix A. This method together with using paramagnetic oxygen analyzer led to very small levels of standard deviation.

Table 3.2 LOI and UL-94 Results of PA6 and PA66 Based Specimens

Specimens	LOI	UL-94 Rating
PA6	24.9 ± 0.4	V-2
PA6-MCA	27.1 ± 0.4	V-2
PA6-GF	22.4 ± 0.3	V-2
PA6-GF-Br/Sb	28.1 ± 0.2	V-0
PA66	26.8 ± 0.5	V-2
PA66-GF	21.3 ± 0.3	V-2
PA66-GF-Br/Sb	31.8 ± 0.3	V-0
PA66-GF-RP	27.6 ± 0.7	V-0

It is seen in Table 3.2 that neat PA6 and PA66 have LOI values of 24.9% and 26.8%, respectively. One should state that: "Improving flame retardancy of PA6 and PA66 is

unnecessary because their LOI values are higher than 21% and they are self-extinguishing.” Unfortunately, this is not true. Both PA6 and PA66 burns with colorless-blue flicker flame and the molten polymer drip down. Due to the dripping of the molten polymer, PA6 and PA66 burns the cotton in UL-94 tests, therefore they could only get V-2 rating. Since many industrial applications require polymers with a V-0 rating in UL-94 test, researchers are continually investigating new additives to improve flame retardancy of polyamides.

When short glass fibers are present without any flame retardant additives, dripping is inhibited but LOI is substantially decreased. For PA6-GF it is reduced from 24.9% to 22.4% while for PA66-GF it decreases from 26.8% to 21.3%. These specimens continue to burn like candle with a stable yellow flame. The easy flammability of glass fiber reinforced polymer composites is well established to be due to “candlewick effect” of the glass fibers [48,50,72]. In “*candlewick effect*”, glass fibers can transport the fuel from the pyrolysis of polymers to the flame by capillary action, speed up the heat flowing back to polymers and thus make the polymers decompose faster and burn more easily. So in order to achieve UL-94 V-0 rating, glass-fiber-reinforced plastics need much higher amount of flame retardants than neat polymers. Zhao et.al [75] explain the reasons behind the increased flammability by candlewick effect: (1) glass fibers have a larger heat conduction coefficient than polyamides, so they can transmit heat to the polymer below the burning region easily; (2) the alignment and contact of the filled glass fibers can form a continuous mass path and thus transport the flammable mass to the burning area.

Addition of MCA has a significant impact on LOI owing to its condensed phase flame retardancy mechanism. It increases LOI of PA6 from 24.9% to 27.1%; however it fails to induce an improvement in UL-94 rating. It is known that, decomposition products of MCA interfere with the main degradation of PA6 leading to dehydration of amide groups and scission of $-\text{CH}_2-\text{C}(\text{O})-$ bonds. Thus, oligomeric chain fragments having much lower molecular weight and viscosity are formed [46]. As a result; material and heat transfer to the flame is decreased by the dripping of the low viscosity decomposition products which cools the flaming material, leading to

self-extinguishment. Furthermore, the nitrogen gas produced by combustion will act as an inert diluent. Another source of inert diluent is the ammonia gas which is released during breakdown of the melamine or self-condensation of the melamine fraction which does not sublime. However, this drip promoting mechanism limits the usage of MCA in glass fiber reinforced polyamides, where the dripping is inhibited.

In the presence of an effective flame retardant, glass fibers may have a positive contribution to flame retardancy due to increased strength of the char and reduced thermal decomposition rate [52,60]. This statement is also validated by LOI and UL-94 results of PA6-GF-Br/Sb, PA66-GF-RP and PA66-GF-Br/Sb in which V-0 rating is achieved and samples are self-extinguishing.

Use of brominated epoxy polymer together with antimony trioxide (Br/Sb) is found to impart dramatic improvements in LOI and UL-94 values for short glass fiber reinforced PA6 and PA66 (Table 3.2). LOI value of PA6-GF-Br/Sb is increased from 22.4% to 28.1% and for PA66-GF-Br/Sb from 21.3% to 31.8%, which is the highest LOI value obtained in this study. The primary flame retardancy mechanism of halogens is the elimination of hot H• and OH• radicals in the gas phase. These reactions are summarized below in Reactions 3.1-3.3, where R-X being the halogenated flame retardant and P-H being the polymer [76].



When halogens are used in combination with antimony oxide, flame retardancy effects are enhanced. In this case, instead of hydrogen halides, metal halides are formed which are more active radical scavengers. The product of bromine compounds with antimony trioxide yields antimony tribromide in the gaseous phase and provides an effective scavenging of free radicals. The elimination reactions of the hydrogen bromide are shown below in Reactions 3.4-3.7 [76].



Then, SbBr_3 scavenges $\text{H}\cdot$, $\text{OH}\cdot$ and $\text{O}\cdot$ radicals as indicated in Reaction 3.8-3.15 [13].



Besides the dominant gas phase activity of Br/Sb systems, antimony trioxide also acts in the condensed phase promoting charring.

The addition of red phosphorus (RP) to glass fiber reinforced PA66 enhances LOI and imparts an UL-94 V-0 rating. LOI value is increased from 21.3% to 26.7% due to the condensed phase flame retardancy action of red phosphorus. This mechanism mainly depends on the formation of the various phosphoric acids upon reaction with polyamides, which covers the burning surface. Formation of phosphoric acid from elemental phosphorus is shown in Reactions 3.16 and 3.17. Moreover, acid promoted dehydration accelerates the formation of a consolidated char layer [50]. This intense char layer limits the oxygen access and heat transfer to the flame.



(ii) Fire Performance Assessment by Mass Loss Cone Calorimeter (MLC)

Fire performance of the PA6 and PA66 based specimens were characterized by using Mass Loss Cone Calorimeter (MLC), at an external heat flux of 35 kW/m². Heat Release Rate vs. Time, Total Heat Evolved vs. Time and Mass Loss Rate vs. Time graphs for PA6 and PA66 based specimens are given in Figure 3.13 and Figure 3.14, respectively. Using the obtained data, Peak Heat Release Rate (PHRR), Total Heat Evolved (THE), Time to Ignition (TTI), Total Burning Time (TBT), Total Mass Loss (TML), Fire Growth Index (FGI = PHRR/TTI) and THE/TML Ratio are calculated and tabulated in Table 3.3.

PHRR and THE are most widely inspected values to assess flame retardancy of the specimen. PHRR is the maximum energy emitted during burning and shows the impact of the fire. THE is the total energy emitted during burning, showing the fire load of the specimen in cone calorimeter scenario. TTI shows the ease of ignitability of the specimen. TBT is the time between ignition and extinguishment of flame.

FGI is firstly stated by Petrella [39] as the ratio of PHRR to TTI. FGI is a value which gives information about the flame spread of the material. Specimens with high FGI values spread the flame further, while the specimens with lower FGI values resist to expansion of the flame.

Schartel et al. [77] stated that, the ratio of THE to TML is proportional to the *Effective Heat of Combustion of the Volatiles* by a factor called *combustion efficiency*. Thus, THE/TML Ratio is employed as an indication of the flame retardancy mechanism. For the flame retardants having a gas phase action; THE/TML Ratio is reduced significantly compared to neat polymer, while for flame retardants with dominant condensed phase mechanism, it does not change much.

Comparing neat glass fiber reinforced polyamides (PA6-GF, PA66-GF) with unreinforced matrices (PA6, PA66), even though Time to Ignition (TTI) values are

not changed significantly, TBT are nearly doubled. Glass fiber reinforced specimens have broader peaks as seen in Figure 3.13 and Figure 3.14. Despite the certain reductions in LOI value upon addition of glass fibers, PHRR and THE values are reduced significantly. Comparing PA6 with PA6-GF, PHRR value decreases about 34%, while THE value is not altered much. Effect of glass fibers are seen more clearly when comparing PA66 and PA66-GF, which contains 25 wt% glass fibers. In this case, PHRR and THE values decrease as much as 57% and 32%, respectively.

It is seen in Table 3.3 that, after addition of MCA, TTI and TBT become shorter. The decrease in TTI value is in agreement with the TGA in which addition of MCA lowers the initial decomposition temperature of PA6 (Section 3.1.5) . PHRR and THE values are decreased about 22% and 25%, respectively compared to neat PA6. In Figure 3.13(a), Heat Release Rate reaches to 625 kW/m² in the early minutes of the combustion, and then it increases to a maximum of 723 kW/m² before the end of the test.

On the other hand, Mass Loss Rate curve has a different shape (Figure 3.13(c)): mass loss rate reaches its highest values after the start and it decreases. The reason behind the different shapes of Heat Release Rate and Mass Loss Rate curves is the evolution of incombustible gases in the first minutes of combustion

Table 3.3 Mass Loss Cone Calorimeter Results of PA6 and PA66 Compounds

Specimens	Total Heat		Peak Heat		Time to		Total Burning		Fire Growth		Total Mass		THE/ TML	
	Evolved (THE) (MJ/m ²)		Release Rate (PHRR) (kW/m ²)		Ignition (TTI) (s)		Time (TBT) (s)		Index (FGI) (PHRR/TTI)		Loss (TML) (g)		Ratio (MJ/m ² :g)	
PA6	180		921		98		394		9.4		43.6		4.1	
PA6- GF	172		611		99		524		6.2		43.6		3.9	
PA6- MCA	135		723		80		325		9.0		43.8		3.1	
PA6 -GF- Br/Sb	66		266		76		358		3.5		36.8		1.8	
PA66	131		683		109		380		6.3		43.2		3.0	
PA66- GF	89		293		91		604		3.2		35.1		2.5	
PA66- GF-RP	32		74		135		702		0.6		27.4		1.2	
PA66- GF- Br/Sb	25		94		53		379		1.5		32.3		0.8	

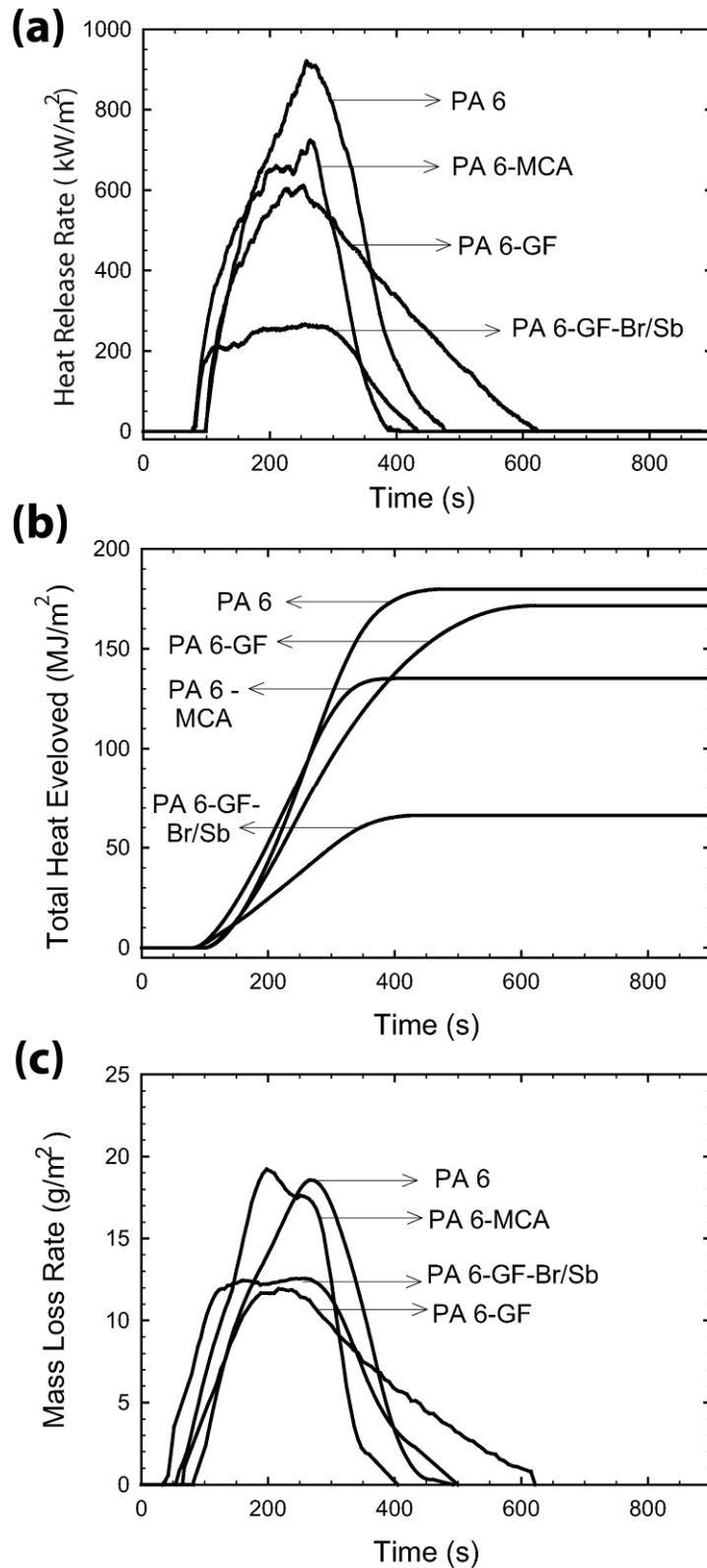


Figure 3.13 (a) Heat Release Rate vs. Time, (b) Total Heat Evolved vs. Time, and (c) Mass Loss Rate vs. Time graphs for PA6 based specimens

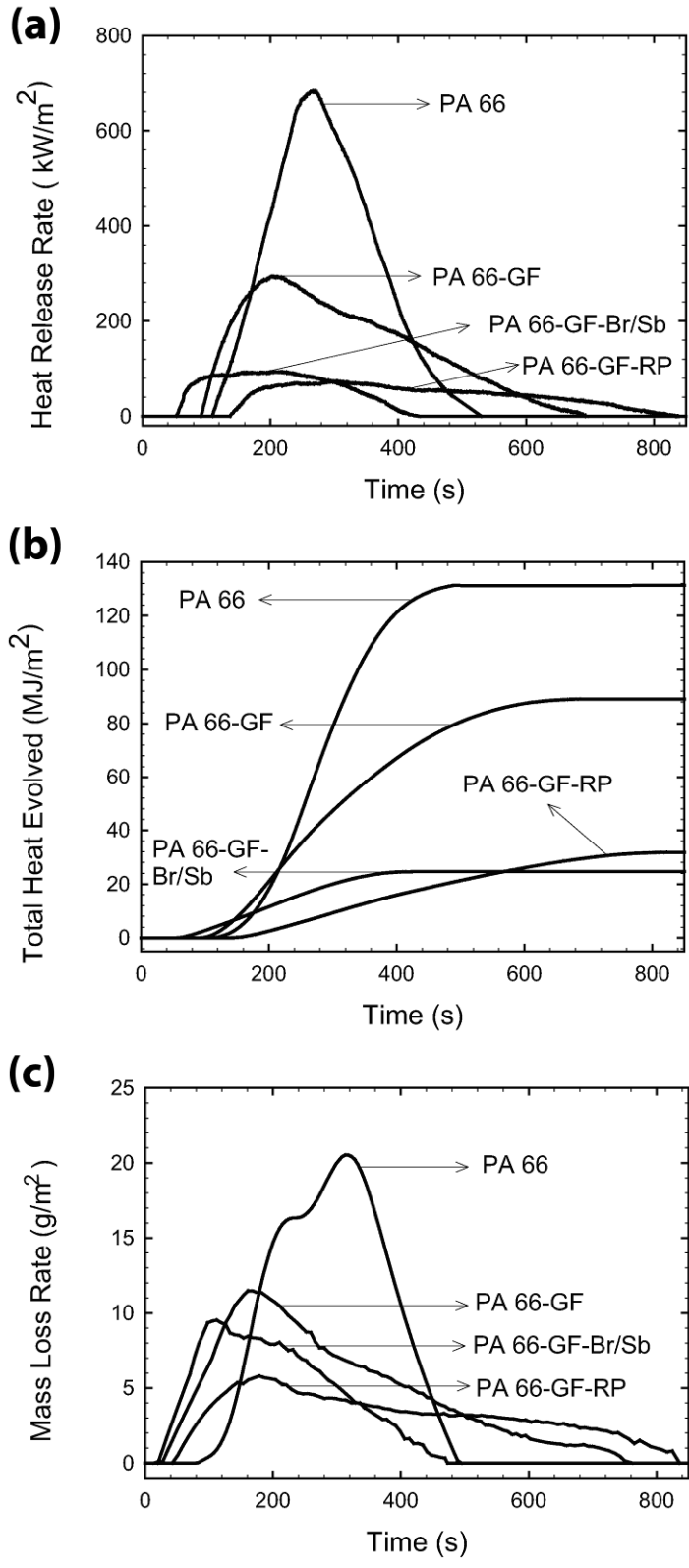


Figure 3.14 (a) Heat Release Rate vs. Time, (b) Total Heat Evolved vs. Time, and (c) Mass Loss Rate vs. Time Graphs for PA66 Based Specimens

As stated previously, flame spread is addressed by comparing FGI values. MCA do not have a significant retardancy effect in the fire spread, as nearly the same results are obtained compared to neat PA6 in the FGI values. In addition, dividing total heat release rate to total mass loss, THE/TML Ratio is obtained which is an indication of the mechanism of the flame retardant. Some minor reductions are observed in THE/TML Ratio of PA6-MCA compared to neat PA6; concluding that melamine cyanurate does not avoid the evolution of combustible gases completely, but the dominant mechanism is in the condensed phase.

Introduction of brominated epoxy in combination with antimony trioxide (Br/Sb) to glass fiber reinforced PA6 and PA66 lead to significant improvements in PHRR and THE values. In PA6-GF-Br/Sb, PHRR and THE values are decreased about 55% and 62%, respectively compared to PA6-GF. In PA66-GF-Br/Sb, PHRR and THE values are dropped as much as 68% and 72%, respectively compared to PA66-GF. Increased efficiency of the Br/Sb flame retardant system in PA66-GF-Br/Sb compared to PA6-GF-Br/Sb may be attributed to increased glass fiber content in which PA66-GF-Br/Sb contains 25 wt% glass fiber while PA6-GF-Br/Sb have 15 wt%. Chen et al. [60] stated that increasing glass fiber content in flame retarded compositions greatly improves flame retardancy as a result of reduced thermal decomposition rate. Moreover, gas phase action of Br/Sb system (scavenging hot radicals) which is explained in the previous section is also validated by the values of THE/TML Ratio. This ratio for PA6-GF-Br/Sb and PA66-GF-Br/Sb are much lower than that for PA6-GF and PA66-GF, indicating the presence of dominant gas phase flame retardancy.

Br/Sb addition decreases the Time to Ignition to and Total Burning Time. Actually, they have a very effective flame retardancy property which extinguishes the flame before all the polymer burns. FGI values are nearly halved to that of PA6-GF and PA66-GF in both cases validating the efficiency of Br/Sb in controlling the flame spread.

Incorporation of red phosphorus (RP) to glass fiber (GF) reinforced PA66, lead to 75% and 65% reductions in PHRR and THE values respectively. Contrary to the most of the other flame retardants, RP increases TTI together with TBT. Delayed TTI is ascribed to thermo-oxidative decomposition reactions that take place on the surface of the sample forming a black skin before ignition [53]. After the ignition has occurred, polymer burns homogenously with a stable flame above the surface showing some intumescent character. Reductions in PHRR and THE values are mainly resulted from the condensed phase mechanism of RP forming a char-like barrier limiting heat and mass transfer to the flaming zone. Besides this dominant flame retardancy mechanism, non-negligible reduction in the THE/TML Ratio for PA66-GF-RP compared to PA66-GF indicates that RP also have some gas phase activity. This gas phase action is explained by Levchik et al. [14] as the scavenging of $O\cdot$ and $OH\cdot$ radicals, which are active in inducing the formation of gaseous species.

Even though, PA66-GF-RP and PA66-GF-Br/Sb have similar PHRR and THE values, their Mass Loss Rate curves are different as shown in Figure 3.14(c) due to the difference in their predominant flame retardancy mechanism. PA66-GF-Br/Sb mainly acts in the gas phase so its mass loss rate is higher, while PA66-GF-RP forms a protective char layer in the condensed phase limiting the mass loss.

3.1.7 Residue Characterization

Photographs of all the specimens taken after LOI test are shown in Figure 3.15. Intense dripping behavior of PA6 and PA66 is clearly observed in these images. Addition of MCA blows the molten polymer and contributes to dripping. In the neat GF reinforced polyamides (PA6-GF and PA66-GF) flaming occurs just on the tip of the specimens without any dripping. This burning behavior of glass fiber reinforced specimens is called “candle wick effect” and increases the flammability as explained in the previous section. For PA6-GF-Br/Sb, PA66-GF- Br/Sb, and PA66-GF-RP specimens, charring was observed in these photos.

SEM micrographs of the flame retarded specimens after LOI are presented in Figure 3.16. Porous and blown char provided by MCA is shown in Figure 3.16(a). MCA shows considerable contribution to the formation of a char layer in the intumescent process. This char layer acts as a barrier between oxygen and polymeric decomposition gases. Char stability is enhanced by multi-ring structures (like melem and melon) formed during self-condensation of melamine. Moreover, melamine can act as blowing agent for the char, enhancing the heat barrier functionality of the char layer.

Figure 3.16 (b) and (c) display the charred fiber networks of PA6-GF-Br/Sb and PA66-GF-Br/Sb. These char networks are ineffective as a barrier due to the open/loose structure caused by the evolution of gases during flaming.

The strong and dense charred fiber residue for PA66-GF-RP displayed in Figure 3.16(d) protects the underlying polymer from heat transfer and oxygen diffusion, and slows down the rate of evolution of gaseous fuels.

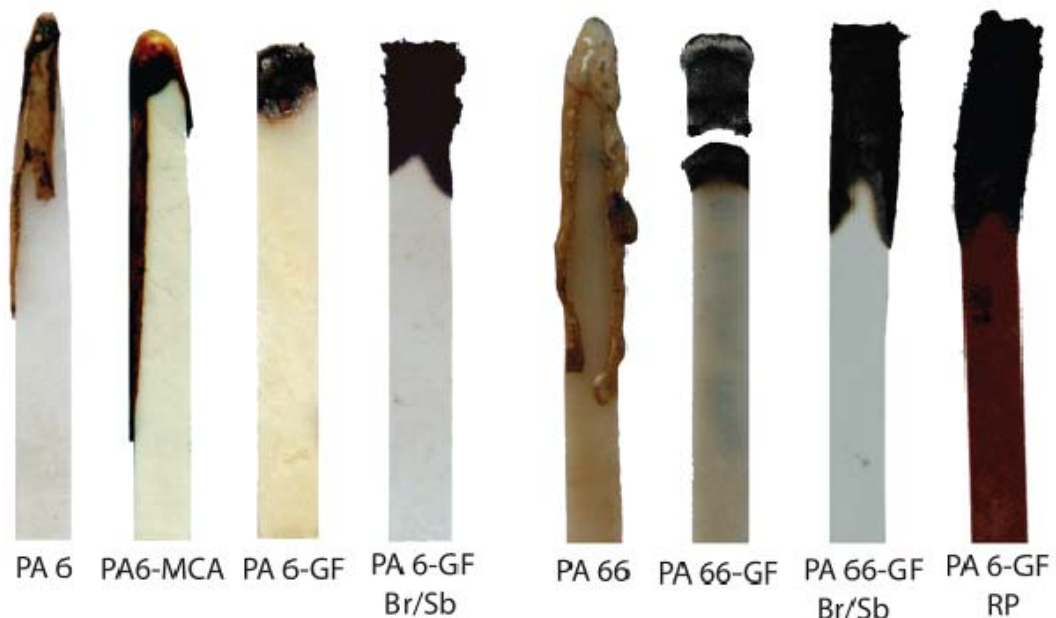


Figure 3.15 Appearances of the PA6 and PA66 Based Specimens after LOI Test

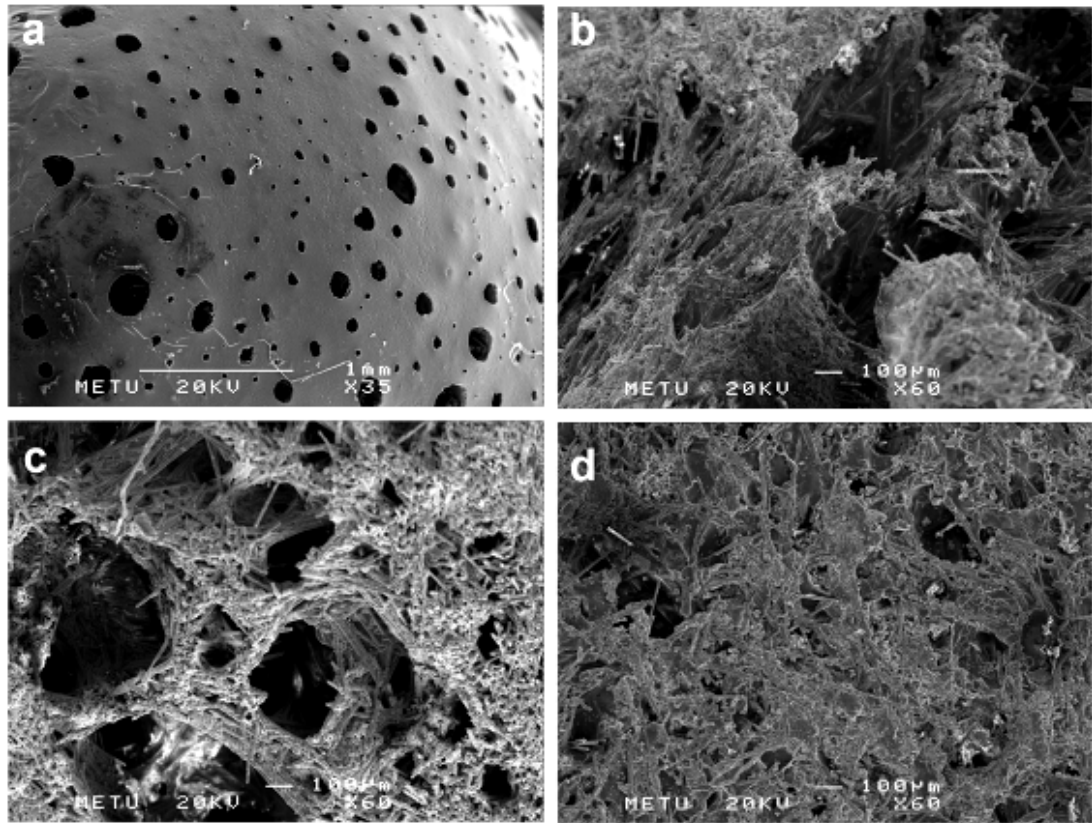


Figure 3.16 SEM Micrographs Taken from Chars of Flame Retarded Specimens (a) PA6-MCA, (b) PA6-GF-Br/Sb, (c) PA66-GF-Br/Sb, (d) PA66-GF-RP

3.2 Short Glass Fiber Reinforced PA6 with a Flame Retardant and Nanoclay

In the second part, another new commercial flame retardant, which is Clariant Exolit OP1312, (OP) was compounded with glass fiber (GF) reinforced PA6 by using a laboratory scale twin screw extruder. Certain nanoclay (*n*), which is Cloisite 30B, was also introduced to flame retarded compositions in order to investigate the synergistic flame retardancy effects. Melt flow indices (MFI) and mechanical properties of the samples were determined; clay dispersion was quantified and morphology was examined. Then thermogravimetric analysis (TGA) and flammability tests of: UL-94, Limiting Oxygen Index (LOI) and Mass Loss Cone

Calorimeter (MLC) were conducted. Finally, the residues of the burnt specimens were characterized by means of ATR-FTIR and SEM.

3.2.1 Melt Flow Index (MFI)

MFI measurements were carried out under a specified load of 2.16 kg and at a temperature of 240°C to determine the effect of glass fibers, nanoclay and flame retardant additives on the processability of PA6. The results of MFI measurements are shown in Figure 3.17.

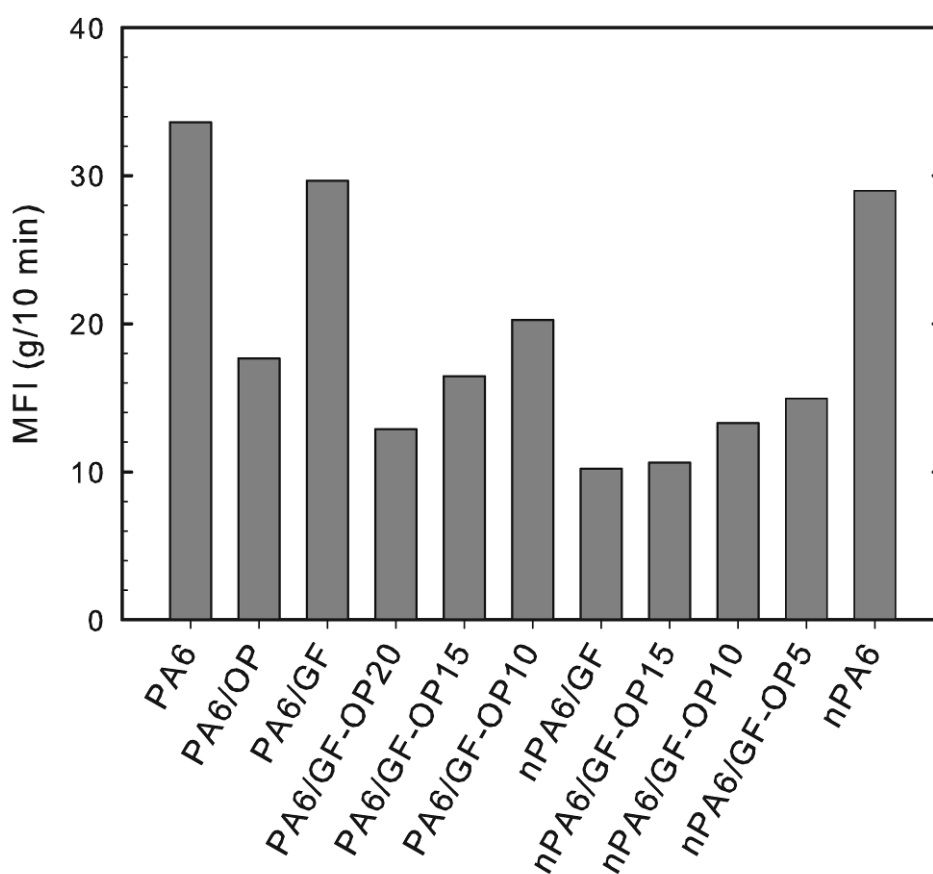


Figure 3.17 Melt Flow Index Values for PA6 Based Specimens

It is clearly deduced from Figure 3.17 that addition of flame retardant (OP) to neat PA6 reduces MFI value from 33.6 g/10min to 17.6 g/10min. However, due to the very short length of the glass fibers (Section 3.2.3) after extrusion, MFI value of PA6-GF is not decreased so significantly compared to PA6. MFI value of *n*PA6 is also quite close to that of PA6, because nanoclays both hinder the flow and decrease the melt viscosity.

For the glass fiber reinforced compositions, MFI value increases with decreasing flame retardant content. Following the introduction of nanoclay, MFI values are further decreased to 10 g/10 min.

3.2.2 Mechanical Properties

Tensile strength, Young's modulus and elongation at break values were calculated from the stress-strain curves of the specimens. Figure 3.18 shows the effect of flame retardant, glass fiber and nanoclay on the mechanical properties of PA6.

Flame retardant additives are generally incompatible with the host polymer matrix resulting in discontinuities at particle/matrix interface in the form of debonding. Consequently, there is a loss of strength and ductility with the incorporation of flame retardant into neat PA6 as shown in Figure 3.18. However, modulus is increased to some extent due to the stiffening effect of the flame retardant.

Figure 3.18 show that reinforcing fillers such as nanoclays and glass fibers provide effective strengthening. It should also be emphasized that: addition of 5 wt% nanoclay, in *n*PA6, gives higher tensile strength than PA6-GF, which contains 15 wt% glass fibers. Thus, reinforcement at the nano-scale is much more effective than that at the micro-scale in terms of composite strength. This is especially attributed to much greater average aspect ratio of nanoclay layers compared to short glass fibers. Additionally, molecular level entanglements of polymer chains with nanoclays having very large surface area ensure highly efficient stress transfer from matrix to reinforcement. Moreover, ductile character of PA6 is preserved after the addition of

nanoclay in *n*PA6 having 28% elongation, while in PA6-GF it is much smaller being only 4.8%.

Introduction of 5 wt% nanoclay into glass fiber reinforced PA6 (*n*PA6-GF) further increases the tensile strength and Young's modulus values and correspondingly leads to no reduction in the ductility level.

Mechanical properties of the samples are also compared with each other at equal total additive content (flame retardant + nanoclay) and the results are shown in Figure 3.19. It can be deduced from this figure that there is a decreasing tendency of tensile strength and elongation in parallel with flame retardant content both for composites with and without nanoclay. On the other hand, modulus increases in both cases by increasing the concentration of the flame retardant.

Flame retardant used in the current study was also shown to deteriorate the apparent interfacial strength between glass fibers and matrix in the case of flame retarded and glass fiber reinforced PA6. Upon replacement of flame retardant with 5 wt% nanoclay, at equal total additive content, tensile strength values are increased as shown in Figure 3.19(a), as a result of the improved interfacial strength between glass fiber and polyamide. The only exception is in *n*PA6/GF-OP15, where tensile strength is decreased as a result of loss of matrix property due to very high loading level.

Young's modulus for every composition is significantly increased upon introduction of very high moduli nanoclays. It is also seen from Figure 3.19(c) that nanoclays have a slightly decreasing effect on the ductility of glass fiber reinforced/flame retarded compositions.

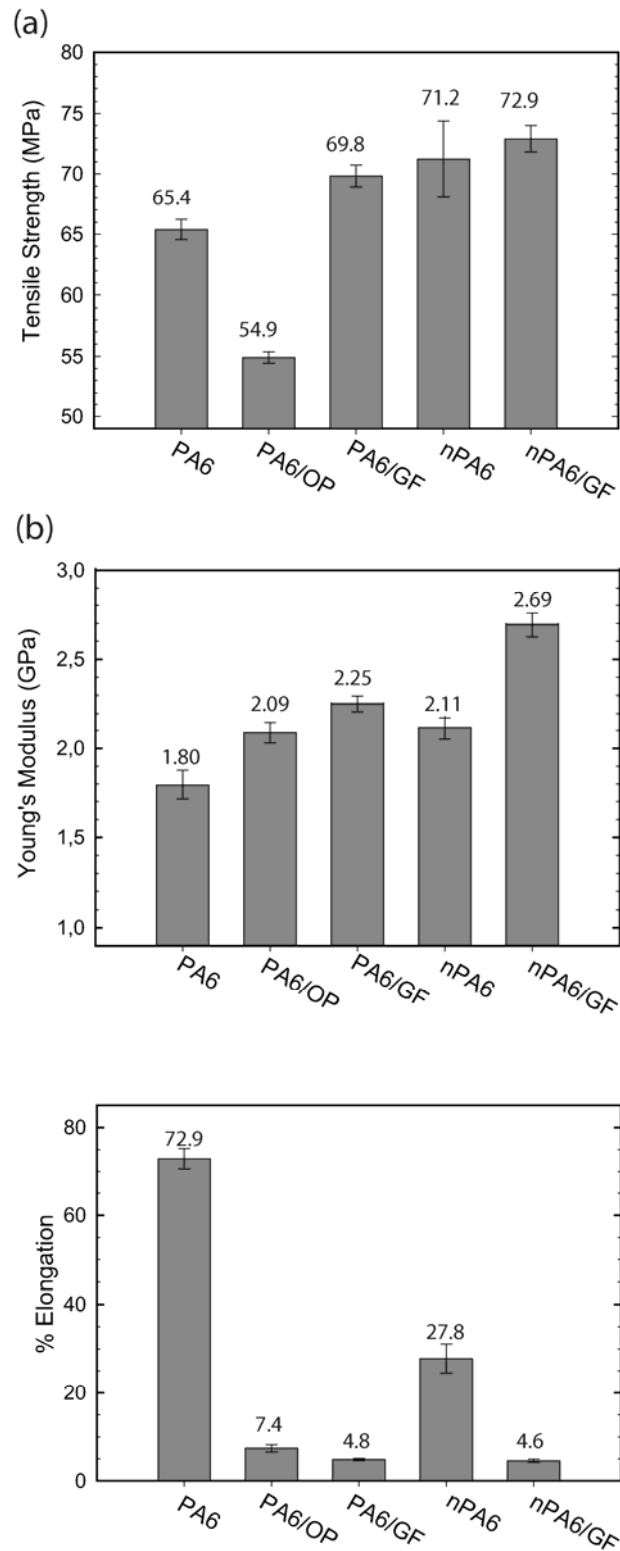


Figure 3.18 Effect of Flame Retardant, Glass Fibers and Nanoclay on the Mechanical Properties of PA6: (a) Tensile Strength, (b) Young's Modulus and (c) Elongation at Break

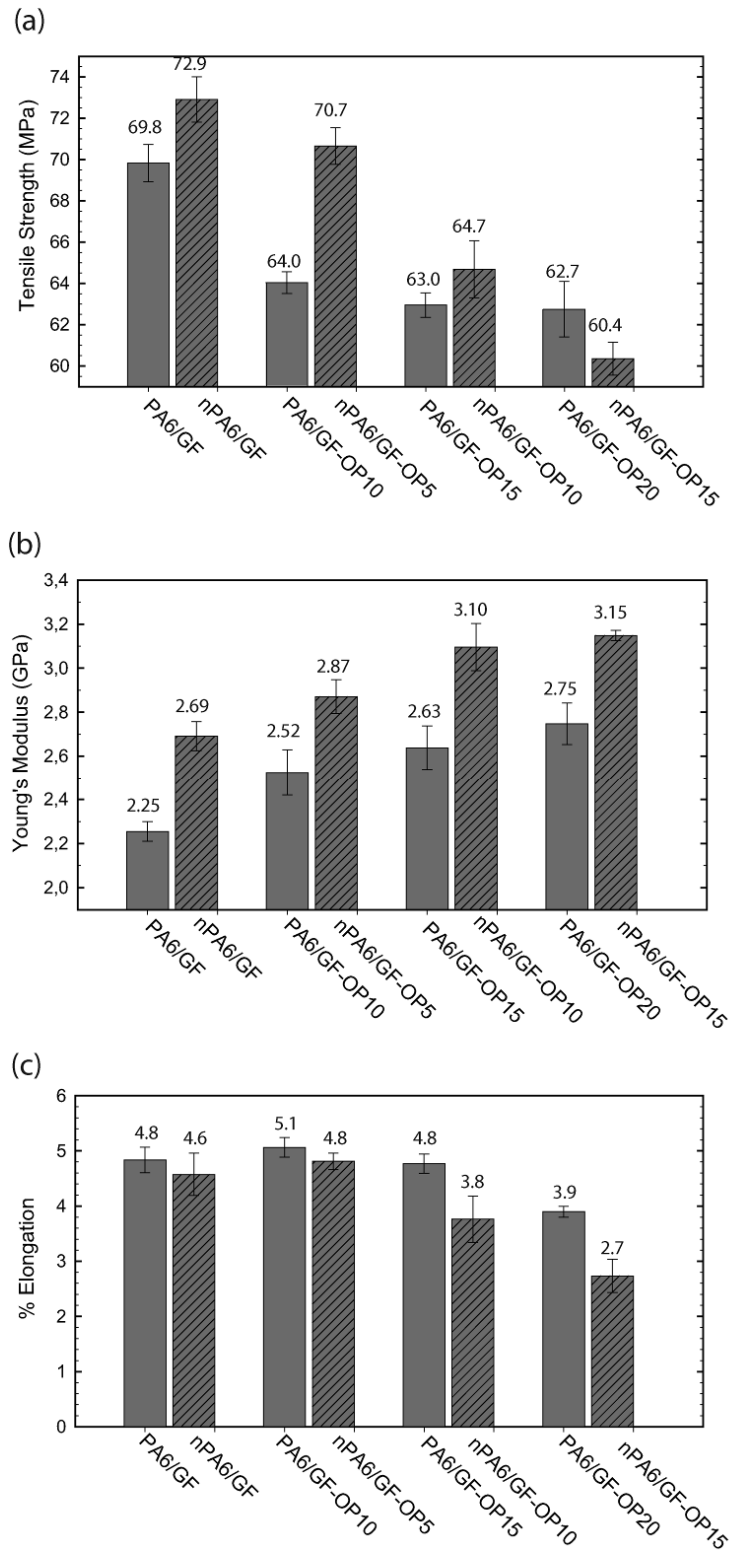


Figure 3.19 Mechanical Properties of Flame Retarded PA6 Specimens with/without Nanoclay at Equal Total Additive Content: (a) Tensile Strength, (b) Young's Modulus and (c) Elongation at Break

3.2.3 Fiber Length Distribution

After burning the samples at 800°C for 15 minutes and dispersing the fibers ultrasonically, approximately 600 fibers were counted using semi-automated image analysis software, and then fiber length distributions were determined as probability density functions. As can be seen in the optical micrograph of PA6/GF-OP15 in Figure 3.20, it is difficult to count the fiber lengths for composites containing additives that induce charring. Here in this case, the char residue produced by OP flame retardant, masks the glass fibers making them difficult to spot from the optical micrograph.

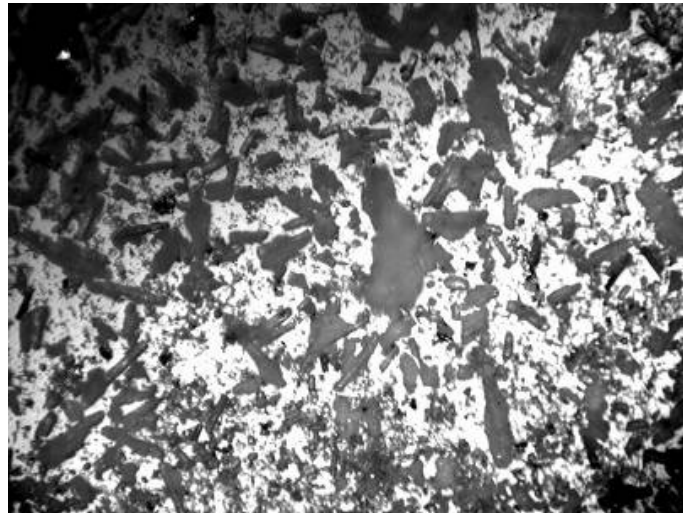


Figure 3.20 Optical Micrograph of PA6/GF-OP15 (40X Magnification)

Fiber length probability densities and number average fiber lengths are determined and given in Figure 3.21 for representative samples. Even for neat glass fiber reinforced composite PA6/GF, glass fibers are fragmented into shorter lengths to a high extend, which results from the increased residence time due to extruding all samples two times. Thus, glass fibers only contribute to a modest increase, less than expected, in the tensile strength of PA6 owing to their smaller aspect ratios.

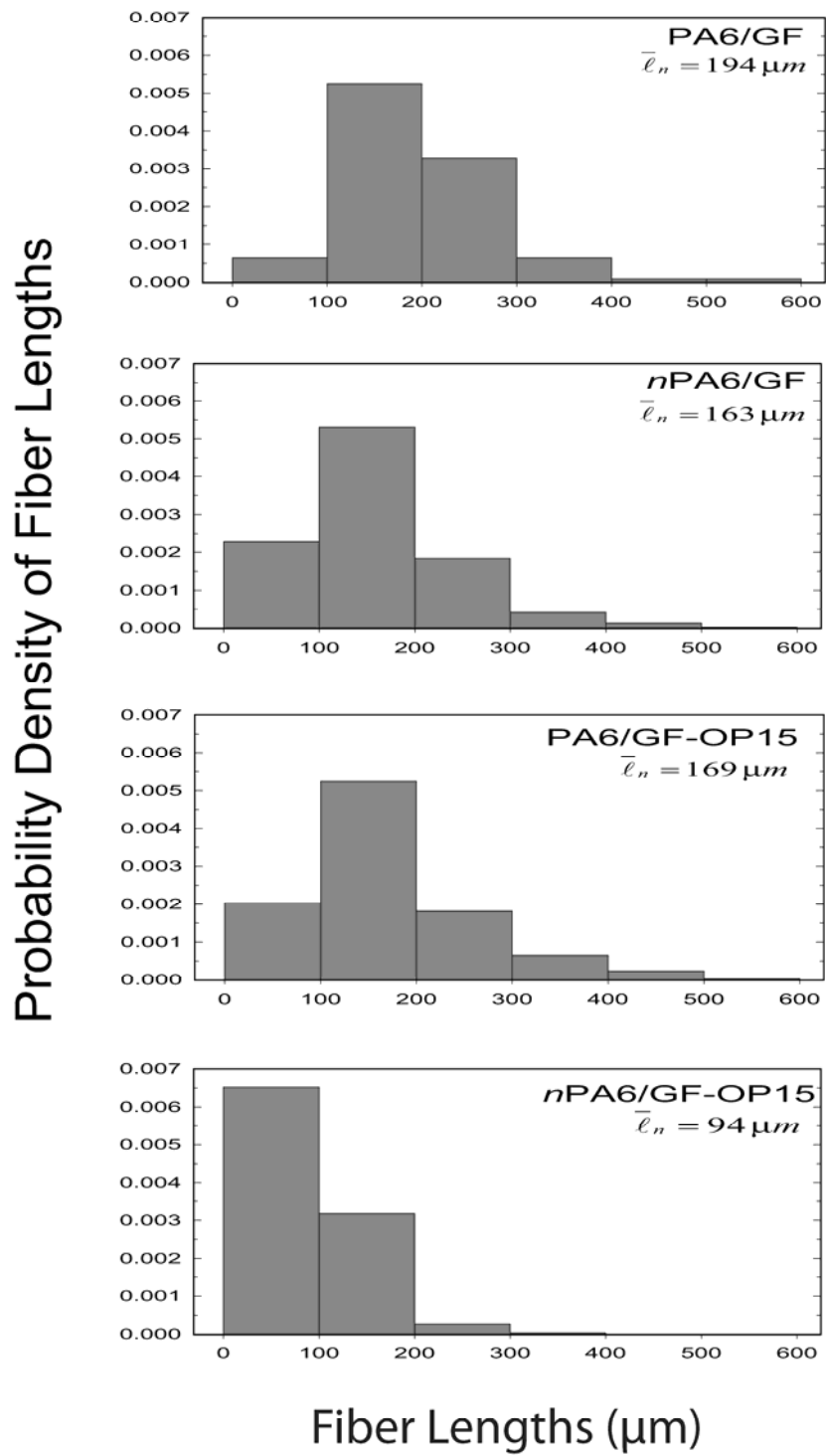


Figure 3.21 Fiber Length Probability Density Functions and Corresponding Mean Fiber Lengths for Representative Composite Samples

Upon introduction of the flame retardant and nanoclay, fiber lengths are decreased further as a result of attrition induced by these particles. As stated in Section 3.2.1, MFI value of specimens containing flame retardants and nanoclay are low. Restricted melt flow increases the residence time, and thus increases the fiber-fiber, fiber-machine and fiber-filler interactions. In the specimen of *n*PA6/GF-OP15, number average length of the fibers is smallest due to presence of both flame retardant and nanoclay.

3.2.4 Fracture Surface Morphology

SEM micrographs were taken from the fracture surfaces of the tensile test specimens at various magnifications. SEM micrograph of PA6/OP is given in Figure 3.22 and for the glass fiber reinforced compositions in Figure 3.23.

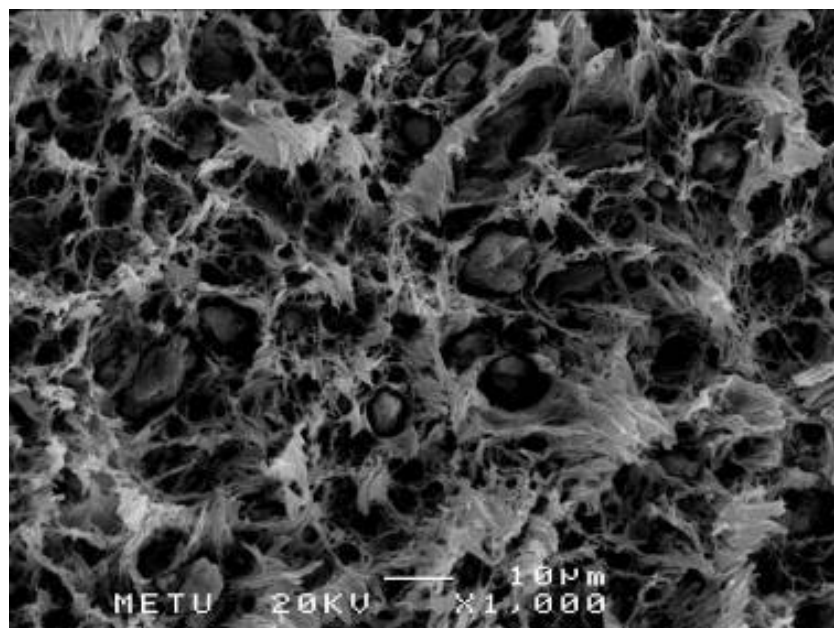


Figure 3.22 Debonding at Flame Retardant/Polymer Interface as a Consequence of Poor Adhesion in PA6/OP

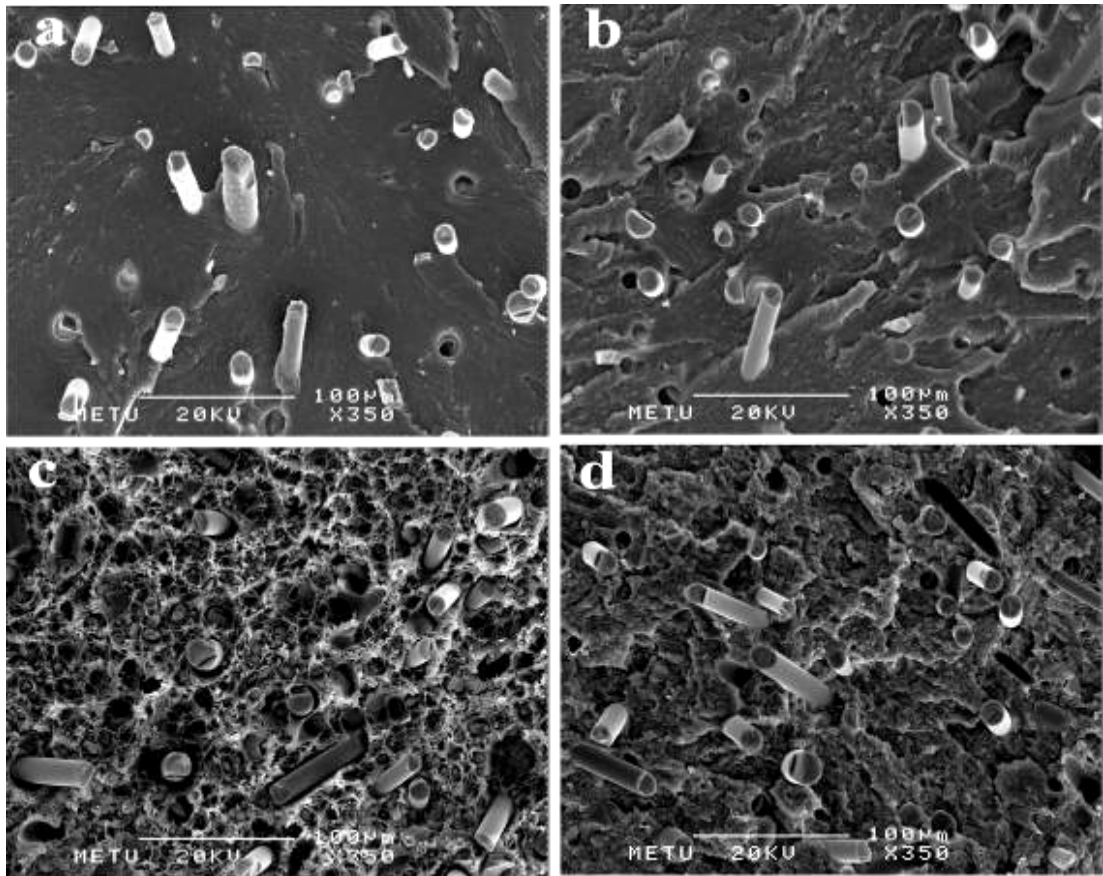


Figure 3.23 SEM Micrographs of (a) PA6/GF, (b) *n*PA6/GF, (c) PA6/GF-OP15, (d) *n*PA6/GF-OP15

Incompatibility of organo-phosphorus (OP) flame retardant with PA6 results in discontinuities in the form of debonding as seen in Figure 3.22. Poor adhesion between PA6 matrix and flame retardant particles is the major reason behind the loss of tensile strength upon addition of flame retardant. Fibrils are observed in the SEM micrograph of PA6/OP as a result of inorganic particles limiting the elongation of polymer. These fibrils start from the circumference of the flame retardant particles and expand throughout the matrix.

Fracture surface of glass fiber reinforced PA6 is given in Figure 3.23(a) showing rather better fiber/polymer adhesion. Mechanical properties are enhanced due to this strong fiber/polymer interfacial bond strength. When nanoclay is introduced, there seems to be no detrimental effect in the interface as seen in Figure 3.23(b).

On the other hand, upon addition of 15 wt% flame retardant to glass fiber reinforced PA6, tensile strength is lowered drastically. This effect can also be deduced from Figure 3.23(c) showing poor fiber/polymer interface leading to many pull-outs and debonding. Addition of nanoclay, (*n*PA6/GF-OP15) somehow decreases the number of pull-outs and the degree of debonding, as seen in Figure 3.23(d).

3.2.5 Nanoclay Dispersion

Physical properties of the polymer/clay nanocomposites are directly related to the dispersion state of the nanoclays. Superior properties are possible if the exfoliation of the clay particles is achieved. In the exfoliated polymer nanocomposites; polymer extensively penetrates between clay layers resulting in disorders and delamination of layers and finally leading to well dispersed individual layers in the thickness of nanometers in the polymer matrix.

Exfoliation can be achieved by the addition of a surfactant to the material, typically a long chain alkylammonium salt. For alkylammonium modified clays, number and magnitude of favorable polymer-surfactant interactions are maximized while minimizing the magnitude and number of apolar interactions [78].

Thus, exfoliation is thermodynamically favored by the large enthalpic contribution of the polar and hydrogen bonding interactions between clay surface modifier (methyl tallow bis-2-hydroxyethyl quaternary ammonium cation) and PA6 chains. In this study, TEM images and XRD patterns of nanocomposites revealed the exfoliated nanomorphology of clay layers.

Low magnification TEM image displayed in Figure 3.24(a) reveals the homogenous dispersion and exfoliation of organoclays in PA6 matrix. Figure 3.24(b) is a higher magnification image showing exfoliated individual clay layers preferentially oriented in the flow direction of injection molding.

XRD reflections of specimens taken after the first and second extrusion are shown in Figures 3.25 and 3.26, respectively. Disrupted registry of silicate layers, i.e. the absence of basal reflections in these XRD patterns (Figure 3.25 and 3.26) support exfoliated morphology for all the specimens containing nanoclays. It can be deduced that, first extrusion might be sufficient to obtain exfoliation. However, the idea behind extruding samples twice was not to achieve exfoliation of clays but to provide even dispersion of pellets since the feeder was not used and ingredients were fed manually. Presence of the flame retardant and/or short glass fibers seems to have no significant influence on the exfoliation of nanoclays assessed by XRD.

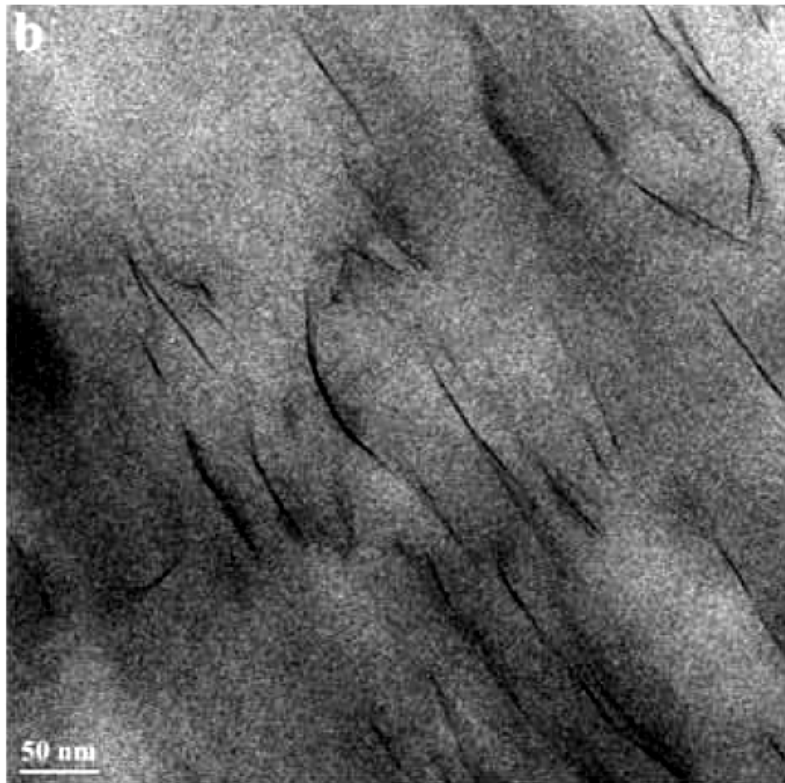
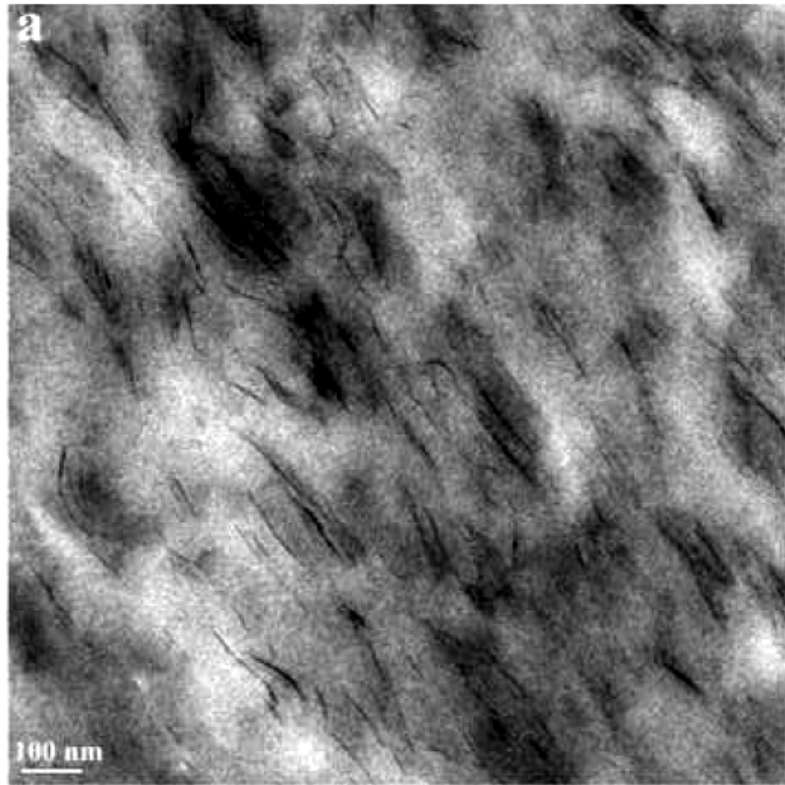


Figure 3.24 TEM images of *n*PA6 Nanocomposite at (a) Low Magnification and (b) High Magnification

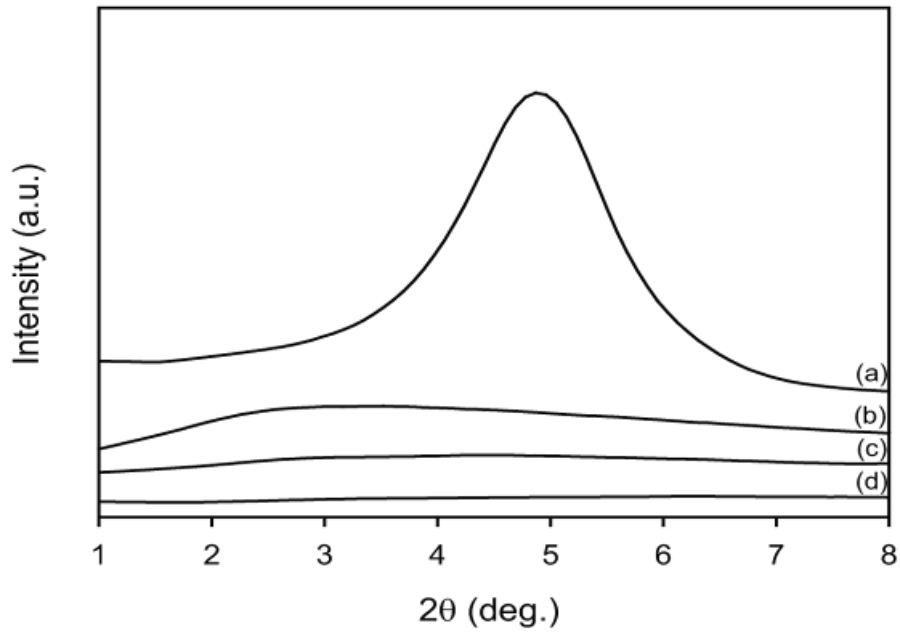


Figure 3.25 XRD Patterns after the First Extrusion of the Specimens (a) Nanoclay, (b) *n*PA6/GF, (c) *n*PA6/GF-OP15, (d) *n*PA6

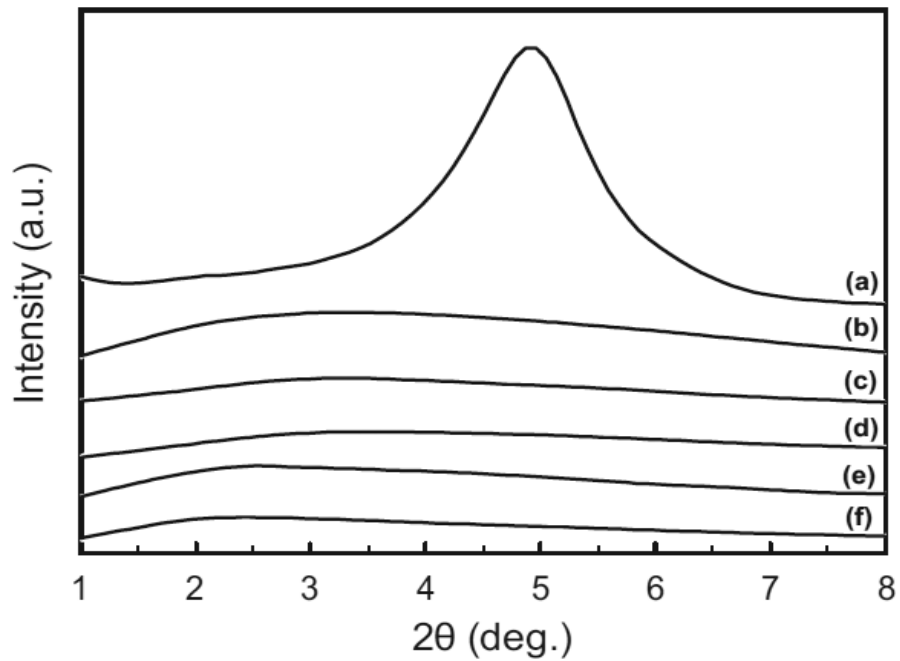


Figure 3.26 XRD Patterns after the Second Extrusion of the Specimens (a) Nanoclay, (b) *n*-PA6, (c) *n*-PA6/GF, (d) *n*-PA6/GF-OP15, (e) *n*-PA6/GF-OP10, and (f) *n*-PA6/GF-OP5

3.2.6 Thermogravimetry

Thermogravimetric analysis was carried out on representative samples to investigate the effects of nanoclay and organo-phosphorus flame retardant (OP) on the thermal decomposition of PA6. Figure 3.27 shows the thermogravimetric (TG) and differential thermogravimetric (DTG) curves of these specimens with/without nanoclay. Effects of flame retardant concentration are evaluated in Figure 3.28. Peak temperatures of differential thermogravimetry ($T_{DTG-Peak}$), 10% mass loss temperature ($T_{10\%}$), and % residue values are given in Table 3.4 for the specimens tested.

Table 3.4 Results of the Thermogravimetric Analysis.

Specimens	$T_{DTG-Peak}$ (°C)	$T_{10\%}$ (°C)	% Residue
PA6/GF	455	416	13.6
PA6/GF-OP15	425	399	18.8
<i>n</i> PA6/GF	455	408	19.6
<i>n</i> PA6/GF-OP5	450	397	21.6
<i>n</i> PA6/GF-OP10	435	384	22.2
<i>n</i> PA6/GF-OP15	418	371	25.1

Figure 3.27 and Figure 3.28 show that all specimens possess a single decomposition step. Although $T_{DTG-Peak}$ of PA6/GF and *n*PA6/GF are almost the same, $T_{10\%}$ is lowered by 8°C as shown in Table 3.4. Likewise, $T_{DTG-Peak}$ and $T_{10\%}$ are lowered 7°C and 28°C respectively in the case of *n*PA6/GF-OP15 compared to PA6/GF-OP15. Lower temperatures corresponding to maximal rate of decomposition and 10% mass loss are attributed to the catalytic activity in the presence of large surface area clay layers with protonic sites; catalyzing the degradation of PA6 [67,79,80].

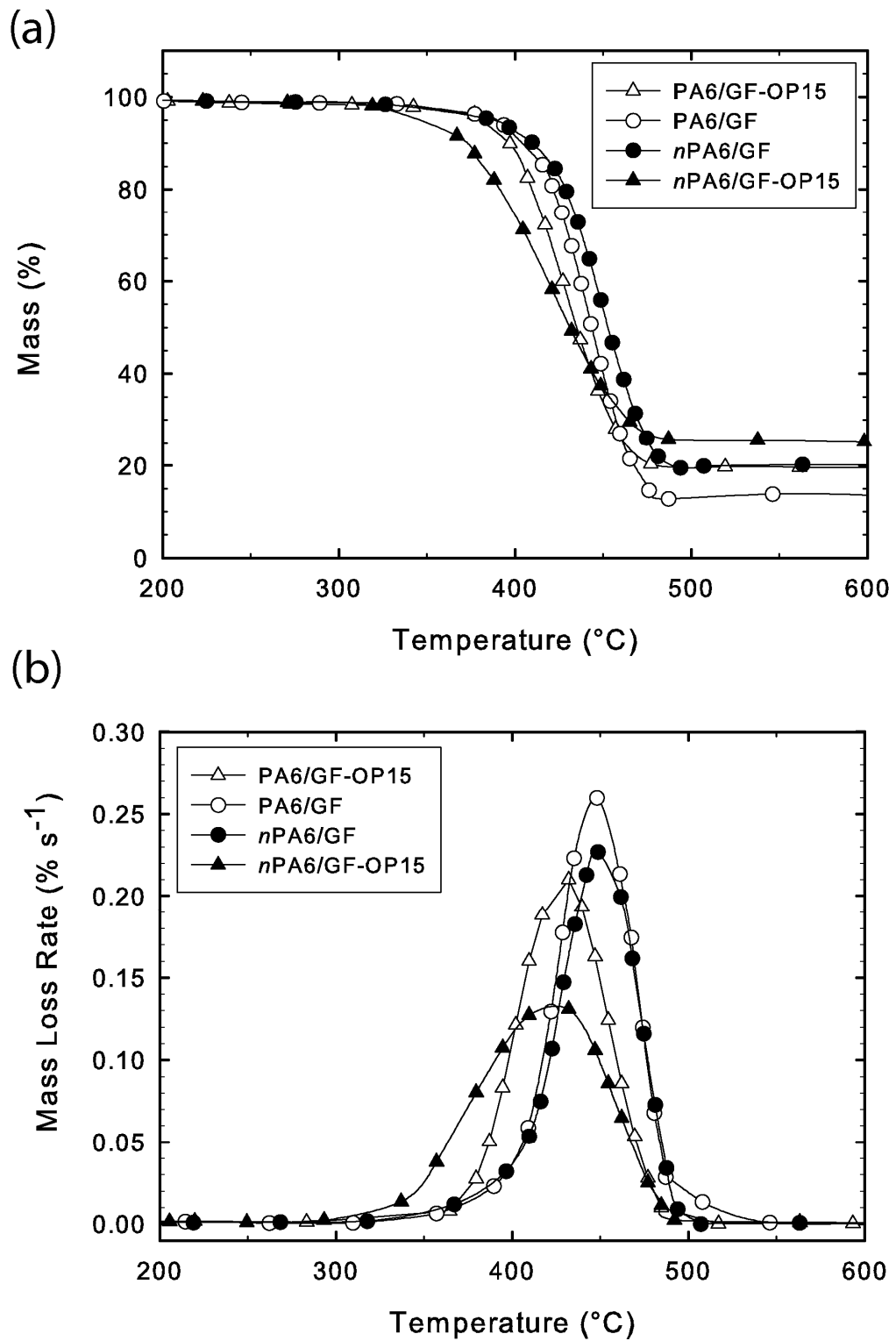
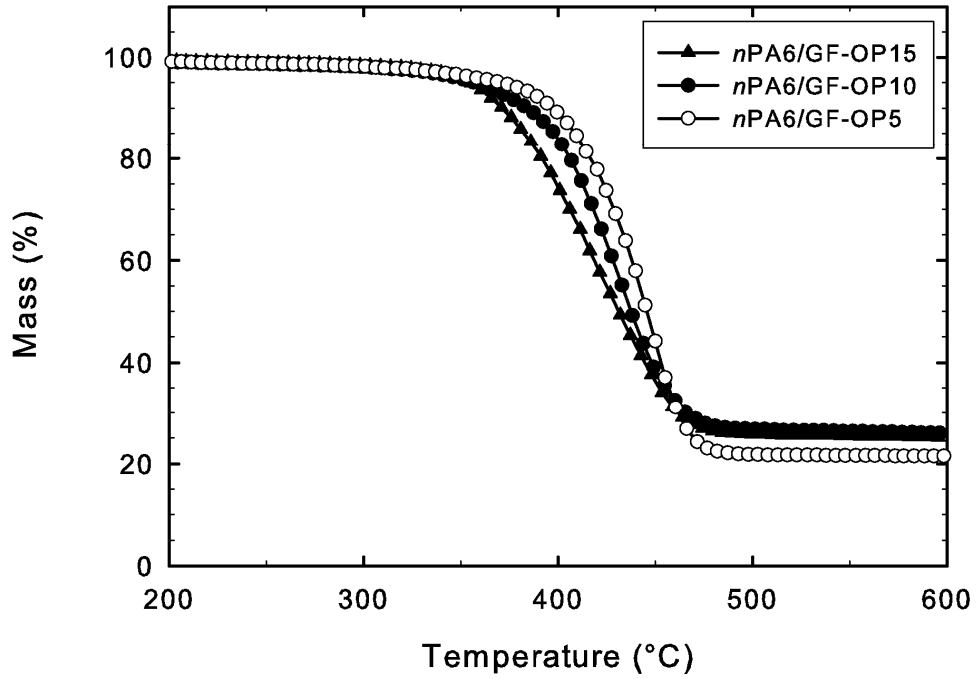


Figure 3.27 (a) Thermogravimetric, and (b) Differential Thermogravimetric Curves of the Specimens Tested

(a)



(b)

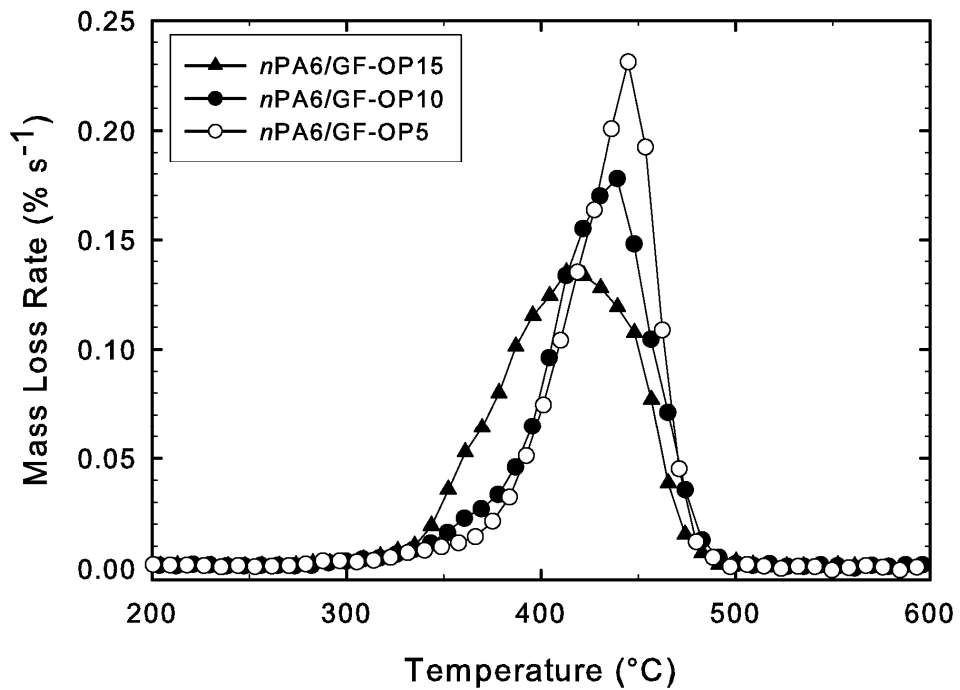


Figure 3.28(a) Thermogravimetric, and (b) Differential Thermogravimetric Curves for the Evaluation of the Effects of Flame Retardant Content

$T_{\text{DTG-Peak}}$ and $T_{10\%}$ for PA6/GF-OP15 is 30°C and 17°C lower, respectively, compared to PA6/GF as a consequence of decomposing flame retardant constituents. Decomposition of melamine polyphosphate at around 350°C [59], and evolution of phosphinates and phosphinic acids into the vapor phase [57] result in lower degradation temperatures. In addition, it is clear from $T_{\text{DTG-Peak}}$ and $T_{10\%}$ for *n*PA6/GF with varying OP content that the flame retardant shifts the degradation temperature progressively to smaller values, material containing the highest flame retardant content being the earliest to degrade as seen in Figure 3.28.

Comparing the DTG curves of PA6/GF and PA6/GF-OP15, in Figure 3.27(b), flame retardant decreases the maximal rate of mass loss by interfering with the main decomposition of PA6 with degrading flame retardant constituents. Formation of flame retarded nanocomposite (*n*PA/GF-OP15) further suppresses the peak of mass loss rate for PA6/GF-OP15. Similarly, lower mass loss rates are obtained with *n*PA6/GF compared to PA6/GF. These are attributed to the retardation of volatile evolution by means of the tortuous pathway formed by exfoliated clay layers of large aspect ratio.

It is given in Table 3.4 that PA6/GF yields a residue of 13.6 wt% corresponding solely to glass fibers. In the case of PA6/GF-OP15, char residue is 18.8 wt% while total concentration of additives is 30 wt%. Therefore, it is concluded that a significant fraction of the flame retardant volatilizes and acts in the gas phase. However, it should be noted that primary flame retardancy mechanism for organophosphorous flame retardant was stated to be a condensed phase action [81,82].

For *n*PA6/GF, considering the weight fractions of nanoclay on silicate basis (~3.5 wt%) and glass fiber residue from the reference measurement (13.6 wt%) of PA6/GF, char yield of 19.6 wt% is higher than the total inorganic filler content (17.1 wt%). This is indicative of certain polymer fraction being retained as a result of charring induced in the presence of nanoclay. Particularly, comparing PA6/GF-OP15 and *n*PA6/GF-OP15, 6.3 wt% higher char yield is obtained with the flame retarded

nanocomposite considering that the inorganic residue from nanoclay is approximately 3.5 wt%. In fact, for materials with same nominal filler content, i.e. PA6/GF-OP15 and *n*PA6/GF-OP10, char yield is still higher with nanocomposites.

Further investigations made by ATR-FTIR (Section 3.2.8 (ii)) on char residues revealed the underlying reasons behind increased amounts of char residues with nanocomposites of both PA/GF and PA6/GF-OP formulations. Finally, considering *n*PA6/GF-OP with different flame retardant contents, it is clearly seen that the amount of char residue increases in parallel with the flame retardant content.

3.2.7 Flammability and Fire Testing

Limiting Oxygen Index Test (LOI), UL-94 Vertical Burning Test and Mass Loss Cone Calorimetry measurements were conducted for all specimens.

(i) Flammability Tests: Limiting Oxygen Index (LOI) and UL-94 Vertical Burning

Results of LOI and UL-94 tests are given in Table 3.5. Despite having LOI values of 24.9% and 21.3% for PA6 and PA6/GF respectively, both being higher than the oxygen concentration in air; their UL-94 ratings are only V-2. The lower LOI value of PA6/GF arises from the “candlewick effect” which is well-established in the literature [75]. Presence of 15 wt% short glass fiber can stabilize the melt in LOI whereas dripping can not be prevented in UL-94 test during which the residue fell off and a V-2 rating of PA6 is retained.

Effectiveness of organo-phosphorus flame retardant (OP) is apparent when LOI values and UL-94 ratings of PA6/OP are compared with PA6. LOI is increased noticeably from 24.9% to 31.7% and a V-0 rating is easily attained with the incorporation of 20 wt% flame retardant.

For glass fiber reinforced PA6, LOI is increased to 24.9% upon addition of 10 wt% OP. LOI value is progressively improved with increasing OP content in flame retarded/glass fiber reinforced PA6, possessing a jump from 24.9% to 29.3% when the flame retardant concentration is changed from 10 wt% to 15 wt%. LOI value increases further to 30.2%, when the flame retardant content is 20 wt%. For flame retarded/glass fiber reinforced PA6, V-0 rating is obtained in UL-94, for all compositions except for the lowest concentration of the flame retardant utilized here, i.e. 10 wt%.

Table 3.5 Results of the Flammability Tests

Specimens	LOI	UL-94
PA6	24.9 ± 0.4	V-2
PA6/OP	31.7 ± 0.6	V-0
PA6/GF	21.3 ± 0.2	V-2
PA6/GF-OP10	24.9 ± 0.2	V-1
PA6/GF-OP15	29.3 ± 0.4	V-0
PA6/GF-OP20	30.2 ± 0.6	V-0
<i>n</i> -PA6/GF	22.4 ± 0.3	Fail
<i>n</i> -PA6/GF-OP5	29.1 ± 0.2	V-1
<i>n</i> -PA6/GF-OP10	30.9 ± 0.4	V-0
<i>n</i> -PA6/GF-OP15	31.7 ± 0.7	V-0

Glass fiber and nanoclay reinforced PA6 without the flame retardant shows only a modest enhancement in LOI compared to PA6/GF. Dripping of PA6/GF is prevented by after the addition of nanoclays, thus the specimen burns for longer periods without dripping, and fails from UL-94 vertical burning test. The disappointing results in LOI and UL-94 have been the discussion of a number of studies investigating the flammability of nanocomposites without conventional flame

retardants stating that for improved flame retardancy they should not be used alone but in combination with conventional flame retardants [31,69].

Flame retarded/glass fiber reinforced nanocomposites have impressive LOI values even at a very low concentration of the flame retardant (5 wt%). Comparing PA6/GF-OP10 and *n*-PA6/GF-OP5 having nominally the same filler concentration of 10 wt% (apart from glass fiber reinforcement), LOI of the nanocomposite (29.1%) is unambiguously superior to that of the conventional composite (24.9%). However, UL-94 classification of V-1 obtained by PA6/GF-OP10 is not improved by nanocomposite formation in *n*PA/GF-OP5 due to the stringent ignition conditions and geometry of the UL-94 test.

To generalize, when 5 wt% of the flame retardant is replaced by the same amount of nanoclays, e.g. PA6/GF-OP10 and *n*-PA6/GF-OP5, improvements in LOI are substantial for all three concentrations of the flame retardant utilized in this study. In *n*PA/GF-OP10, it increased to 30.9% from 29.3% of PA6/GF-OP15. Likewise, comparing *n*PA/GF-OP15 with PA6/GF-OP20; LOI is improved to 31.7% from 30.2%. UL-94 classifications of the flame retarded/glass fiber reinforced materials are maintained as either V-1 or V-0 with the mentioned replacements of 5 wt% of flame retardant with nanoclay, contrary to the deteriorated ratings reported previously [69,83].

(ii) Fire Performance Assessment by Mass Loss Cone Calorimeter (MLC)

Fire performances of the samples were characterized by using Mass Loss Cone Calorimeter (MLC), at an external heat flux of 35 kW/m². Data are evaluated in the forms of (a) Heat Release Rate (HRR) versus Time, (b) Total Heat Evolved (THE) versus Time, and (c) Mass Loss Rate (MLR) versus Time curves.

These curves are drawn for three different cases; Figure 3.29 to compare the effects of glass fibers (GF), organo-phosphorus flame retardant (OP) and nanoclay (*n*) generally; Figure 3.30 and 3.31 for the effects of OP content and nanoclay in the

glass fiber reinforced PA6, respectively. Then, interpreted data are also tabulated in Table 3.6.

Figure 3.29(a) shows that PA6/GF possesses extended total burning time and a lower peak heat release rate (PHRR) through slowing down of polymer transport into the pyrolysis zone. However, Figure 3.29(b) indicates that THE values are not altered much considering the diluting effect of glass fibers. Upon formation of nanocomposite (*n*PA6/GF) PHRR value is reduced and burning time is increased. Incorporation of an organophosphorous flame retardant into PA6, leads to the largest suppression in PHRR together with longest burning time. Longer burning times were previously reported when the flame retardants promoting the charring are employed [66]. Significant decrease in THE value, after the addition of flame retardant is seen in Figure 3.29 (b).

Mass Loss Rate (MLR) curves displayed in Fig. 3.29(c) shows that, for PA6 and PA6/GF, shapes of HRR and MLR curves are similar as an indication of a condensed phase action of glass fibers. Particularly for *n*-PA6/GF, MLR curve possess an initial increase in rate of mass loss followed by a gradual smooth decrease until extinction by the act of the established barrier. More importantly, even though *n*-PA6/GF and PA6/OP have similar mass loss rates, heat release rates are remarkably different due to the fact that PA6/OP shows an effective gas phase action reducing PHRR.

HRR, THE and MLR curves of PA6 glass fiber reinforced composites, at varying flame retardant concentrations are shown in Figure 3.30. As can be seen in Figure 3.30(a), addition of 10 wt% flame retardant to PA6/GF suppresses PHRR value by 52%. Increasing the flame retardant concentration to 15 wt% and 20 wt% causes further reductions in PHRR decreasing it by 57% and 62%, respectively compared to PA6/GF. However, total heat evolved (THE) values are not altered with flame retardant concentration as shown in Figure 3.30(b). Mass loss rate (MLR) curves shown in Figure 3.30(c) have an initial increase before a char barrier is formed and then they decrease gradually.

Figure 3.31 shows HRR, THE and MLR curves of glass fiber and nanoclay reinforced PA6 with various flame retardant content. It is seen that PHRR and THE values decrease with increasing OP content (Figure 3.11 (a),(b)). In the mass loss rate curves (Figure 3.31(c)), a hunchback like pattern is observed in the early minutes of the combustion. This pattern is a characteristic of thick-charring materials. MLR increases until a consolidated char layer is formed. After the formation of the char barrier mass loss is restricted and MLR decreases.

In order to show the synergistic effect of nanoclay, heat release curves of PA6/GF-OP15 and *n*PA6/GF-OP10 (each having same nominal additive concentration) together with their non-flame retarded compositions are re-drawn in Figure 3.32. It is inferred from Figure 3.32 that burning characteristics of PA6/GF is altered such that PHRR is largely suppressed and burning time is extended with the incorporation of the flame retardant. Clay nanocomposite, *n*-PA/GF-OP10, provides further extension of burning time owing to the formation of a thick and consolidated barrier char layer. In fact, the initial increase of heat release rate and following steady burning plateau possessed by *n*-PA/GF-OP10 is a reflection of thick charring on the heat release behavior [77].

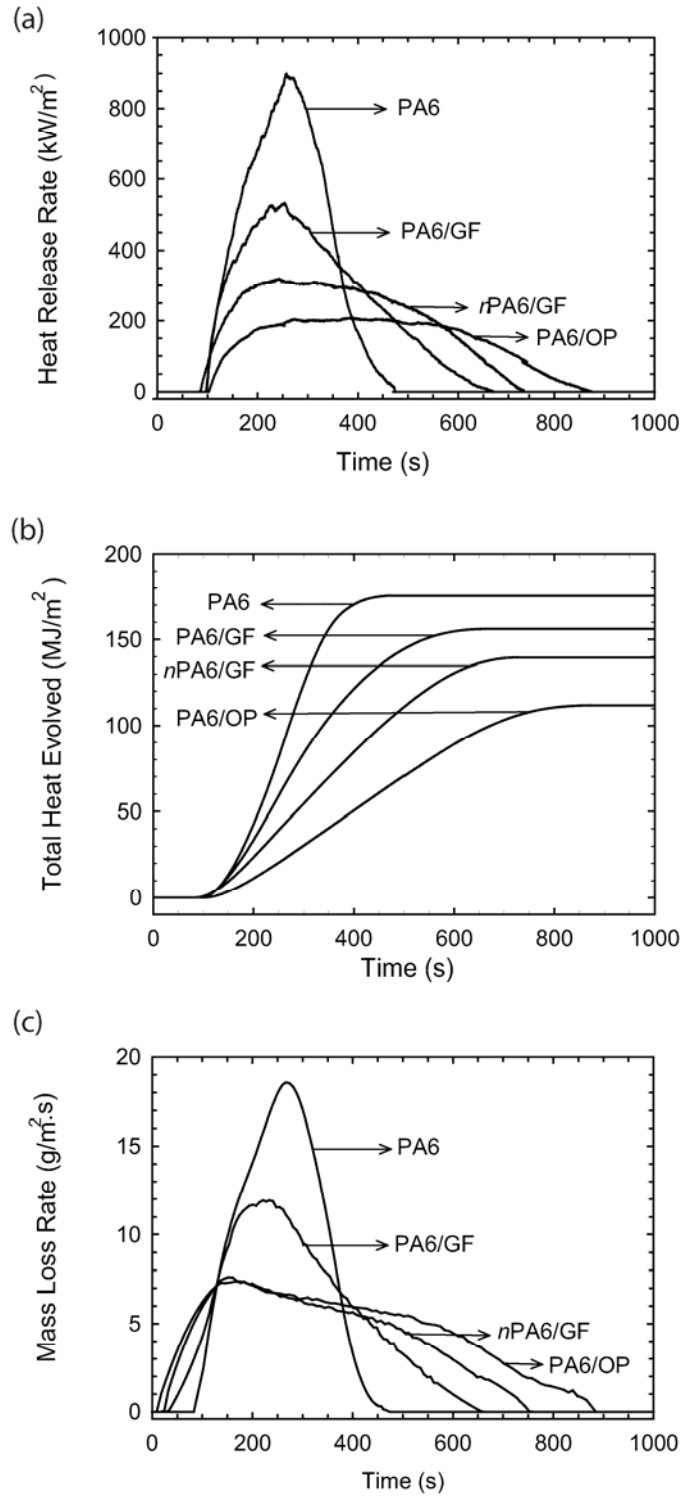


Figure 3.29 Cone Calorimeter Data to Compare generally the Effects of Glass Fibers (GF), Organo-phosphorus Flame Retardant (OP) and Nanoclay (*n*): (a) HRR, (b) THE and (c) MLR Curves

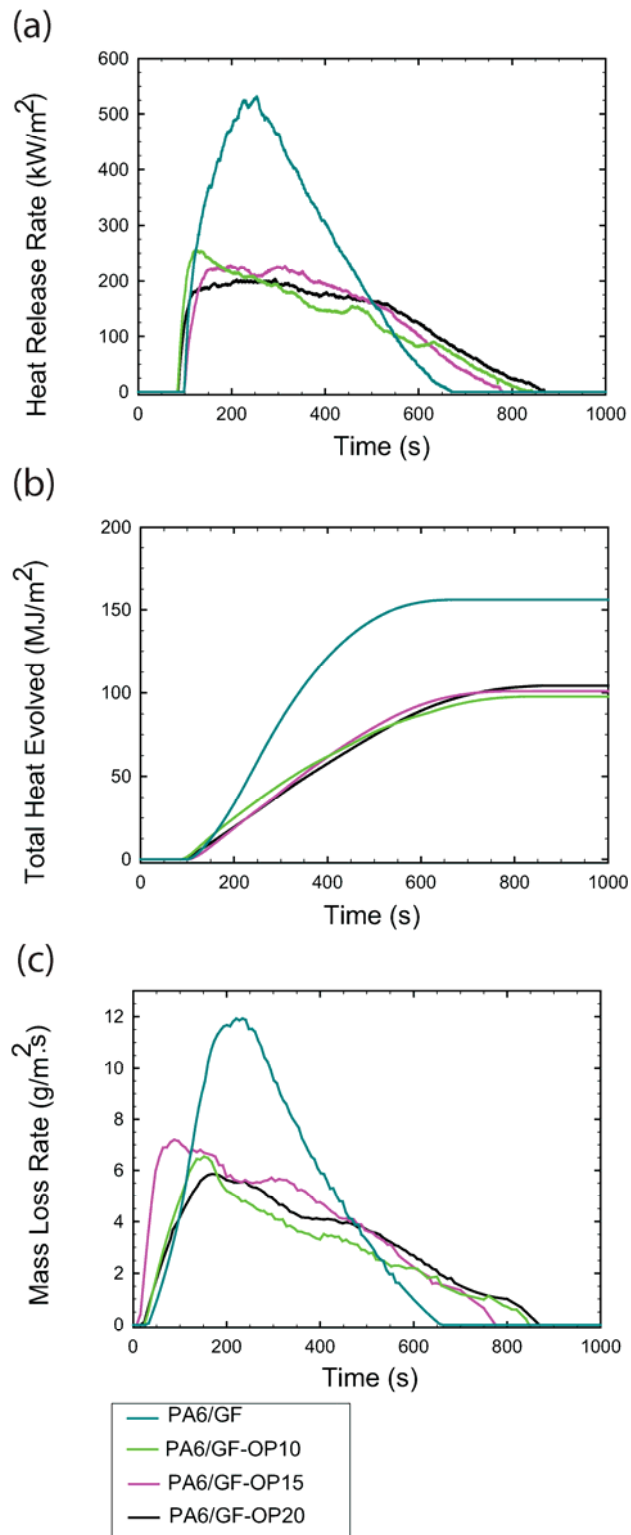


Figure 3.30 Cone Calorimeter Data to Compare the Effects of OP Content in the Glass Fiber Reinforced PA6.

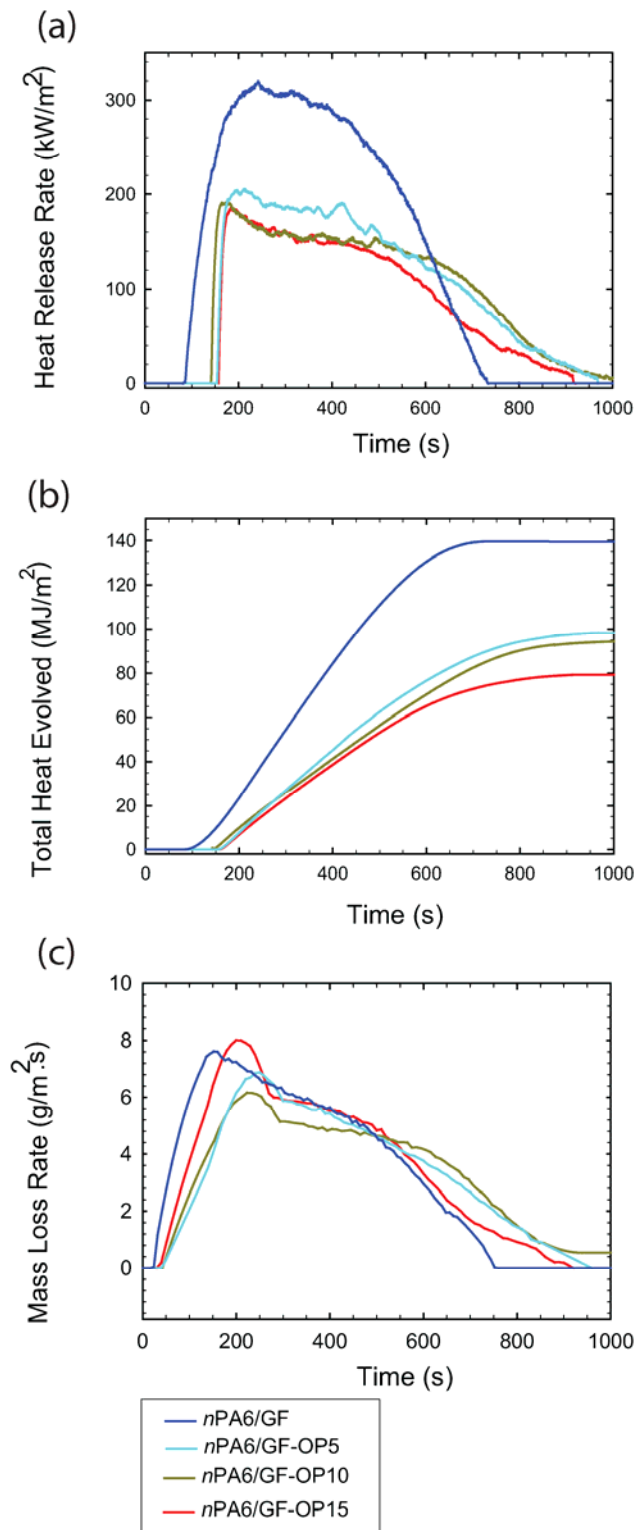


Figure 3.31 Cone Calorimeter Data to Compare the Effects of OP Content in the Glass Fiber and Nanoclay Reinforced PA6.

Table 3.6 Cone Calorimetry Results for Glass Fiber and Nanoclay Reinforced PA6

Specimens	Total Heat Evolved (THE) (MJ/m ²)	Peak Heat Release Rate (PHRR) (kW/m ²)	Time to Ignition (TTI) (s)	Total Burning Time (TBT) (s)	Fire Growth Index (FGI) (PHRR/TTI)	Total Mass Loss (TML) (g)	THE/TML ratio (MJ/m ² .g)
PA6	175	899	98	376	9.2	43.6	4.1
PA6/OP	112	208	101	774	2.1	38.9	2.9
PA6/GF	156	532	99	570	5.4	40.3	3.9
PA6/GF-OP20	104	203	85	784	2.4	36.9	2.8
PA6/GF-OP15	101	228	97	679	2.4	37.4	2.7
PA6/GF-OP10	98	255	84	761	3.0	36.3	2.7
<i>n</i> PA6/GF	139	320	80	653	4.0	37.4	3.7
<i>n</i> PA6/GF-OP15	76	178	157	757	1.1	36.8	2.1
<i>n</i> PA6/GF-OP10	94	191	141	861	1.4	35.8	2.6
<i>n</i> PA6/GF-OP5	98	205	154	815	1.3	36.4	2.7

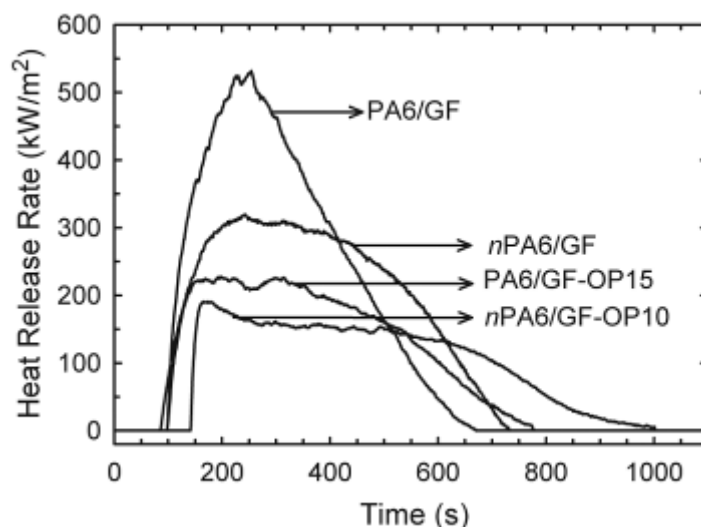


Figure 3.32 Heat Release Rate Curves Showing the Synergistic Effect of Nanoclay with OP

In order to emphasize nanoclay synergism, cone calorimeter data are reevaluated in Figure 3.33 in the form of Peak Heat Release Rates (PHRR), Total Heat Evolved (THE), Time to Ignition (TTI) and Fire Growth Index (FGI) charts. In Figure 3.33, open circles shows glass fiber reinforced PA6 composites with varying OP content, while filled circles represent nanoclay and glass fiber reinforced composites of PA6 with varying OP content.

Figure 3.33(a) and Table 3.6 show that *n*PA6/GF nanocomposite suppresses the PHRR of PA6/GF by 40% owing to the carbonaceous barrier formed on the exposed surface of the specimen by migration and accumulation of clay layers dispersed at the nano-scale. Considering PA6/GF-OP formulations, PHRR is reduced in parallel with flame retardant contents by 52%, 58% and 62%, with respect to PA6/GF. In the nanoclay containing specimens, similar reductions are obtained with flame retardant contents of by 36%, 41%, 45%, with respect to *n*-PA6/GF. When PA6/GF-OP and *n*-PA6/GF-OP with same nominal filler contents (dashed lines in Figure 3.33(a)) are considered, further PHRR reductions of 20%, 16% and 13% could be attained with nanocomposite formulations in the order of increasing total filler content.

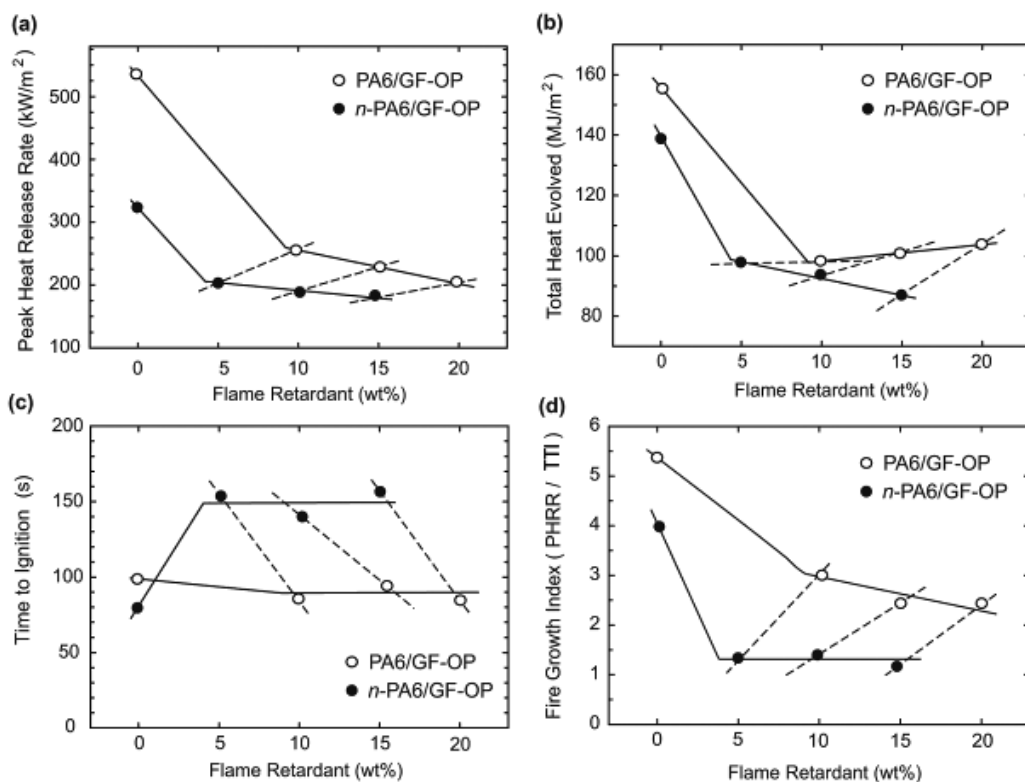


Figure 3.33 Re-evaluation of Cone Calorimeter Data for Nanoclay Synergism; (a) Peak Heat Release Rate, (b) Total Heat Evolved, (c) Time to Ignition, and (d) Fire Growth Index. (Dashed lines indicate equal nominal filler contents, i.e. nanoclay + flame retardant)

Comparing PA6/GF with *n*PA6/GF, total heat evolved (THE) values given in Figure 3.33(b) and Table 3.6 a minor reduction caused mainly by dilution of fuel via inorganic filler content. Due to stabilization of a certain PA6 fraction by catalytic charring, THE is remarkably lowered with the addition of the flame retardant in PA6/GF and *n*-PA6/GF. It can be inferred from Figure 3.33(b) that THE is more or less independent of flame retardant content with PA/GF-OP formulations, whereas a progressive reduction is obtained as a result of char enhancement and strengthening in the presence of the nanoclay. Furthermore, regarding materials with same nominal filler content (dashed lines in Figure 3.33(b)), increasing flame retardant loading leads to larger reductions in THE obtained by nanocomposite formulations.

It is given in Figure 3.33(c) that *n*-PA6/GF ignites earlier than PA6/GF as a result of acid catalyzed degradation of polyamides[75] via protonic sites formed within clay galleries upon degradation of the organic modifier [67,79,80]. However, for *n*-PA/GF-OP formulations, an opposite effect is observed such that strong and consolidated char impedes the evolution of flammable volatiles. Consequently, ignition is delayed in nanocomposites when materials with same nominal filler content are considered, indicated by dashed lines in Figure 3.30(c). Time to ignition (TTI) values suggest that flame retardant content imparts no alteration in ignitability for both PA/GF-OP and *n*-PA/GF-OP formulations.

It is discussed in the work of Petrella [39] that Fire Growth Index (FGI) defined by PHRR/TTI makes a reasonable attempt at assessing the flame spread as a fire hazard. It can be inferred from Figure 3.33(d) that substitution of 5 wt% flame retardant with nanoclays significantly lowers FGI owing to reduced PHRR and delayed ignition.

It is well established that the mechanism of flame retardancy can be addressed considering the ratio of Total Heat Evolved to Total Mass Loss (THE/TML) which helps to investigate the availability of gas phase action. Table 3.6 shows that, THE/TML Ratio for PA6 is reduced from 4.1 MJ/m²g to 2.9 MJ/m²g with the addition of the flame retardant. PA/GF gives a THE/TML value of 3.9 MJ/m²g, which is reduced on the average to 2.8 with PA6/GF-OP formulations. Therefore, it can be concluded that, in addition to a dominant condensed phase action by means of barrier formation, flame inhibition and dilution are also present as gas phase flame retarding mechanisms. As a matter of fact, Braun et al [57] have shown that evolution of melamine, diethyl phosphinic acid and aluminum-zinc phosphinates constitute the gas phase action of OP flame retardant.

Considering nanocomposites of PA6/GF-OP formulations, no significant alteration is observed in the values of THE/TML Ratio. The average value of 2.8 MJ/m²g for PA6/GF-OP becomes 2.6 MJ/m²g on the average for *n*-PA6/GF-OP formulations, the change being in the range of experimental error margin. Hence, combining the reductions in PHRR and unaltered THE/TML values, it is concluded that the

condensed phase action is amplified, mainly owing to the formation of a stronger boron-aluminum phosphate barrier reinforced at the nanoscale.

3.2.8 Residue Characterization

Burnt specimens after Mass Loss Cone Calorimetry (MLC) analysis are further analyzed for their char structures.

(i) Morphology of the Char

Macroscopic appearances of char residues serving as barriers during cone calorimetry are given in Figure 3.34 while their microscopic morphology by SEM micrographs are shown in Figure 3.35.

Figure 3.34(a) and Figure 3.35(b) show that the residue of *n*-PA6/GF possesses a loose structure suffering from major cracks. It is once again to be noted that improved cone calorimetric performance can be obtained with the incorporation of nanoclays into glass fiber reinforced polymer. However, legitimate flame retardancy is known to be obtained if a nanoclay and a conventional flame retardant is used in combination.

Residue from PA6/OP displayed in Figure 3.35(a) shows intumescence. Similarly, PA6/GF-OP residue shown in Figure 3.34(b) and Figure 3.35(c) possesses intumescent natures with the carbonaceous char being thin and mechanically weak.

It is clear that the residues reinforced at the nanoscale (Figure 3.34(c),(d) and Figure 3.35 (b),(d)) are much more effective barriers in impeding mass and heat transfer when compared to residues without the nanoclay (Figure 3.34(b) and Figure 3.35(c)). Figure 3.34(c),(d) reveal that the structure of the barrier is improved with increasing flame retardant content. Thus, as concluded above, strong nature of the chars formed from flame retarded and glass fiber reinforced nanocomposites provides significant improvements in flame retardancy.

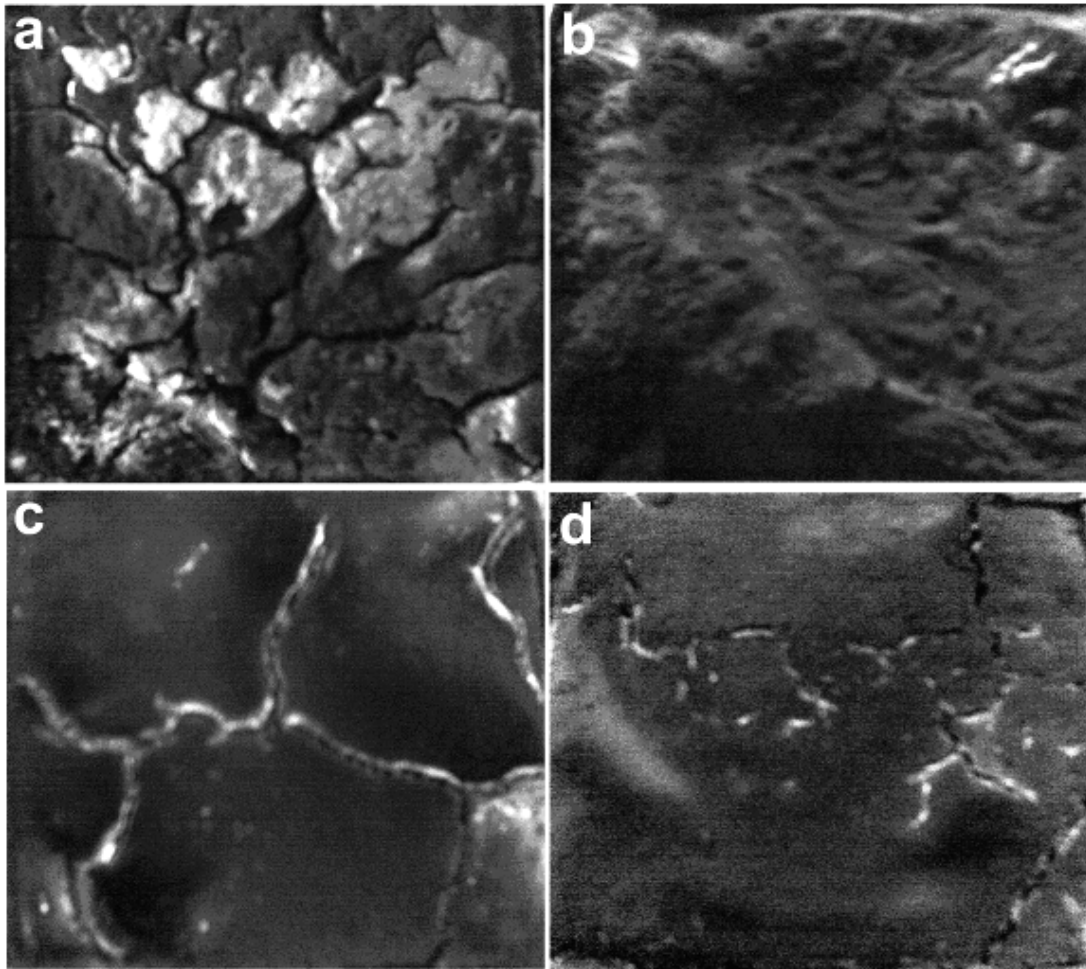


Figure 3.34 Macroscopic Appearances of Char Residues after Cone Calorimetry (Full Upper Surfaces of 100x100 mm Specimens are Displayed): (a) *n*-PA6/GF, (b) PA6/GF-OP15, (c) *n*-PA6/GF-OP5, and (d) *n*-PA/GF-OP15

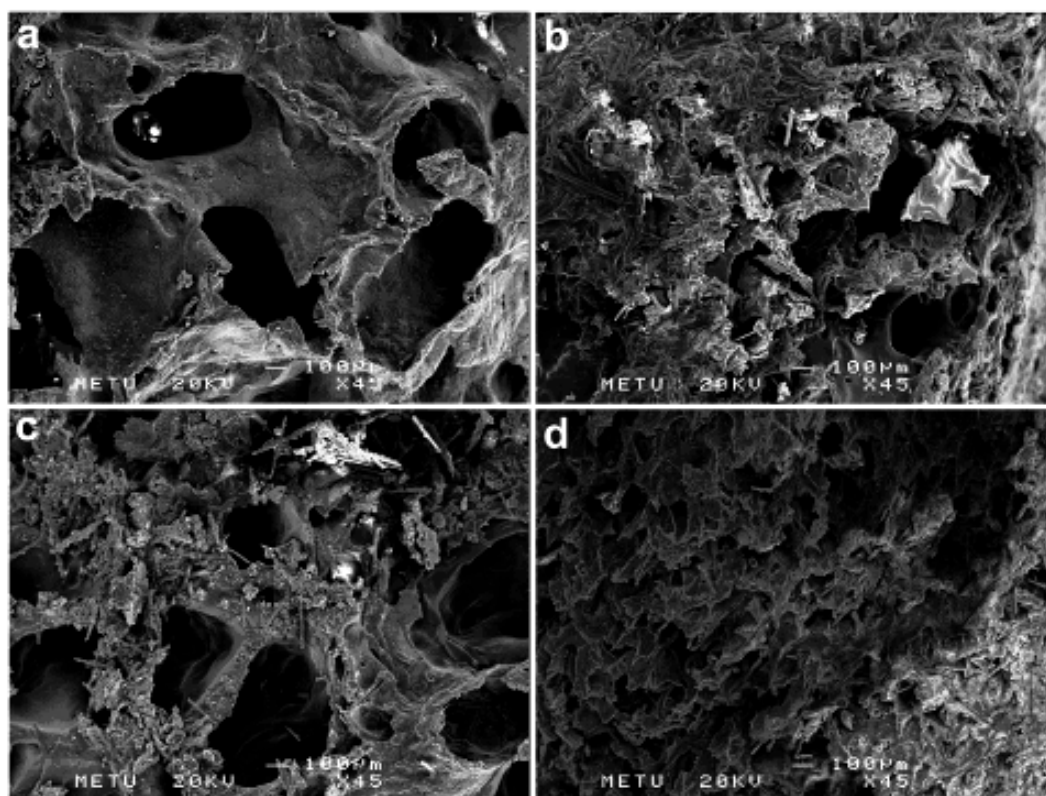


Figure 3.35 SEM Micrographs Displaying the Char Morphologies of (a) PA6/OP, (b) *n*-PA6/GF, (c) PA6/GF-OP15, and (d) *n*-PA6/GF-OP

(ii) Infrared Spectroscopy

ATR-FTIR spectra of the burnt specimens with and without nanoclay are given in Figure 3.36 and 3.37, respectively. The spectrum for PA6/GF residue (Figure 3.36(a)) includes a diffuse band around 930 cm^{-1} which corresponds to the superposition of bridging oxygen in Si-O-Si and terminal Si-O stretching vibrations [84]. The small band around 680 cm^{-1} is attributed to bending vibrations of Si-O-Si bridging oxygen atoms, and an additional small band around 1400 cm^{-1} corresponds to glass fibers [57].

The spectra recorded from PA6/OP residue (Figure 3.36(b)) involve a sharp peak at 1080 cm^{-1} and a shoulder around 1020 cm^{-1} which are attributed to asymmetric stretching (ν_3) of PO_4^{3-} in boron phosphates. Small shoulder appearing near 960 cm^{-1} arises from symmetric stretching vibrations (ν_1) of PO_4^{3-} . Small signal at 780 cm^{-1}

matches with the most intense signal of neat organic phosphinate (characterized by reference measurements) which indicates that certain amount of flame retardant remains without decomposing. An additional broad peak appears at 1600 cm^{-1} which indicates the formation of an aromatic ring breathing mode or C=C of conjugated polyene structure. It was shown by Holland and Hay [2] that it is practically impossible to identify whether the band at 1600 cm^{-1} corresponds to aromatic or conjugated species. Nevertheless, aromatic or conjugated species indicate a partial stabilization of polymer degradation product in the condensed phase by the act of OP flame retardant. Residue from PA6/GF-OP15 (Figure 3.36(c)) contains an additional shoulder around 930 cm^{-1} , which is characteristic of glass fibers, when compared with the residue of PA6/OP (Figure 3.36(b)).

Figure 3.36 shows the spectra of the residues from *n*-PA6/GF-OP15, *n*-PA6/GF, and PA6/GF. Absorption band for Si-O stretching in montmorillonite is at 1030 cm^{-1} determined by measuring reference spectra, and from the literature [85]. Spectrum for the residue of *n*-PA6/GF, given in Figure 3.37(b), contains a sharp peak around 1030 cm^{-1} which is characteristic of montmorillonite and a shoulder around 930 cm^{-1} corresponding to Si-O-Si and Si-O stretching in glass fibers. Similar to previous discussions regarding specimens with no nanoclays, formation of a band at 1600 cm^{-1} indicates the presence of aromatic or conjugated degradation products of nylon stabilized in the residue.

Considering the residue of *n*-PA/GF-OP15 (Figure 3.37(c)), an additional shoulder appears around 1115 cm^{-1} as an evidence for the formation of aluminum phosphates such as aluminum ortho-, pyro- and poly-phosphates [57]. Here, bands for phosphate absorption in boron phosphates are masked by the strong absorption of montmorillonite in nanoclay containing residue. This restricts further conclusions on the composition of the residue. Nevertheless, presence of the nanoclay altered the reactivity of aluminum phosphinate, melamine polyphosphate and zinc borate flame retarding species in such a way that aluminum phosphates are preferentially formed contrary to the specimens without nanoclay.

The mechanism for this behavior can be explained by considering the well-known barrier effect of nano-dispersed clay layers. Diffusion of volatile species generated at elevated temperatures attained during cone calorimeter test is restricted by the tortuous pathway formed by the clay layer network [86]. Of particular interest to our case, retardation of gaseous aluminum phosphinate evolution by means of the nanoconfinement effect of exfoliated clay layers provide the formation of aluminum phosphates. Similarly, Braun et al [57] previously showed that when the vaporization of aluminum phosphinates is restricted through the utilization of large external heat fluxes in the cone calorimeter test, aluminum phosphate is formed instead acting as an effective flame retardant in the condensed phase.

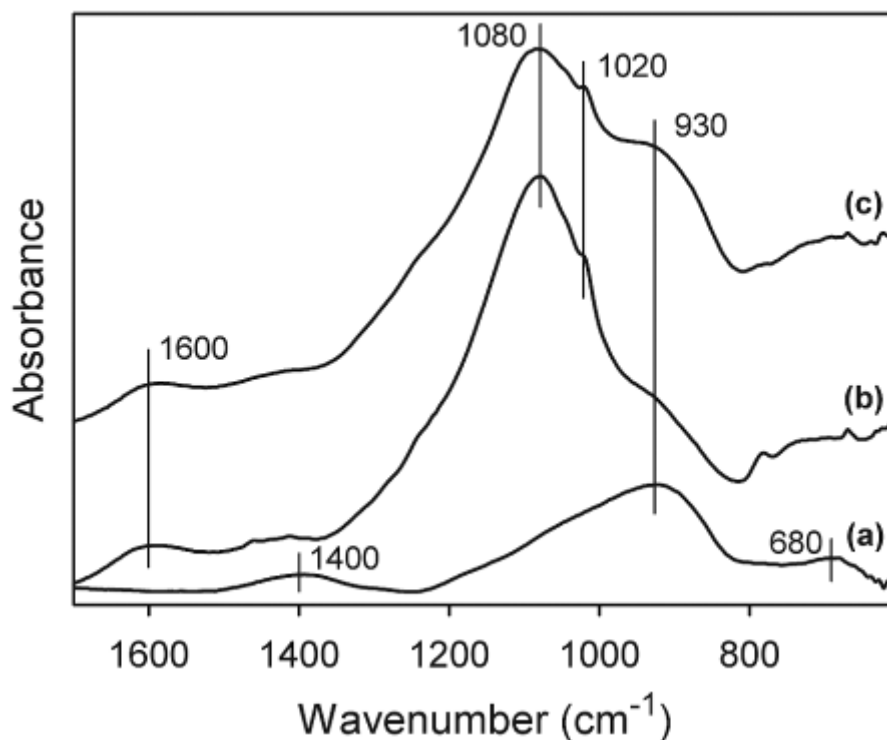


Figure 3.36 ATR-FTIR Spectra of Combustion Residues from Specimens without Nanoclay: (a) PA6/GF, (b) PA6/OP, (c) PA6/GF-OP15

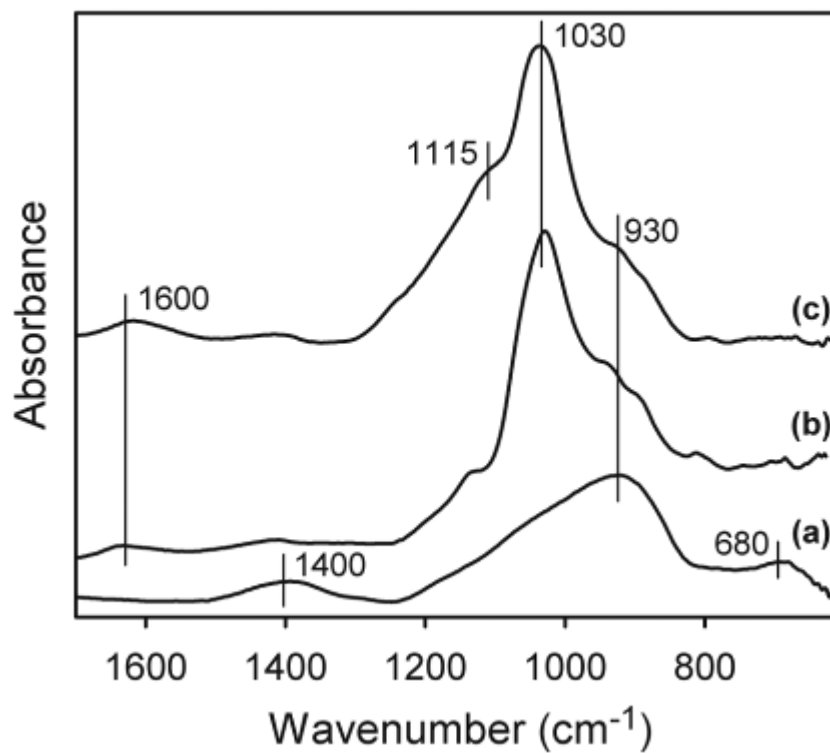


Figure 3.37 ATR-FTIR Spectra of Combustion Residues from Specimens with Nanoclay: (a) PA6/GF, (b) *n*-PA6/GF, and (c) *n*-PA6/GF-OP15

CHAPTER 4

CONCLUSIONS

Flammability properties of both neat PA6 and PA66 are far from the certain requirements in the industry. Although LOI values are higher than the oxygen concentration of air; both PA6 and PA66 continue to burn after ignition, and drip down. Thus, they could only satisfy V-2 rating in UL-94 vertical burning test. When glass fibers are introduced, LOI values further decrease drastically. Therefore, increasing flame retardancy of polyamides is essential.

In the first part of this study, three different flame retardants (MCA, Br/Sb, RP) were compounded with unreinforced/reinforced PA6 and PA66. Then, their mechanical properties (tensile test), thermal stability (TGA) and flame retardancy (UL-94, LOI, MLC) were studied. Main conclusions drawn from this part are:

- Addition of melamin cyanurate (MCA) decreased tensile strength of PA6 from 73.2 MPa to 55.8 MPa. The reason behind this decrease was the poor compatibility of MCA with PA6, which was observed as debonding at the polymer/additive interface in the SEM micrographs.
- When brominated epoxy with antimony trioxide (Br/Sb) was introduced into glass fiber reinforced polyamides; fiber/polymer adhesion became weaker (again observed as debonding in the SEM micrographs), and average fiber lengths were also reduced, thus tensile strength was decreased significantly from 102.1 MPa to 86.4 MPa for PA6-GF-Br/Sb and from 133.8 to 83.1 for PA66-GF-Br/Sb compared to their neat glass fiber reinforced specimens.

- Addition of red phosphorus (RP) to glass fiber reinforced PA66, did not interfere with the interfacial strength of glass fibers much and therefore tensile strength reduction was in tolerable limits (it is reduced from 133.8 MPa to 117.8 MPa).
- On the other hand, it was observed that, all flame retardants increased the Young's Modulus values due to their stiffening effects.
- When MCA was incorporated to unreinforced PA6, degradation products with lower molecular weight and viscosity were formed. The formation of low viscosity products were also observed in the TGA curves as shifting from single step decomposition to a two step decomposition. As a result, molten polymer drips away decreasing the amount of fuel in the flaming zone.
- When 12 wt% MCA was added to PA6, it only induced an increase in LOI value from 24.9% to 27.1% and a minor decrease (21.5%) in Peak Heat Release Rate (PHRR). However, there was no change in the UL-94 rating. In conclusion, MCA was found to be the least effective flame retardant investigated in this study. It was also observed from TGA that MCA gives no charring.
- Halogenated flame retardants still have far better flame retardancy effects compared to other commercial flame retardants. This was also validated in this study, in the glass fiber reinforced polyamides with Br/Sb flame retardant.
- With the very effective gas phase radical scavenging mechanism of this brominated system, V-0 rating was reached in UL-94 test, and LOI values were increased to the highest levels obtained in this study, which were increased from 22.4% to 28.1% for PA6-GF-Br/Sb and from 21.3% to 31.8% for PA66-GF-Br/Sb compared to their neat glass fiber reinforced specimens.

Moreover, PHRR values decreased to 1/3 of the neat glass fiber reinforced specimens.

- After addition of Br/Sb flame retardant; degradation pathway of the polyamides was also altered, decreasing $T_{DTG-Peak}$ value by 100°C due to acid catalysis of the gases formed. As a consequence of the reduced thermal stability, Br/Sb containing specimens became harder to process and shape.
- Considering the % residue values from TGA of Br/Sb containing specimens, it can be stated that, charring induced by Br/Sb was negligible. Considering the SEM micrographs of the burnt specimens, it was observed that residue of Br/Sb containing specimens was loose due to the gases evolved.
- RP was also an efficient flame retardant in glass fiber reinforced PA66. Only 7.2 wt% RP (12 wt% RP containing phenolic resin) was sufficient to impart an UL-94 V-0 rating and improvement in LOI value from 21.3% to 27.6%. PHRR was also decreased by 75% compared to PA66-GF. Moreover, RP increased charring and shifted $T_{DTG-Peak}$ value 20°C lower.
- The main reason behind the efficiency of RP was the formation of protective glassy barrier promoted by the catalysis of phosphoric acids. The strong and consolidated barrier was observed in the SEM micrographs of burnt specimens.

In the second part of this study, a certain nanoclay was compounded with short glass fiber reinforced PA6, containing organo-phosphorus flame retardant (OP). Then, synergism of nanoclay with OP flame retardant was studied on the thermal stability (TGA) and flame retardancy (UL-94, LOI, MLC) of these specimens. Furthermore, burnt residues were characterized by ATR-FTIR and SEM. The following are the main conclusions drawn from this part:

- First of all, XRD and TEM studies proved that dispersion and exfoliation of nanoclay layers in the PA6 matrix was successful.
- Like most of the flame retardants, OP was incompatible with PA6 matrix (validated by SEM micrographs). Thus, addition of OP decreased fiber/matrix interfacial strength in glass fiber reinforced specimens leading to lower tensile strength values. For example, comparing PA6/GF-OP10 with PA6/GF, tensile strength was decreased from 69.8 MPa to 64 MPa.
- On the other hand, upon replacement of flame retardant with 5 wt% nanoclay, at equal total additive content, tensile strength values were increased (e.g. 70.7 MPa for *n*PA6/GF-OP5), as a result of the improved interfacial strength between glass fibers and PA6 matrix.
- It was also observed that, synergism of both OP and nanoclay increased Young's Modulus values. For instance, neat glass fiber reinforced specimen (PA6/GF) had the Young's Modulus value of 2.25 GPa, upon introduction of 5 wt% nanoclay (*n*PA6/GF) it increased to 2.69 GPa, while after introduction of 10 wt% OP (PA6/GF-OP10) it increased to 2.52 GPa. However, when both 5 wt% nanoclay and 10 wt% OP were introduced together (*n*PA6/GF-OP10), Young' Modulus value was reached to 3.10 GPa.
- When only nanoclays were introduced to PA6; no significant improvement was observed in the LOI, UL-94, and PHRR values. Therefore, to impart flame retardancy they should not be used alone but in combination with commercial flame retardants.
- OP used in this study contains aluminum phosphinate, melamine polyphosphate and zinc borate. Upon flaming, aluminum phosphates as well as boron phosphates were formed leading to carbonaceous barrier.

- Thus, LOI values and UL-94 ratings were improved significantly, while PHRR values were reduced. For example, comparing PA6/GF-OP15 with PA6/GF, LOI value increased from 21.3% to 29.3%, and UL-94 rating improved from V-2 to V-0. Additionally, PHRR and THE values decreased by 57% and 35%, respectively.
- When 5 wt% of OP was replaced by nanoclay, significant PHRR reductions (e.g. 20% comparing *n*PA6/GF-OP5 with PA6/GF-OP10), and remarkably delayed Time to Ignition (TTI) periods were observed. Hence, Fire Growth Index (FGI=PHRR/TTI), as an assessment of flame spread, was lowered.
- Additionally, substantial improvements in LOI value were obtained in the nanocomposites of flame retarded and glass fiber reinforced PA6 even when the nominal filler content was kept constant. For example, LOI value of PA6/GF-OP10 (24.9%) increased to 29.1% in *n*PA6/GF-OP5.
- The improved flammability and fire properties of nanocomposites were attributed to the formation of strong and consolidated barrier owing to the reinforcement of the char at nanoscale by clay layers. This was validated by the SEM micrographs of burnt nanocomposite specimens. ATR-FTIR studies also revealed that this char barrier was mainly consisted of boron-aluminum phosphates.
- It was observed from TGA that, degradation temperatures of nanocomposites were shifted to lower temperatures as a result of the catalytic activity of protonic sites within clay galleries.
- Evolution of the volatiles was retarded by the act of the tortuous pathway formed by exfoliated clay layers. This was determined from mass loss rates in TGA curves. Regarding the same nominal filler content, char yields of flame retarded nanocomposites in TGA were also higher compared to conventionally flame retarded formulations.

REFERENCES

- [1] Kirk-Othmer Encyclopedia of Chemical Technology, John Wiley & Sons Inc. (2009)
- [2] Holland, B. J. and Hay, J. N. "Thermal degradation of nylon polymers." *Polymer International* 49(9): 943-948. (2000).
- [3] Levchik, S. V., Weil, E. D. and Lewin, M. "Thermal decomposition of aliphatic nylons." *Polymer International* 48(6-7): 532-557. (1999).
- [4] Holland, B. J. and Hay, J. N. "The dependence of non-volatile residue formation in nylon 6 and nylon 6,6 during thermal degradation on hydrogen bonding in the melt." *Polymer* 42(10): 4759-4761. (2001).
- [5] Curtis, P. T., Bader, M. G. and Bailey, J. E. "The stiffness and strength of a polyamide thermoplastic reinforced with glass and carbon fibres." *Journal of Materials Science* 13(2): 377-390. (1978).
- [6] "DuPont Zytel Material Data Sheets". Retrieved from "http://www2.dupont.com/Plastics/en_US/Products/Zytel/zytel_europe_data_sheets.html." at "07.05.2009"
- [7] Cho, J. W. and Paul, D. R. "Nylon 6 nanocomposites by melt compounding." *Polymer* 42(3): 1083-1094. (2001).
- [8] Carter, L. W., Hendricks, J. G. and Bolley, D. S., "US Patent 2531396" (1950)
- [9] Nahin, P. G. and Backlund, P. S., "US Patent 3084117" (1963)
- [10] Fujiwara, S. and Sakamoto, T. "Japanese Kokai Patent 109998." (1976).
- [11] Kawasumi, M., Kohzaki, M. and Kojima, Y., "US Patent 4810734" (1989)
- [12] Lyon, R. E. and Janssens, M. L. "Polymer Flammability." US Department of Transportation Federal Aviation Administration Office of Aviation Research Technical Report. (2005).
- [13] Grand, A. F. and Wilkie, C. A. "Fire Retardancy of Polymeric Materials". New York, Marcel Dekker Inc.(2000)

- [14] Levchik, S. V. and Weil, E. D. "Combustion and fire retardancy of aliphatic nylons." *Polymer International* 49(10): 1033-1073. (2000).
- [15] Galip, H., Hasipoglu, H. and Gunduz, G. "Flame-retardant polyester." *Journal of Applied Polymer Science* 74(12): 2906-2910. (1999).
- [16] Wu, Z., Shu, W. and Hu, Y. "Synergist flame retarding effect of ultrafine zinc borate on LDPE/IFR system." *Journal of Applied Polymer Science* 103(6): 3667-3674. (2007).
- [17] He, Q., Song, L., Hu, Y. and Zhou, S. "Synergistic effects of polyhedral oligomeric silsesquioxane (POSS) and oligomeric bisphenyl A bis(diphenyl phosphate) (BDP) on thermal and flame retardant properties of polycarbonate." *Journal of Materials Science* 44(5): 1308-1316. (2009).
- [18] Hull, T. R., Quinn, R. E., Areri, I. G. and Purser, D. A. "Combustion toxicity of fire retarded EVA." *Polymer Degradation and Stability* 77(2): 235-242. (2002).
- [19] Xiao, W. D. and Kibble, K. A. "Comparison of aluminium hydroxide and magnesium hydroxide as flame retardants in SEBS-based composites." *Polymers and Polymer Composites* 16(7): 415-422. (2008).
- [20] Almeras, X., Le Bras, M., Poutch, F., Bourbigot, S., Marosi, G. and Anna, P. "Effect of fillers on fire retardancy of intumescent polypropylene blends." *Macromolecular Symposia* 198: 435-447. (2003).
- [21] Casu, A., Camino, G., De Giorgi, M., Flath, D., Morone, V. and Zenoni, R. "Fire-retardant mechanistic aspects of melamine cyanurate in polyamide copolymer." *Polymer Degradation and Stability* 58(3): 297-302. (1997).
- [22] Zaikov, G. E. and Lomakin, S. M. "Ecological issue of polymer flame retardancy." *Journal of Applied Polymer Science* 86(10): 2449-2462. (2002).
- [23] Green, J. "Mechanisms for flame retardancy and smoke suppression - A review." *Journal of Fire Sciences* 14(6): 426-442. (1996).
- [24] Kashiwagi, T., Harris Jr, R. H., Zhang, X., Briber, R. M., Cipriano, B. H., Raghavan, S. R., Awad, W. H. and Shields, J. R. "Flame retardant mechanism of polyamide 6-clay nanocomposites." *Polymer* 45(3): 881-891. (2004).
- [25] Gilman, J. W., Kashiwagi, T. and Lichtenhan, J. D. "Nanocomposites: A revolutionary new flame retardant approach." *SAMPE Journal* 33(4): 40-46. (1997).
- [26] Bourbigot, S., Duquesne, S. and Jama, C. "Polymer nanocomposites: How to reach low flammability?" *Macromolecular Symposia* 233: 180-190. (2006).

- [27] Shanmuganathan, K., Deodhar, S., Dembsey, N. A., Fan, Q. and Patra, P. K. "Condensed-phase flame retardation in nylon 6-layered silicate nanocomposites: Films, fibers, and fabrics." *Polymer Engineering and Science* 48(4): 662-675. (2008).
- [28] Song, L., Hu, Y., He, Q. and You, F. "Study on crystallization, thermal and flame retardant properties of nylon 66/organoclay nanocomposites by in situ polymerization." *Journal of Fire Sciences* 26(6): 475-492. (2008).
- [29] Samyn, F., Bourbigot, S., Jama, C. and Bellayer, S. "Fire retardancy of polymer clay nanocomposites: Is there an influence of the nanomorphology?" *Polymer Degradation and Stability* 93(11): 2019-2024. (2008).
- [30] Bourbigot, S., Duquesne, S., Fontaine, G., Bellayer, S., Turf, T. and Samyn, F. "Characterization and Reaction to Fire of Polymer Nanocomposites with and without Conventional Flame Retardants." *Molecular Crystals and Liquid Crystals* 486: 325/[1367]-339/[1381]. (2008).
- [31] Bartholmal, M. and Schartel, B. "Layered silicate polymer nanocomposites: New approach or illusion for fire retardancy ? Investigations of the potentials and the tasks using a model system." *Polymers for Advanced Technologies* 15(7): 355-364. (2004).
- [32] Zhang, S. and Horrocks, A. R. "A review of flame retardant polypropylene fibres." *Progress in Polymer Science (Oxford)* 28(11): 1517-1538. (2003).
- [33] Camino, G., Costa, L. and Martinasso, G. "Intumescent fire-retardant systems." *Polymer Degradation and Stability* 23(4): 359-376. (1989).
- [34] Carpentier, F., Bourbigot, S., Le Bras, M., Delobel, R. and Foulon, M. "Charring of fire retarded ethylene vinyl acetate copolymer - magnesium hydroxide/zinc borate formulations." *Polymer Degradation and Stability* 69(1): 83-92. (2000).
- [35] Samyn, F., Bourbigot, S., Duquesne, S. and Delobel, R. "Effect of zinc borate on the thermal degradation of ammonium polyphosphate." *Thermochimica Acta* 456(2): 134-144. (2007).
- [36] Levchik, S. V. and Weil, E. D. "A review of recent progress in phosphorus-based flame retardants." *Journal of Fire Sciences* 24(5): 345-364. (2006).
- [37] Laoutid, F., Bonnaud, L., Alexandre, M., Lopez-Cuesta, J. M. and Dubois, P. "New prospects in flame retardant polymer materials: From fundamentals to nanocomposites." *Materials Science and Engineering R: Reports* 63(3): 100-125. (2009).
- [38] Fenimore, C. P. and Martin, F. J. "Flammability of polymers." *Combustion and Flame* 10(2): 135-139. (1966).

- [39] Petrella, R. V. "The Assessment of Full-Scale Fire Hazards from Cone Calorimeter Data." *Journal of Fire Sciences* 12(1): 14-43. (1994).
- [40] Richardson, P. N., "US Patent 4 373 049 " (1983)
- [41] Yamanaka, K., Okamoto, K. and Mizukami, Y., "US Patent 4 144 225 " (1979)
- [42] Kohan, M. I., "US Patent 4 410 653" (1983)
- [43] Tjahjadi, M., "EP Patent Application 0855421 A1 " (1998)
- [44] Williams, I. G., "US Patent 4 696 966 " (1987)
- [45] Yaakov, Y. B. and Minke, R., "US Patent 4 605 708 " (1986)
- [46] Levchik, S. V., Balabanovich, A. I., Levchik, G. F. and Costa, L. "Effect of melamine and its salts on combustion and thermal decomposition of polyamide 6." *Fire and Materials* 21(2): 75-83. (1997).
- [47] Gijsman, P., Steenbakkers, R., Fu^lrst, C. and Kersjes, J. "Differences in the flame retardant mechanism of melamine cyanurate in polyamide 6 and polyamide 66." *Polymer Degradation and Stability* 78(2): 219-224. (2002).
- [48] Liu, Y., Wang, Q., Fei, G. and Chen, Y. "Preparation of polyamide resin-encapsulated melamine cyanurate/melamine phosphate composite flame retardants and the fire-resistance to glass fiber-reinforced polyamide 6." *Journal of Applied Polymer Science* 102(2): 1773-1779. (2006).
- [49] Liu, Y. and Wang, Q. "Preparation of microencapsulated red phosphorus through melamine cyanurate self-assembly and its performance in flame retardant polyamide 6." *Polymer Engineering and Science* 46(11): 1548-1553. (2006).
- [50] Liu, Y. and Wang, Q. "Melamine cyanurate-microencapsulated red phosphorus flame retardant unreinforced and glass fiber reinforced polyamide 66." *Polymer Degradation and Stability* 91(12): 3103-3109. (2006).
- [51] Davis, J. and Huggard, M. "The Technology of Halogen-Free Flame Retardant Phosphorus Additives for Polymeric Systems." *Journal of Vinyl and Additive Technology* 2(1): 69-75. (1996).
- [52] Jou, W. S., Chen, K. N., Chao, D. Y., Lin, C. Y. and Yeh, J. T. "Flame retardant and dielectric properties of glass fibre reinforced nylon-66 filled with red phosphorous." *Polymer Degradation and Stability* 74(2): 239-245. (2001).
- [53] Schartel, B., Kunze, R. and Neubert, D. "Red phosphorus-controlled decomposition for fire retardant PA 66." *Journal of Applied Polymer Science* 83(10): 2060-2071. (2002).

- [54] Levchik, G. F., Vorobyova, S. A., Gorbarenko, V. V., Levchik, S. V. and Weil, E. D. "Some mechanistic aspects of the fire retardant action of red phosphorus in aliphatic nylons." *Journal of Fire Sciences* 18(3): 172-182. (2000).
- [55] Balabanovich, A. I. and Schnabel, W. "Fire retardance in polyamide-6,6. The effects of red phosphorus and radiation-induced cross-links." *Macromolecular Materials and Engineering* 287(3): 187-194. (2002).
- [56] Levchik, S. V. and Weil, E. D. "Flame retardancy of thermoplastic polyester - A review of the recent literature." *Polymer International* 54(1): 11-35. (2005).
- [57] Braun, U., Scharrel, B., Fichera, M. A. and Jager, C. "Flame retardancy mechanisms of aluminum phosphinate in combination with melamine polyphosphate and zinc borate in glass-fibre reinforced polyamide 6,6." *Polymer Degradation and Stability* 92(8): 1528-1545. (2007).
- [58] Liping, L., Bin, L. and Feitang "Thermal stability and properties of flame retarded glass fiber reinforced polyamide 66 composite." *Journal of Reinforced Plastics and Composites* 27(3): 277-285. (2008).
- [59] Jahromi, S., Gabrielise, W. and Braam, A. "Effect of melamine polyphosphate on thermal degradation of polyamides: A combined X-ray diffraction and solid-state NMR study." *Polymer* 44(1): 25-37. (2002).
- [60] Chen, Y. and Wang, Q. "Preparation, properties and characterizations of halogen-free nitrogen-phosphorous flame-retarded glass fiber reinforced polyamide 6 composite." *Polymer Degradation and Stability* 91(9): 2003-2013. (2006).
- [61] Wang, Z. Y., Feng, Z. Q., Liu, Y. and Wang, Q. "Flame retarding glass fibers reinforced polyamide 6 by melamine polyphosphate/polyurethane-encapsulated solid acid." *Journal of Applied Polymer Science* 105(6): 3317-3322. (2007).
- [62] Gilman, J. W. "Flammability and thermal stability studies of polymer layered-silicate (clay) nanocomposites." *Applied Clay Science* 15(1-2): 31-49. (1999).
- [63] Wang, S., Hu, Y., Zong, R., Tang, Y., Chen, Z. and Fan, W. "Preparation and characterization of flame retardant ABS/montmorillonite nanocomposite." *Applied Clay Science* 25(1-2): 49-55. (2004).
- [64] Lu, H., Hu, Y., Li, M. and Song, L. "Effects of charring agents on the thermal and flammability properties of intumescent flame-retardant HDPE-based clay nanocomposites." *Polymer - Plastics Technology and Engineering* 47(2): 152-156. (2008).
- [65] Bourbigot, S., Le Bras, M., Dabrowski, F., Gilman, J. W. and Kashiwagi, T. "PA-6 clay nanocomposite hybrid as char forming agent in intumescent formulations." *Fire and Materials* 24(4): 201-208. (2000).

- [66] Shanmuganathan, K., Deodhar, S., Dembsey, N., Fan, Q., Calvert, P. D., Warner, S. B. and Patra, P. K. "Flame retardancy and char microstructure of nylon-6/layered silicate nanocomposites." *Journal of Applied Polymer Science* 104(3): 1540-1550. (2007).
- [67] Song, L., Hu, Y., Lin, Z., Xuan, S., Wang, S., Chen, Z. and Fan, W. "Preparation and properties of halogen-free flame-retarded polyamide 6/organoclay nanocomposite." *Polymer Degradation and Stability* 86(3): 535-540. (2004).
- [68] Dong, W., Zhang, X., Liu, Y., Wang, Q., Gui, H., Gao, J., Song, Z., Lai, J., Huang, F. and Qiao, J. "Flame retardant nanocomposites of polyamide 6/clay/silicone rubber with high toughness and good flowability." *Polymer* 47(19): 6874-6879. (2006).
- [69] Hu, Y., Wang, S., Ling, Z., Zhuang, Y., Chen, Z. and Fan, W. "Preparation and combustion properties of flame retardant Nylon 6/montmorillonite nanocomposite." *Macromolecular Materials and Engineering* 288(3): 272-276. (2003).
- [70] Kiliaris, P., Papaspyrides, C. D. and Pfaendner, R. "Polyamide 6 filled with melamine cyanurate and layered silicates: Evaluation of flame retardancy and physical properties." *Macromolecular Materials and Engineering* 293(9): 740-751. (2008).
- [71] Zhang, J., Lewin, M., Pearce, E., Zammarano, M. and Gilman, J. W. "Flame retarding polyamide 6 with melamine cyanurate and layered silicates." *Polymers for Advanced Technologies* 19(7): 928-936. (2008).
- [72] Huang, X., Li, B., Shi, B. and Li, L. "Investigation on interfacial interaction of flame retarded and glass fiber reinforced PA66 composites by IGC/DSC/SEM." *Polymer* 49(4): 1049-1055. (2008).
- [73] Akkapeddi, M. K. "Glass fiber reinforced polyamide-6 nanocomposites." *Polymer Composites* 21(4): 576-585. (2000).
- [74] Wu, S. H., Wang, F. Y., Ma, C. C., Chang, W. C., Kuo, C. T., Kuan, H. C. and Chen, W. J. "Mechanical, thermal and morphological properties of glass fiber and carbon fiber reinforced polyamide-6 and polyamide-6/clay nanocomposites." *Materials Letters* 49(6): 327-333. (2001).
- [75] Zhao, C. S., Huang, F. L., Xiong, W. C. and Wang, Y. Z. "A novel halogen-free flame retardant for glass-fiber-reinforced poly(ethylene terephthalate)." *Polymer Degradation and Stability* 93(6): 1188-1193. (2008).
- [76] Troitzsch, J. "Plastics Flammability Handbook". Munich, Hanser Publications.(2004)
- [77] Schartel, B. and Hull, T. R. "Development of fire-retarded materials - Interpretation of cone calorimeter data." *Fire and Materials* 31(5): 327-354. (2007).

- [78] Vaia, R. A. and Giannelis, E. P. "Lattice model of polymer melt intercalation in organically-modified layered silicates." *Macromolecules* 30(25): 7990-7999. (1997).
- [79] Morgan, A. B., Chu, L. L. and Harris, J. D. "A flammability performance comparison between synthetic and natural clays in polystyrene nanocomposites." *Fire and Materials* 29(4): 213-229. (2005).
- [80] Dasari, A., Yu, Z. Z., Mai, Y. W., Cai, G. and Song, H. "Roles of graphite oxide, clay and POSS during the combustion of polyamide 6." *Polymer* 50(6): 1577-1587. (2009).
- [81] Samyn, F., Bourbigot, S., Jama, C., Bellayer, S., Nazare, S., Hull, R., Fina, A., Castrovinci, A. and Camino, G. "Characterisation of the dispersion in polymer flame retarded nanocomposites." *European Polymer Journal* 44(6): 1631-1641. (2008).
- [82] Laachachi, A., Cochez, M., Leroy, E., Ferriol, M. and Lopez-Cuesta, J. M. "Fire retardant systems in poly(methyl methacrylate): Interactions between metal oxide nanoparticles and phosphinates." *Polymer Degradation and Stability* 92(1): 61-69. (2007).
- [83] Lewin, M., Zhang, J., Pearce, E. and Gilman, J. "Flammability of polyamide 6 using the sulfamate system and organo-layered silicate." *Polymers for Advanced Technologies* 18(9): 737-745. (2007).
- [84] Stoch, L. and Siroda, M. "Infrared spectroscopy in the investigation of oxide glasses structure." *Journal of Molecular Structure* 511-512: 77-84. (1999).
- [85] Madejova, J. "FTIR techniques in clay mineral studies." *Vibrational Spectroscopy* 31(1): 1-10. (2003).
- [86] Adame, D. and Beall, G. W. "Direct measurement of the constrained polymer region in polyamide/clay nanocomposites and the implications for gas diffusion." *Applied Clay Science* 42(3-4): 545-552. (2009).

APPENDIX A

AN EXAMPLE OF THE CALCULATION OF LIMITING OXYGEN INDEX BY DIXON'S UP AND DOWN METHOD

Test Results Sheet For Oxygen Index According To ISO 4589

Test Laboratory: Polymers and Nanocomposites Lab.
 Date Of Test: 10.10.2008 Test Performed By: H. Özgür Gündüz
 Material: PA 6 Ignition Procedure: A / B A (Top Surface Ignition)
 Density (kg m⁻³): 1.13 Oxygen Concentration Increment, *d* (%): 0.2
 Specimen Form: Rigid bar
 Specimen Dimensions (mm)
 Length: 100 Oxygen Index, *OI*, (%): 24.9
 Width: 10 Standard Deviation, $\hat{\sigma}$, (%): 0.21
 Thickness: 4
 Conditioning Procedure: 24 hours at room atmosphere

Part 1: Determination of the preliminary oxygen concentration from one pair of "X" and "O" response at $\leq 1\%$ O₂ concentration interval

Oxygen concentration (%)	19	20	21	22	23	24	25	26	
Burning Period (s)	NO Ign.	NO Ign.	5	10	10	17	90		
Length Burnt (mm)								>50	
Response (X or O)	O	O	O	O	O	O	O	X	

Preliminary oxygen concentration (%) = 25

Part 2: Determination Of The Oxygen Index Value

		<i>N_i</i> series measurements										
		<i>N_i</i> series measurements					<i>c_P</i>					
Oxygen concentration (%)		25	25.2					25.2	25.0	24.8	24.6	24.8
Burning Period (s)		90									40	50
Length Burnt (mm)			>50					>50	>50	>50		
Response (X or O)		O	X					X	X	X	O	O
		Column (2, 3, 4 or 5): 2					Row (1 to 16): 13					
		<i>k</i> value from table: 0.50										
		<i>k</i> value, with correct sign: 0.50										

$$OI = c_P + k \cdot d = 24.8 + (0.50)(0.2) = 24.9$$

[To one decimal place for reporting *OI* and two decimal places for calculating the standard deviation]

Part 3: Verification Of The Oxygen Concentration Increment, d

Last six results	Oxygen concentration (%)			
	c_i	OI	$c_i - OI$	$(c_i - OI)^2$
c_{i1} 1	24.8	24.9	- 0.1	0.01
2	24.6	24.9	- 0.3	0.09
3	24.8	24.9	- 0.1	0.01
4	25.0	24.9	0.1	0.01
5	25.2	24.9	0.3	0.09
n 6	25.0	24.9	0.1	0.01
Total $\Sigma (c_i - OI)^2$				0.22

Standard deviation

$$\hat{\sigma} = \left[\frac{\sum (c_i - OI)^2}{n-1} \right]^{1/2}$$

$$= \left(\frac{0.22}{5} \right)^{1/2} = 0.21$$

$$\frac{2\hat{\sigma}}{3} = 0.14 < d = 0.2 < \frac{3\hat{\sigma}}{2} = 0.32$$

If $\frac{2\hat{\sigma}}{3} < d < \frac{3\hat{\sigma}}{2}$ OR if $d > \frac{3\hat{\sigma}}{2}$ and $d = 0.2\%$ then OI is valid.

Otherwise...

If $d < \frac{2\hat{\sigma}}{3}$, repeat part 2 of the test using an increased value of d .

OR If $d > \frac{3\hat{\sigma}}{2}$, repeat part 2 of the test using a decreased value of d .

Part 4: Additional Information

Colorless to blue, hesitating flame

Burning polymer drips away

Drips can extinguish the flame.

The test results relate only to the behaviour of the test specimens under the condition of this test and these results must not be used to infer fire hazards of the material in other forms or under other fire conditions

LOI value is calculated from the Equation A.1.

$$OI = c_F + k.d \tag{A.1}$$

Where:

“ c_F ” is the final value of oxygen concentration

“ d ” is the step size between oxygen concentration levels.

“ k ” is a factor to be obtained from Table A.1.

For determining value of k : if the response of the first specimen tested in the N_L series gave an “O” response then refer to column 1 of Table A.1 to select the row for which the last five response symbols correspond to those found when testing the last five specimens. If the response of the first specimen tested in the N_L series gave an “X” response then refer to column 6 of Table A.1 to select the row for which the last five response symbols correspond to those found when testing the last five specimens.

Table A.1 Values of k for calculating Limiting Oxygen Index

1	2	3	4	5	6
Responses for the last five measurements	Values of k for which the first N_L determinations are:				
	(a) O	OO	OOO	OOOO	
XOOOO	-0.55	-0.55	-0.55	-0.55	OXXXX
XOOOX	-1.25	-1.25	-1.25	-1.25	OXXXO
XOOXO	0.37	0.38	0.38	0.38	OXXOX
XOOXX	-0.17	-0.14	-0.14	-0.14	OXXOO
XOXOO	0.02	0.04	0.04	0.04	OXOXX
XOXOX	-0.50	-0.46	-0.45	-0.45	OXOXO
XOXOX	1.17	1.24	1.25	1.25	OXOOX
XOXXX	0.61	0.73	0.76	0.76	OXOOO
XXOOO	-0.30	-0.27	-0.26	-0.26	OXXXX
XXOOX	-0.83	-0.76	-0.75	-0.75	OXXXO
XXOXO	0.83	0.94	0.95	0.95	OXXOX
XXOXX	0.30	0.46	0.50	0.50	OXXOO
XXXOO	0.50	0.65	0.68	0.68	OXXOX
XXXOX	-0.04	0.19	0.24	0.25	OXXO
XXXO	1.60	1.92	2.00	2.01	OXXOX
XXXXX	0.89	1.33	1.47	1.50	OXXXX
	Values of k for which the first N_L determinations are:				Responses for the last five measurements
	(b) X	XX	XXX	XXXX	
	are as given in the above table opposite the appropriate response in column 6, but with the sign of k reversed.				

APPENDIX B

AN EXAMPLE OF THE CALIBRATION OF THE MASS LOSS CONE CALORIMETER

B.1 Calibration of the Heater Thermocouples to External Heat Flux Values

The value of the external heat flux was determined from the temperature of the cone. First, the cone temperature was set to different values. Then, heat flux meter was placed at the center of the cone and exactly 25 mm from the bottom of the cone heater plate. Finally, the readings of the heat flux meter, which is in the units of milivolts, were correlated to heat fluxes, in the units of kW/m^2 by employing the calibration graph provided by the producer (FTT). Set cone temperatures, corresponding heat flux meter readings, and their converted heat fluxes are given in Table B.1.

Table B.1 Calibration Data for Converting Cone Temperature to External Heat Flux

Set Cone Temperature (°C)	Heat Flux Meter Reading (mV)	Heat Flux (kW/m^2)
565	3,5	18,0
625	5,0	21,5
702	6,6	30,0
724	7,5	35,0

Therefore in order to conduct the test at an external heat flux of 35 kW/m^2 (corresponds to mild fire scenario) the temperature of the cone is set to 724°C . Then, another heat flux meter reading was taken to ensure that the calibration was not

changed. If this reading is deviated, it is necessary to increase or decrease the cone temperature a few degrees.

B.2 Calibration of the Chimney and Thermopile

Calibration burner, in which propane passes through a layer of glass wool, having the same shape with the specimen heater was placed in its position. Then, the cone temperature was set to the value, which corresponds to the desired external heat flux. For example temperature is 724°C for obtaining 35 kW/m² external heat flux.

Finally, propane flow rate was adjusted, gas was ignited and the readings of the thermopiles positioned above the chimney were recorded. The flow rate of the propane was altered and different temperature values were recorded. Flow rate of the propane was correlated to heat release by Equation B.1. Propane flow rates, corresponding heat release rates and thermopile readings are given in Table B.2.

$$\text{Heat Release of Propane} = (\Delta H_{\text{propane}}) \cdot (\text{Propane Flow rate}) \quad (\text{B.1})$$

Propane used for the calibration was purchased from AYGAZ and it has calorific value of 22100 kcal/m³, as stated in its data sheet.

$$\Delta H_{\text{propane}} = 22100 \text{ kcal/m}^3 = 92466 \text{ J/lt}$$

When testing a polymer at a certain external heat flux (e.g. 35 kW/m²), thermopile readings were correlated by using the Equation B.1 obtained from the propane calibration, for the observed temperature range.

For example, for neat PA6; observed maximum thermopile reading, during the testing of a 4mm specimen at 35 kW/m² external heat flux, is round 500°C. Using all data points in Table B.2, correlation of heat release rate (HRR) to thermopile temperature (T) is found from Figure B.1, as:

$$HRR = 2.3916(T) - 342.59 \quad (B.2)$$

Table B.2 Calibration Data for Converting Thermopile Reading to Heat Release Rate

Propane Flow Rate (l/min)	Heat Release Rate of Propane (kW/m²)	Thermopile Reading (°C)
0.6	92.47	171
1.0	154.11	203
1.4	215.75	237
1.6	246.58	255
2.0	308.22	272
2.4	369.86	299
2.6	400.69	315
2.8	431.51	326
3.0	462.33	335
4.0	616.44	410
5.0	770.55	462
6.0	924.66	521
7.0	1078.77	595

As another example, when testing a 4 mm specimen of PA66 containing 25% glass fiber and Br/Sb flame retardant (PA66-GF-Br/Sb), at 35 kW/m² external heat flux, the maximum thermopile reading is around 200°C. Therefore, only first four data of Table B.2 is employed. Correlation of heat release rate (HRR) to thermopile temperature (T) is found from Figure B.2, as:

$$HRR = 1.836(T) - 220.26 \quad (B.3)$$

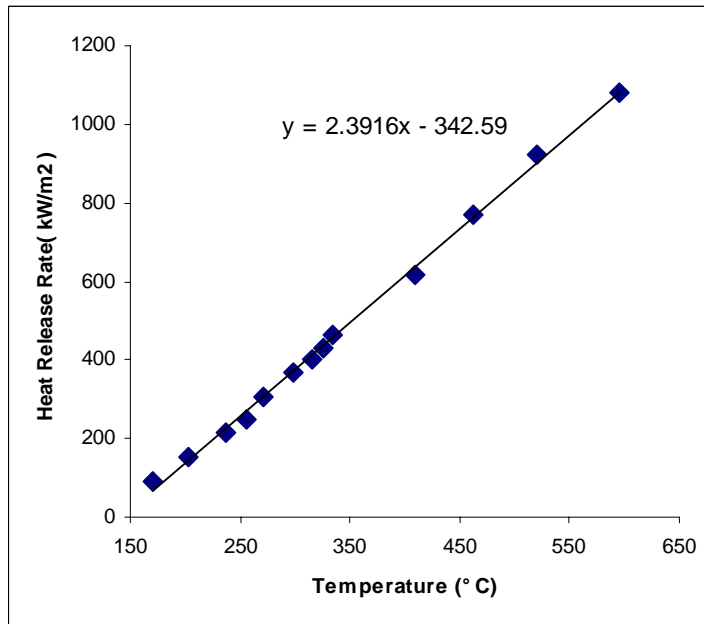


Figure B.1 Correlation of Thermopile Reading to Heat Release Rate for a neat PA6 specimen

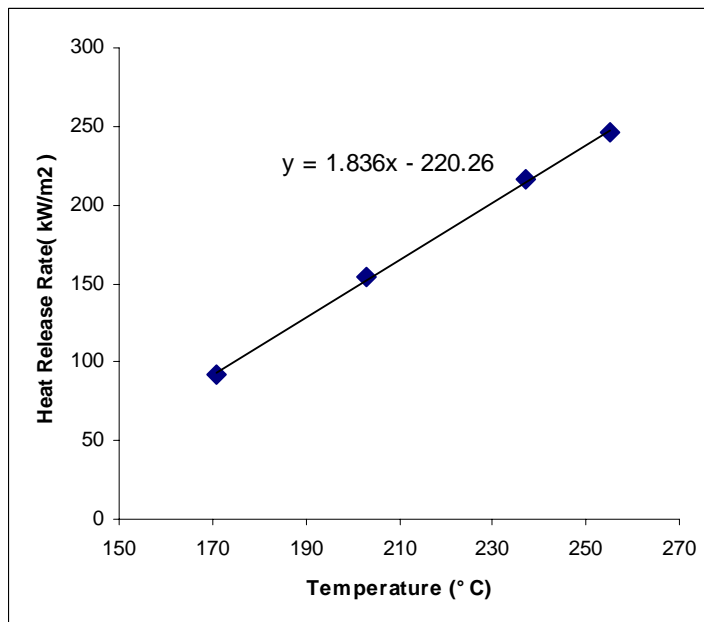


Figure B.2 Correlation of Thermopile Reading to Heat Release Rate for a PA66-GF-Br/Sb specimen

APPENDIX C

REPRESENTATIVE STRESS-STRAIN CURVES FOR EACH SPECIMEN GROUPS

C.1 Specimens Compounded in the Industrial Scale Extruder

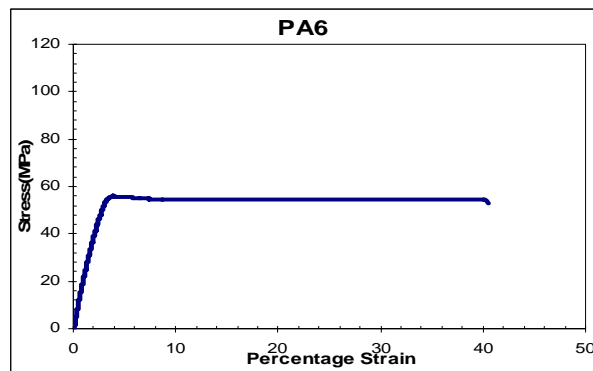


Figure C.1 Representative Stress vs. Strain Curve for a PA6 specimen

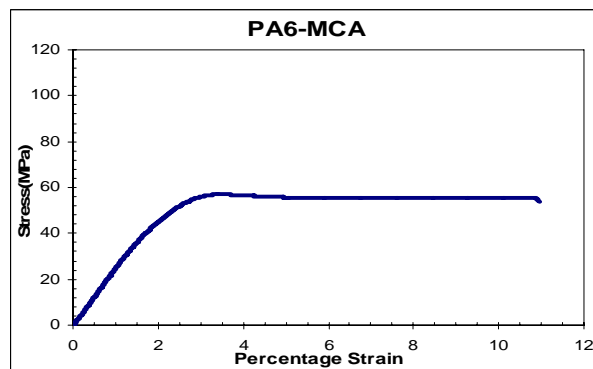


Figure C.2 Representative Stress vs. Strain Curve for a PA6-MCA specimen

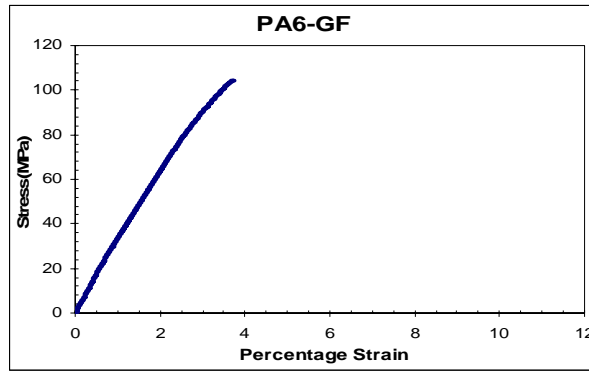


Figure C.3 Representative Stress vs. Strain Curve for a PA6-GF specimen

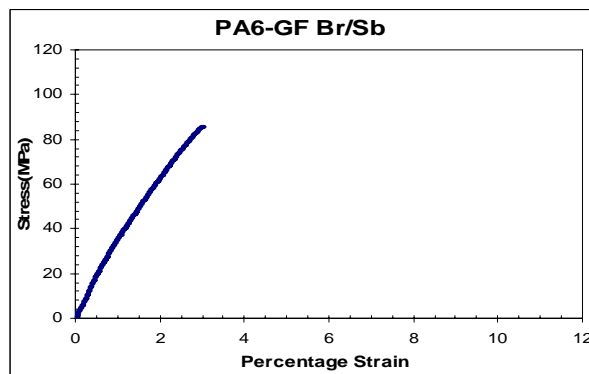


Figure C.4 Representative Stress vs. Strain Curve for a PA6-GF-Br/Sb specimen

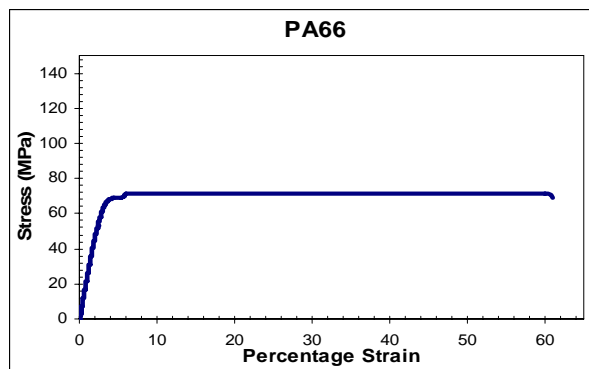


Figure C.5 Representative Stress vs. Strain Curve for a PA66 specimen

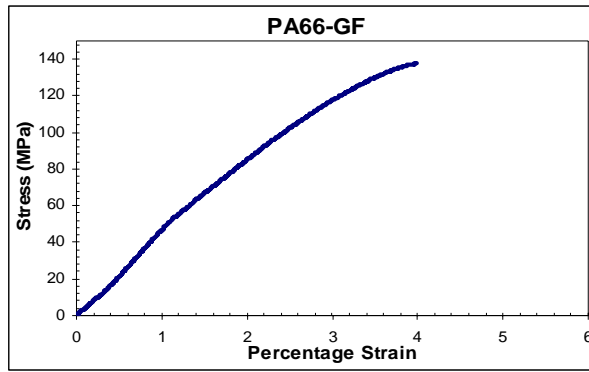


Figure C.6 Representative Stress vs. Strain Curve for a PA66-GF specimen

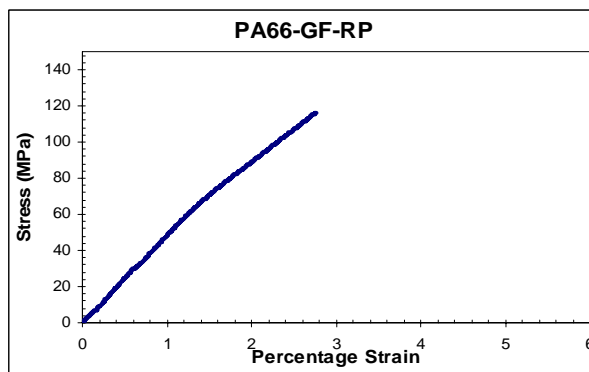


Figure C.7 Representative Stress vs. Strain Curve for a PA66-GF-RP specimen

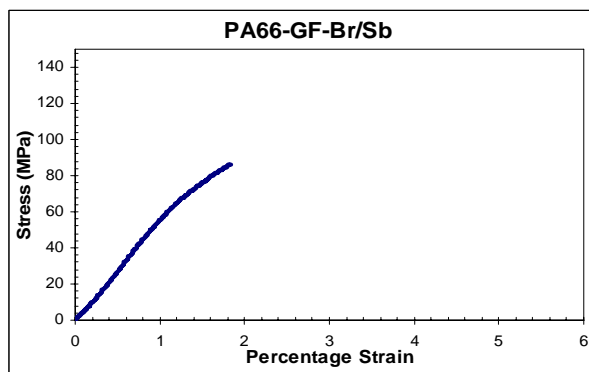


Figure C.8 Representative Stress vs. Strain Curve for a PA66-GF-Br/Sb specimen

C.2 Specimens Compounded in the Laboratory Scale Extruder

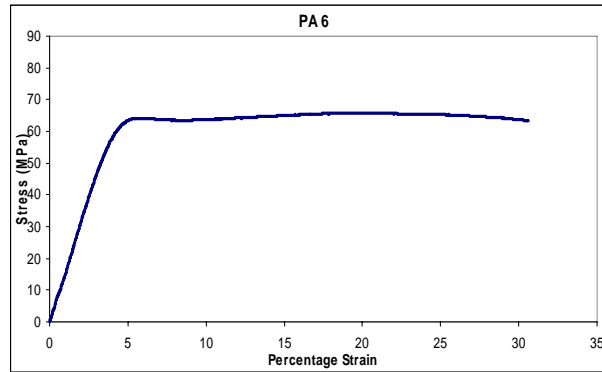


Figure C.9 Representative Stress vs. Strain Curve for a PA6 specimen

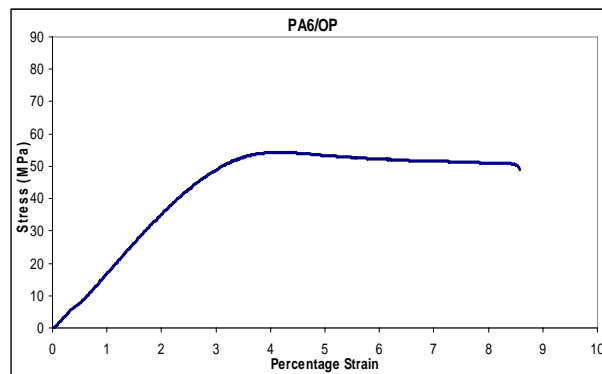


Figure C.10 Representative Stress vs. Strain Curve for a PA6/OP specimen

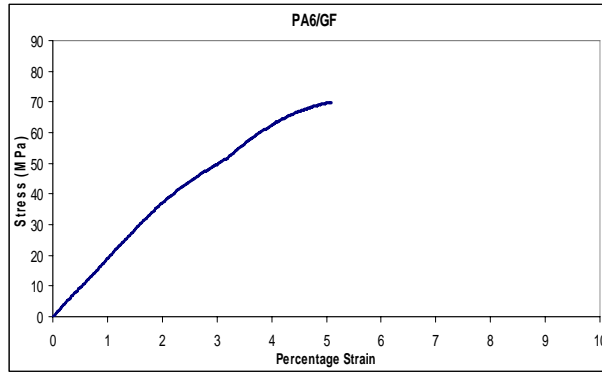


Figure C.11 Representative Stress vs. Strain Curve for a PA6/GF specimen

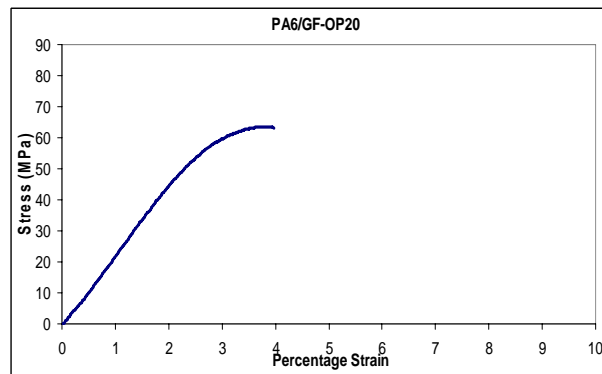


Figure C.12 Representative Stress vs. Strain Curve for a PA6/GF-OP20 specimen

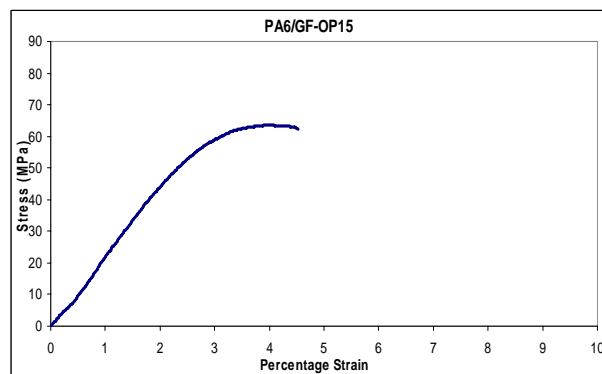


Figure C.13 Representative Stress vs. Strain Curve for a PA6/GF-OP15 specimen

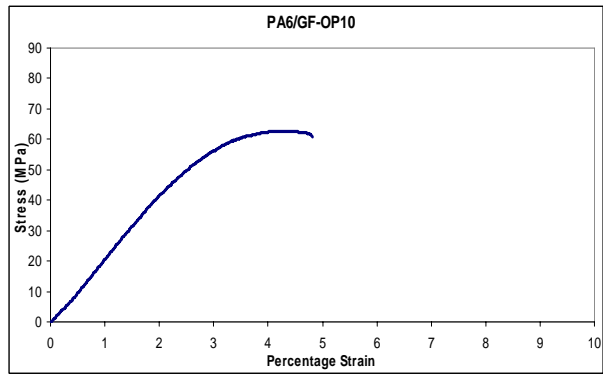


Figure C.14 Representative Stress vs. Strain Curve for a PA6/GF-OP10 specimen

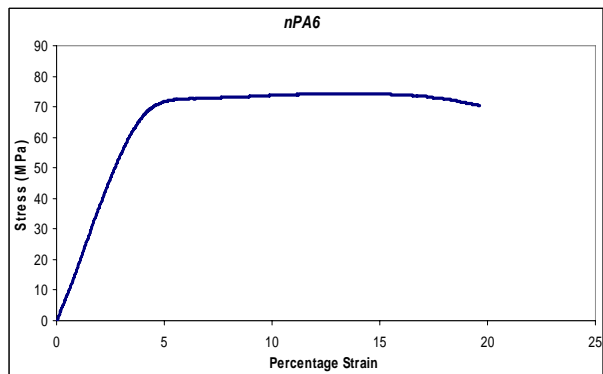


Figure C.15 Representative Stress vs. Strain Curve for an nPA6 specimen

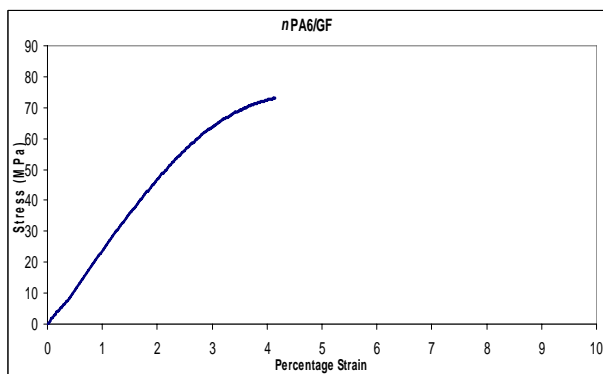


Figure C.16 Representative Stress vs. Strain Curve for an nPA6/GF specimen

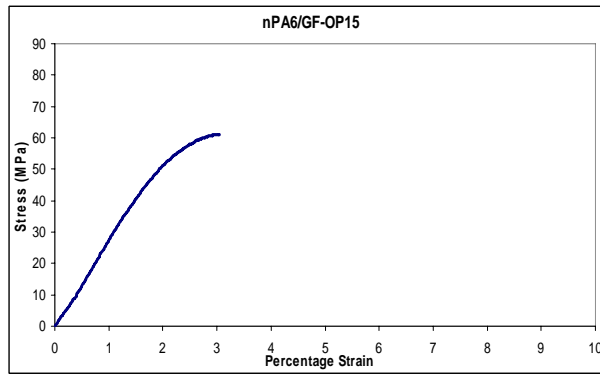


Figure C.17 Representative Stress vs. Strain Curve for an *nPA6/GF-OP15* specimen

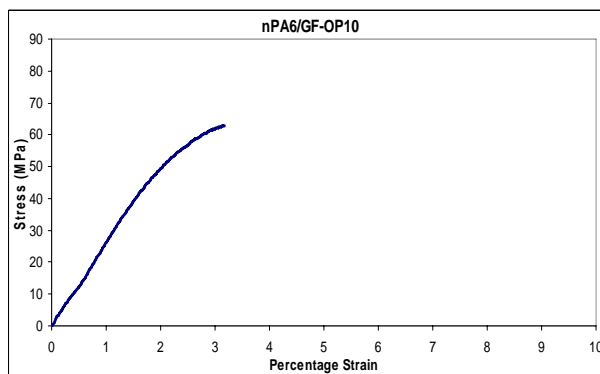


Figure C.18 Representative Stress vs. Strain Curve for an *nPA6/GF-OP10* specimen

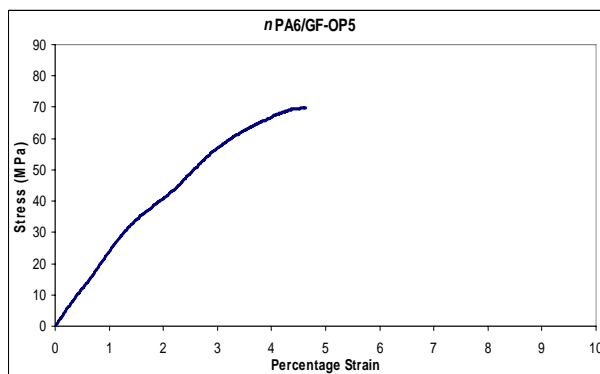


Figure C.19 Representative Stress vs. Strain Curve for an *nPA6/GF-OP5* specimen